Published for SISSA by Springer

Received: *September 10, 2020*
Accepted: *November 10, 2020*
Published: *December 16, 2020*

QED corrections in $\bar{B} \to \bar{K}\ell^+\ell^-$ at the double-differential level

Gino Isidori,[a] **Saad Nabeebaccus**[b] **and Roman Zwicky**[b]

[a] *Department of Physics, Universität Zürich, Winterthurerstrasse 190, CH-8057 Zürich, Switzerland*

[b] *Higgs Centre for Theoretical Physics, School of Physics and Astronomy, University of Edinburgh, Edinburgh EH9 3JZ, Scotland, U.K.*

E-mail: isidori@physik.uzh.ch, saad.nabeebaccus@ed.ac.uk, roman.zwicky@ed.ac.uk

Abstract: We present a detailed analysis of QED corrections to $\bar{B} \to \bar{K}\ell^+\ell^-$ decays at the double-differential level. Cancellations of soft and collinear divergences are demonstrated analytically using the phase space slicing method. Whereas soft divergences are found to cancel at the differential level, the cancellation of the hard-collinear logs $\ln m_\ell$ require, besides photon-inclusiveness, a specific choice of kinematic variables. In particular, hard-collinear logs in the lepton-pair invariant mass distribution (q^2), are sizeable and need to be treated with care when comparing with experiment. Virtual and real amplitudes are evaluated using an effective mesonic Lagrangian. Crucially, we show that going beyond this approximation does not introduce any further infrared sensitive terms. All analytic computations are performed for generic charges and are therefore adaptable to semileptonic decays such as $\bar{B} \to D\ell\bar{\nu}$.

Keywords: Heavy Quark Physics, Precision QED

ArXiv ePrint: 2009.00929

https://doi.org/10.1007/JHEP12(2020)104

Contents

JHEP12(2020)104

1 Introduction

Rare semileptonic B decays of the type $\bar{B} \to \bar{K}^{(*)}\ell^+\ell^-$ have received significant interest in the last few years because of the hints of Lepton Flavour Universality (LFU) violations reported by the LHCb experiment [1–3] and [4] for a review, which could be due to physics beyond the Standard Model (SM). In view of higher statistics results on these modes, a detailed study of this phenomenon requires an accurate estimate of all possible sources of LFU violation present within the SM.

Besides trivial kinematic mass effects, the only potential large source of LFU violation present in the SM are hard-collinear singularities in QED. These can induce non-universal corrections of order $\mathcal{O}(\alpha)\ln(m_\ell/m_B)$ to the physical decay rates (depending on the definition of the observables), which can be large for light leptons. These effects are well known and, to a large extent, corrected for in the experimental analyses through Monte Carlo simulations (e.g. PHOTOS [5]). In order to cross-check the reliability of the approximations which are behind this treatment, a detailed analytic analysis of QED corrections is desirable. A first step in this direction was undertaken in [6], where semi-analytic results for the LFU ratios R_K and R_{K^*} have been presented. Here we go one step further: we focus our attention on the process $\bar{B} \to \bar{K}\ell_1\bar{\ell}_2$ (which is a good prototype for a wide class of interesting semi-leptonic decays, including charged-current transitions such as $\bar{B} \to \pi\ell\nu$), and analyse QED corrections at a fully differential level in terms of the "visible" kinematics (i.e. in terms of the two variables that fully specify the kinematics of the non-radiative mode). Moreover, we present a complete analysis of the problem of evaluating both real and virtual corrections within an effective meson approach which is an improvement over scalar QED. As we demonstrate, this approach is sufficient to trace back the origin of all "dangerous" collinear singularities.

JHEP12(2020)104

While soft QED singularities cancel out at the differential level in any infrared-safe observable, the cancellation of the collinear singularities, which are actually physical effects regulated by the lepton mass, is more subtle. As we show, the choice of kinematic variables plays a key role in obtaining a differential distribution that is not only infrared-safe, but also free from the sizeable LFU violating terms of order $\mathcal{O}(\alpha)\ln(m_\ell)$. In particular, as far as the invariant mass of the two lepton system is concerned, the following two options can be considered: $q^2_\ell = (\ell_1+\ell_2)^2$ and $q^2_0 = (p_B - p_K)^2$. The first case (q^2_ℓ), which is the natural choice for experiments where the B momentum is not known (such as those performed at hadron colliders), corresponds to defining the invariant mass of the charged lepton system from the measured lepton momenta ($\ell_{1,2}$), i.e. after radiation has occurred. Whereas in the second case (q^2_0), the hadronic momenta ($p_{B,K}$) are used to define the momentum transfer to the lepton system before radiation. These two choices coincide in the non-radiative case, but are different in the presence of radiation. We show that it is only by using q^2_0, as the relevant kinematic variable, that the differential distribution is free from $\mathcal{O}(\alpha)\ln(m_\ell)$-terms. This does not imply that one cannot perform clean tests of LFU at hadron colliders, but rather that in such cases, the collinear singularities are unavoidable and should be properly corrected for.

The paper is organised as follows. In section 2 the computation of real and virtual amplitudes is presented, as well as the phase space measure including the physical cut-off on the photon energy. Treatment and cancellation of infrared divergences is discussed at length in section 3. Numerical results, in form of plots, showing the size of the radiative corrections, are presented in section 4. An outlook on open issues and future directions is presented in section 5. The paper is concluded in section 6. The appendices contain additional plots, comparison with older work, comments on R_K A, amplitudes B, the parametrisation of kinematic variables C, the soft integrals D and the explicit Passarino-Veltman functions E.

2 Computation

The two sets of variables we introduce to describe the differential distribution of the $\bar{B}(p_B) \to \bar{K}(p_K)\ell_1(\ell_1)\bar{\ell}_2(\ell_2) + \gamma(k)$ process, assuming that radiation is not detected, are

$$\{q^2_a, c_a\} = \begin{cases} q^2_\ell = (\ell_1+\ell_2)^2, \quad c_\ell = -\left(\frac{\vec{\ell}_1\cdot\vec{p}_K}{|\vec{\ell}_1||\vec{p}_K|}\right)_{q-\text{RF}} & [\text{“Hadron collider” variables}]\,, \\ q^2_0 = (p_B - p_K)^2\,,\ c_0 = -\left(\frac{\vec{\ell}_1\cdot\vec{p}_K}{|\vec{\ell}_1||\vec{p}_K|}\right)_{q_0-\text{RF}} & [\text{“B-factory” variables}]\,, \end{cases} \tag{2.1}$$

where $q-\text{RF}$ and $q_0-\text{RF}$ denotes the rest frames of

$$q \equiv \ell_1 + \ell_2\,, \quad q_0 \equiv p_B - p_K = q + k\,, \tag{2.2}$$

as illustrated in figure 1 (to conform to standard notations, throughout the paper $q_\ell \equiv q$). As indicated, the set $a = \ell$ is the natural choice for a hadron-collider experiment, while the set $a = 0$ can be implemented only in an experiment where the B momentum is known.

JHEP12(2020)104

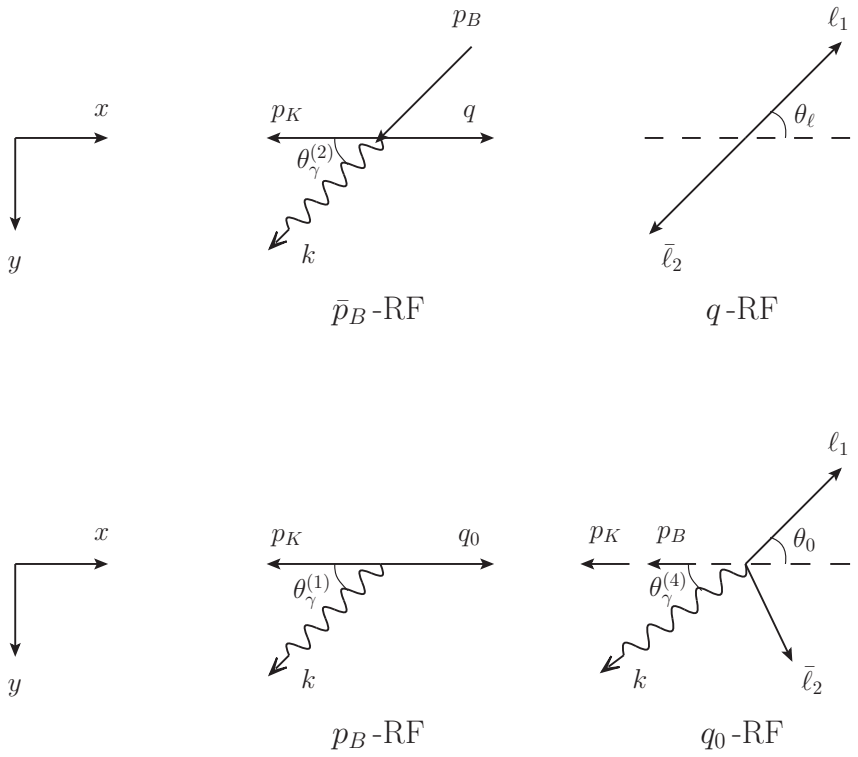

Figure 1. Decay kinematics for the different RFs of interest. The dashed line corresponds to what is deferred to as the decay axis. For brevity we drop the frame-label on the lepton angles, $\theta_\ell \equiv \theta_\ell^{(3)}$ and $\theta_0 \equiv \theta_0^{(4)}$, and if no frame-label is indicated on the photon angle, $\theta_\gamma = \theta_\gamma^{(2)}$ is usually understood.

However, as we shall discuss later on, both sets can be applied to describe appropriate integrated distributions in any kind of experiment.

A further variable that plays a key role in defining infrared-safe observables is

$$\bar{p}_B \equiv p_B - k = \ell_1 + \ell_2 + p_K \,, \tag{2.3}$$

which equals the sum of all visible final-state momenta. The kinematic invariant $\bar{p}_B^2$ is the reconstructed B-meson mass in the hadronic set-up, where p_B is not known, and the variable

$$\delta_{\rm ex} > 1 - \frac{\bar{p}_B^2}{m_B^2} \,, \tag{2.4}$$

provides the most natural choice for the physical cut-off regulating soft divergences. The complete decomposition of all momenta in the p_B, $\bar{p}_B$, q and q_0 RFs is presented in appendix C, and frames are denoted as (1), (2), (3) and (4), respectively.

Schematically, we decompose the double differential rate as

$$d^2\Gamma_{\bar{B}\to\bar{K}\ell_1\bar{\ell}_2}(\delta_{\rm ex}) = \frac{1}{m_B}\left(\rho_a(m_B^2)|\mathcal{A}_V|^2 + \int_{\delta_{\rm ex}} d\Phi_\gamma\, \rho_a(\bar{p}_B^2)\,|\mathcal{A}_R|^2\right) dq_a^2 dc_a \,, \tag{2.5}$$

where $\rho_a(m_B^2)$ and $\rho_a(\bar{p}_B^2)$ denote the 3-body and "effective-3-body" phase space factors, and $d\Phi_\gamma$ indicates the integration over the undetected photon variables over a phase space

JHEP12(2020)104

region specified by the physical cut-off $\delta_{\rm ex}$. In the following, we first introduce the effective Lagrangians used in our analysis, and then present the calculation of the real emission amplitude ($\mathcal{A}_R$) and the one-loop virtual corrections to the tree-level 3-body amplitude ($\mathcal{A}_V$), and finally discuss the corresponding phase space factors. Soft divergences and ultraviolet (UV) divergences are regulated in dimensional regularisation (DR).[1]

2.1 Mesonic effective Lagrangian

Generically, we consider non-radiative processes of the type $M_H \to M_L \ell_1 \bar{\ell}_2$, where $M_{H,L}$ are generic scalar mesons (of either parity). In what follows we take $M_H = \bar{B}$ and $M_L = \bar{K}$ and the mediation is described by the following effective partonic Lagrangian

$$\mathcal{L}_{\rm int}^{\rm parton} = g_{\rm eff} L_\mu V^\mu + \text{h.c.}\,, \quad L_\mu \equiv \bar{\ell}_1 \Gamma^\mu \ell_2\,, \quad V_\mu \equiv \bar{q}\gamma_\mu(1-\gamma_5)b\,, \quad g_{\rm eff} \equiv -\frac{G_F}{\sqrt{2}}\lambda_{\rm CKM}\,, \tag{2.6}$$

where $\Gamma^\mu \equiv \gamma^\mu(C_V + C_A\gamma_5)$. The quark field q, the values of C_V and C_A, and $\lambda_{\rm CKM}$ can be adapted to describe different processes. Processes mediated by the $b \to u(c)\ell\nu$ charged-current interaction correspond to $q = u(c)$, with $(C_V, C_A) = (1, -1)$ and $\lambda_{\rm CKM} = V_{ub}(V_{cb})$. Processes mediated by the flavour changing neutral transition $b \to (d, s)\mu^+\mu^-$ are obtained by setting $C_{V(A)} = \alpha C_{9(10)}/(4\pi)$ and $\lambda_{\rm CKM} = V^*_{t(d,s)}V_{tb}$.

The corresponding effective mesonic weak Lagrangian describing the $\bar{B} \to \bar{K}\ell_1\bar{\ell}_2$ process reads

$$\mathcal{L}_{\rm int}^{\rm EFT} = g_{\rm eff}\, L^\mu V_\mu^{\rm EFT} + \text{h.c.}\,, \quad V_\mu^{\rm EFT} = \sum_{n\geq 0} \frac{f_\pm^{(n)}(0)}{n!}(-D^2)^n[(D_\mu B^\dagger)K \mp B^\dagger(D_\mu K)]\,, \tag{2.7}$$

where $D_\mu = (\partial + ieQA)_\mu$ is the covariant derivative and $f_\pm^{(n)}(q^2)$ denotes the $n^{\rm th}$ derivative of the form factor $f_\pm(q^2)$. This Lagrangian maps the q^2-dependence of the non-radiative $B \to K$ form factor into a tower of derivative operators, such that the hadronic matrix element of V_μ is reproduced to LO in the electromagnetic coupling,

$$H_0^\mu(q_0^2) \equiv \langle \bar{K}|V_\mu|\bar{B}\rangle = f_+(q_0^2)(p_B+p_K)^\mu + f_-(q_0^2)(p_B-p_K)^\mu = \langle \bar{K}|V_\mu^{\rm EFT}|\bar{B}\rangle + \mathcal{O}(e), \tag{2.8}$$

where $\langle 0|B^\dagger|\bar{B}(p_B)\rangle = e^{-ip_B\cdot x}$ and $\langle \bar{K}(p)|K(x)|0\rangle = e^{ip\cdot x}$, and $f_0 = f_+ + \frac{q^2}{m_B^2 - m_K^2}f_-$ is the scalar part of the form factor. The radiative amplitude at $\mathcal{O}(e)$ is computed at the tree level by combining the gauge-invariant Lagrangian in (2.7) with the ordinary QED Lagrangian for fermions and mesons,

$$\mathcal{L}_{\rm QED} \equiv \mathcal{L}_\xi(A) + \sum_{\psi=\ell_1,\ell_2} \bar{\psi}(i\not{D} - m_\ell)\psi + \sum_{M=B,K} (D_\mu M)^\dagger D^\mu M - m_M^2 M^\dagger M\,, \tag{2.9}$$

where $\mathcal{L}_\xi(A)$ denotes the Maxwell Lagrangian with the covariant gauge-fixing term, resulting in the photon propagator given in section 2.3. Matters related to going beyond this approximation, at the form factor level, are discussed in sections 3.4 and 5.1.

[1] Often in QED calculations soft divergences are regulated via an explicit photon mass. For this reason, whenever possible, we will indicate how results change when using this regulator. However, we found that DR is more convenient in performing the soft integrals, this is why we adopt it as default approach.

JHEP12(2020)104

The non-radiative amplitude is decomposed as

$$\mathcal{A}_{\bar{B}\to\bar{K}\ell_1\bar{\ell}_2} \equiv \langle \bar{K}\ell_1\bar{\ell}_2|(-\mathcal{L}_{\rm int})|\bar{B}\rangle = \mathcal{A}^{(0)} + \mathcal{A}^{(2)} + \mathcal{O}(e^4)\,, \tag{2.10}$$

where the superscript indicates the order in the electromagnetic coupling and the phase follows the Particle Data Group (PDG) convention [7]. The lowest-order (LO) amplitude reads

$$\mathcal{A}^{(0)}_{\bar{B}\to\bar{K}\ell_1\bar{\ell}_2} = -g_{\rm eff}\, L_0\cdot H_0\,, \tag{2.11}$$

with

$$L_0^\mu \equiv \langle \ell_1\bar{\ell}_2|L^\mu|0\rangle = \bar{u}(\ell_1)\Gamma^\mu v(\ell_2)\,. \tag{2.12}$$

For flavour changing neutral currents (FCNCs), such as $\bar{B}\to\bar{K}\ell^+\ell^-$, there are additional contributions originating from four-quark operators, dipole and chromomagnetic penguin operators which are apparently not described by the mesonic Lagrangian in (2.7). Some of these effects, in particular the long-distance contribution associated to the charmonium resonances introduce sizeable distortions of the kinematical distribution in specific regions of q^2. However, in the case of a scalar meson final state, such effects can partially be absorbed for moderate $q^2 \ll m^2_{J/\Psi}$ into a reparametrisation of the $f_\pm$ form factors.[2] Approaches of this type can be found in the literature in the framework of e.g. QCD factorisation [8] and/or light-cone sum rules [9–11].

At this point we wish to comment on the QED corrections performed in $K\to\pi\ell^+\ell^-$ [12]. Formally the main difference is that we perform a form factor expansion (2.7) whereas they work with constant form factor which is a good approximation for Kaon physics. In terms of the kinematics they directly work with q_0^2-variable (denoted by s in [12]) since this variable is accessible in Kaon experiments. Moreover, the photon energy cut-off is implemented in the q_0-RF.

2.2 Real radiation

The five diagrams relevant to compute real emission amplitude at $\mathcal{O}(e)$ are shown in figure 2. The result can be expressed as follows[3]

$$\begin{aligned}\mathcal{A}^{(1)} = -e g_{\rm eff}\Bigg\{ & \bar{u}(\ell_1)\left[\hat{Q}_{\ell_1}\frac{2\epsilon^*\cdot\ell_1 + \not{\epsilon}^*\not{k}}{2k\cdot\ell_1}\Gamma\cdot H_0(q_0^2) + \hat{Q}_{\bar{\ell}_2}\,\Gamma\cdot H_0(q_0^2)\frac{2\epsilon^*\cdot\ell_2 + \not{k}\not{\epsilon}^*}{2k\cdot\ell_2}\right] v(\ell_2) \\ & + \hat{Q}_{\bar{B}}\, L_0\cdot\bar{H}_0^{(B)}(q^2)\frac{\epsilon^*\cdot(p_B+\bar{p}_B)}{2k\cdot p_B} + \hat{Q}_{\bar{K}}\, L_0\cdot\bar{H}_0^{(K)}(q^2)\frac{\epsilon^*\cdot(p_K+\bar{p}_K)}{2k\cdot p_K} \\ & + (\hat{Q}_{\bar{B}}-\hat{Q}_{\bar{K}})\, L_0\cdot\epsilon^*\, f_+(q^2) + (\hat{Q}_{\bar{B}}+\hat{Q}_{\bar{K}})\, L_0\cdot\epsilon^*\, f_-(q^2) \\ & + (\hat{Q}_{\bar{B}}+\hat{Q}_{\bar{K}}) L_0\cdot(p_B \pm p_K)(\epsilon^*\cdot(q+q_0))\sum_{n\geq 1}\frac{f_\pm^{(n)}(0)}{n!}P_{n-1}\Bigg\}\,,\end{aligned} \tag{2.13}$$

[2] Of course there are additional long-distance effect, such as the photon exchange between a charm-loop and the B-meson which cannot be captured in this way. We expect the simplified procedure outlined above to absorb the main effect at moderate q^2.

[3] Note that, in order to recover the photon mass regularisation, the following substitutions in the denominators are sufficient: $2k\cdot p \to 2k\cdot p \pm m_\gamma^2$ with plus sign for outgoing and minus sign for ingoing momenta.

JHEP12(2020)104

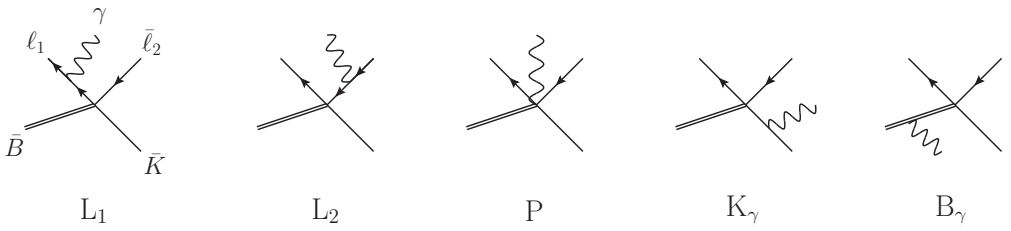

Figure 2. $\mathcal{O}(e)$-graphs with nomenclature referring to photon-emission and the P stands for point-like and can also be interpreted as a contact term.

$\bar{B} \to \bar{K}\ell_1\bar{\ell}_2$	$\hat{Q}_{\bar{B}}$	$\hat{Q}_{\bar{K}}$	$\hat{Q}_{\ell_1}$	$\hat{Q}_{\bar{\ell}_2}$
$\bar{B}^- \to \bar{K}^-\mu^-\mu^+$	$+1$	-1	-1	$+1$
$\bar{B}_s \to \bar{K}^-\nu\mu^+$	0	-1	0	$+1$

Table 1. Example of charge assignment for FCNC and semileptonic decay which obey (2.14). Note that generally $Q_P = -Q_{\bar{P}}$, rules for the hatted charges are given in the text and by convention $\bar{B}$ and $\bar{K}$ correspond to mesons with a $b\bar{q}$ and $s\bar{q}$ valence quarks.

where $P_n = \sum_{m=0}^{n}(q^2)^{(n-m)}(q_0^2)^m$ (with $P_0 = 1$), $\bar{H}_0^{(X)} = H_0|_{p_X \to \bar{p}_X}$ for $X = B, K$ and $\bar{p}_K \equiv p_K + k$.

The rules for the hatted charges are: $\hat{Q}^{\text{in}} = -Q^{\text{in}}$ and $\hat{Q}^{\text{out}} = Q^{\text{out}}$. Furthermore we use $Q_{\bar{\ell}_2} = -Q_{\ell_2}$ such that $Q_{\bar{\ell}_2} + Q_{\ell_1} = 0$ in the case where the lepton pair is charge neutral, cf. table 1 for an illustration. Charge conservation then implies

$$\sum_{i=\bar{B},\bar{K},\ell_1,\bar{\ell}_2} \hat{Q}_i = 0\,. \tag{2.14}$$

Hereafter the $\sum_i$ is defined by the left-hand side (l.h.s.) of the equation above. Keeping the leading terms in the $k \to 0$ limit, i.e. at $\mathcal{O}(1/E_\gamma)$, $\mathcal{A}^{(1)}$ assumes the Low or eikonal form,

$$\mathcal{A}^{(1)}_{\text{Low}} = e\mathcal{A}^{(0)} \sum_i \hat{Q}_i \frac{\epsilon^* \cdot p_i}{k \cdot p_i}\,, \tag{2.15}$$

which is manifestly gauge invariant as a result of eq. (2.14). The subleading terms of $\mathcal{O}(E_\gamma^0)$ are also universal and are proportional to the angular momentum operator (e.g. $\sigma_{\mu\nu}k^\mu\epsilon^{*\nu}$ terms in the first line of (2.13)).

It is instructive to discuss gauge invariance of the amplitude beyond the $k \to 0$ limitas it comes in rather disguised form. Here we summarise the essence and defer some detail to appendix B.3. A gauge transformation ($\epsilon \to k$) of the first line in (2.13), omitting common prefactors, leads to

$$\mathcal{A}^{(1)}_{\text{1st line}}\Big|_{\epsilon\to k} \propto (\hat{Q}_{\bar{\ell}_2} + \hat{Q}_{\ell_1}) L_0 \cdot H_0(q_0^2)\,, \tag{2.16}$$

whilst the second and third line combine to $(\hat{Q}_{\bar{B}} + \hat{Q}_{\bar{K}})L_0 H_0(q^2)$. This is would signify gauge invariance if $q^2 = q_0^2$ and that's where the contact term (P-graph) comes into play. The latter, fourth line, leads to $(\hat{Q}_{\bar{B}} + \hat{Q}_{\bar{K}})L_0[H_0(q_0^2) - H_0(q^2)]$, such that $\mathcal{A}^{(1)}|_{\epsilon\to k}$ is proportional to the sum of charges in (2.14), assuring gauge invariance of the whole amplitude.

JHEP12(2020)104

2.3 Virtual corrections

The diagrams for the virtual corrections are depicted in figure 3 and decompose into

$$\mathcal{A}^{(2)} = \mathcal{A}^{(2)}_{1PI} + \frac{1}{2}\frac{\alpha}{\pi}\left[(Q^2_{\ell_1}+Q^2_{\ell_2})\delta Z^{(1)}_2 + (Q^2_{\bar{B}}+Q^2_{K})\delta Z^{(1)}_S\right]\mathcal{A}^{(0)}\,, \tag{2.17}$$

where 1PI stands for one particle irreducible and δZ correspond to the self-energy corrections. The amplitudes for the 1PI graphs are given in appendix B.2. We have explicitly computed corrections up to the second derivative but in the actual plots we restrict ourselves to the first derivative as they already are numerically time-consuming.

For the Z-factors, decomposed as $Z_i = 1 + Q_i^2\frac{\alpha}{\pi}\delta Z_i^{(1)} + \mathcal{O}(\alpha^2)$, we find, adapting the on-shell scheme,

$$\begin{aligned}
\delta Z^{(1)}_S &= \frac{1}{4}\left((3-\xi)\left(\frac{1}{\hat{\epsilon}_{\rm UV}} - r_{\rm soft}\right) + (1-\xi)\right)\,,\\
\delta Z^{(1)}_2 &= \frac{1}{4}\left(-\xi\frac{1}{\hat{\epsilon}_{\rm UV}} - (3-\xi)r_{\rm soft} + 3\ln\left(\frac{m^2}{\mu^2}\right) - (3+\xi)\right)\,,
\end{aligned} \tag{2.18}$$

with

$$\frac{1}{\hat{\epsilon}} = \frac{1}{\epsilon} - \gamma_E + \ln 4\pi\,. \tag{2.19}$$

The gauge parameter ξ enters the photon propagator as in $\Delta_{\mu\nu}(k) = \frac{-1}{k^2-m_\gamma^2}\left(g_{\mu\nu} - (1-\xi)\frac{k_\mu k_\nu}{k^2}\right)$. The factor $r_{\rm soft}$ reads

$$r_{\rm soft} = \begin{cases} \ln\left(\frac{m_\gamma^2}{\mu^2}\right) & m_\gamma \neq 0\\ \frac{1}{\hat{\epsilon}_{\rm IR}} & m_\gamma = 0 \end{cases}\,, \tag{2.20}$$

in the case of a photon mass and DR respectively.

As far as $\mathcal{A}^{(2)}_{1PI}$ is concerned, soft singularities can be isolated as follows

$$\mathcal{A}^{(2)}_{1PI} = \frac{1}{2}\frac{\alpha}{\pi}\mathcal{A}^{(0)}\sum_{i\neq j}\hat{Q}_i\hat{Q}_j(\hat{p}_i\cdot\hat{p}_j)C_0(m_i^2,m_j^2,(\hat{p}_i+\hat{p}_j)^2,m_i^2,m_\gamma^2,m_j^2) + \text{non-soft}\,, \tag{2.21}$$

where the explicit expression of the C_0 function can be found in appendix E. Here $\hat{p}^{\rm in} = -p^{\rm in}$, $\hat{p}^{\rm out} = p^{\rm out}$ in analogy with the hatted charges (and $p_{\ell_{1,2}} \equiv \ell_{1,2}$). Note that (2.21) is consistent with the crossing rule of reversing momenta and charge when passing from in(out)- to out(in)-state. We explicitly checked that the gauge dependent part of the amplitude vanishes as a consequence of charge conservation:

$$\mathcal{A}^{(2)}|_\xi = \frac{\xi}{2}\frac{\alpha}{4\pi}\mathcal{A}^{(0)}\left(r_{\rm soft} - \frac{1}{\hat{\epsilon}_{\rm UV}} - 1\right)(\sum_i \hat{Q}_i)^2 = 0\,. \tag{2.22}$$

Let us turn to the UV divergences. There are no UV divergences in the neutral meson case since the leptonic currents do not renormalise (at our level of approximation). This does not change when the tower of operators $\mathcal{L}^{\rm EFT}_{\rm int}$ (2.7) is added as the derivatives acts on the mesons only. As previously mentioned, we restrict ourselves to the first form factor derivative approximation or to dimension-eight operators (the explicit form factors are given in section 4). In the case of charged mesons, there are UV divergences associated

JHEP12(2020)104

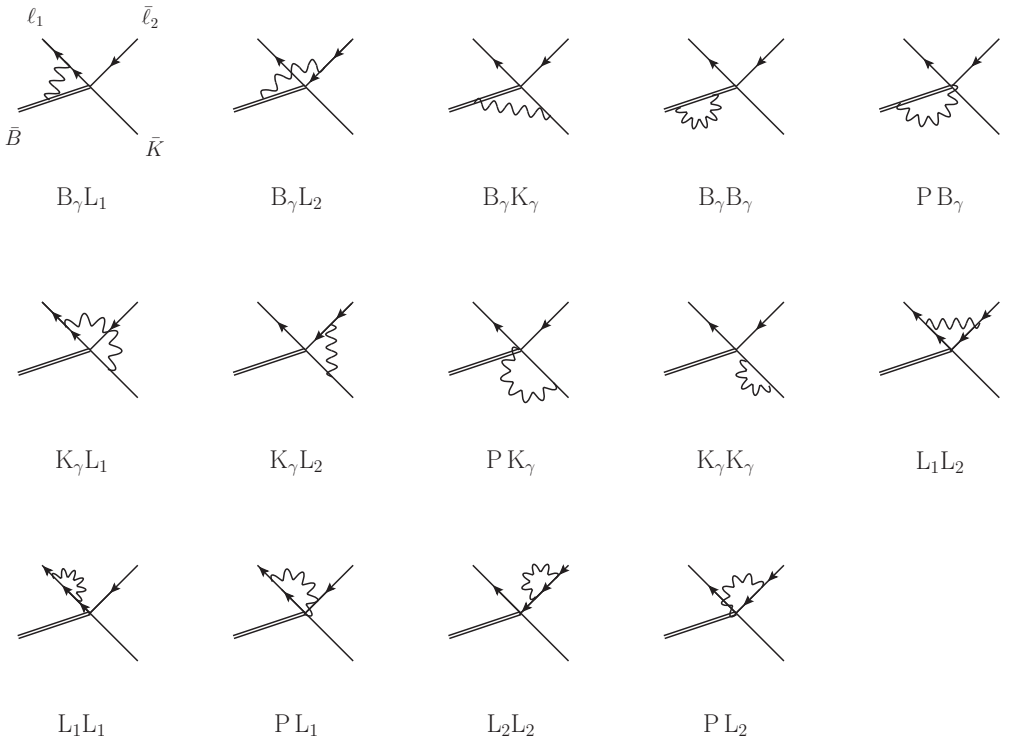

Figure 3. $\mathcal{O}(e^2)$-graphs with nomenclature adapted for tracking the cancellation of IR-divergences.

with operators of dimension six and eight in (2.7) and there is an additional one proportional to $p_B \cdot \ell_1 \, f_\pm^{(1)}(0)$ which can be interpreted as a t-channel operator.[4] Since $f_\pm$ are to be counted separately this means that there are six counterterms to be fixed at our level of approximation. The appropriate counterterms can be determined by matching to QCD which we hope to address in a forthcoming publication. In this work, we treat the divergences with minimal subtraction. We comment in section 4 on the numerical impact of the undetermined finite counterterms.

2.4 Phase space

Below we give the 3- and 4-particle phase space measures. For the photon phase space measure we need a regularised version in order to properly account for finite terms. Here, we find it more instructive to discuss explicitly results obtained using a non-vanishing photon mass. We refer the reader to appendix D.1 for the adaptation to DR.

2.4.1 Phase space for the radiative and non-radiative decay

The radiative rate $\bar{B} \to \bar{K} \ell_1 \bar{\ell}_2 \gamma$, without energy cut-off on the photon, is given by

$$d^2\Gamma_{\bar{B}\to\bar{K}\ell_1\bar{\ell}_2\gamma} = \frac{1}{m_B} \left(\int \rho_a \left[|\mathcal{A}^{(1)}|^2 + \mathcal{O}(e^4) \right] d\Phi_\gamma \right) dq_a^2 dc_a \,, \tag{2.23}$$

[4] The set of operators (2.7) does not close under renormalisation and needs to be completed by the t-channel operator at dimension eight.

JHEP12(2020)104

where

$$\rho_\ell = \frac{1}{2^6(2\pi)^3}\frac{\lambda^{1/2}(\bar{p}_B^2, q^2, m_K^2)}{\bar{p}_B^2 q^2}\lambda^{1/2}(q^2, m_{\ell_1}^2, m_{\ell_2}^2)\,,$$
$$\rho_0 = \frac{1}{2^6(2\pi)^3}\frac{\lambda^{1/2}(m_B^2, q_0^2, m_K^2)}{m_B^2 q_0^2}\frac{1}{\omega^2}\lambda(q_0^2, m_{\ell_1}^2, (k+\ell_2)^2)\,, \tag{2.24}$$

with λ the Källén function (C.3), and ω^2 is given in (C.14). Thus, $\frac{\rho_0}{\rho_\ell} = \det\frac{\partial(q^2, c_\ell)}{\partial(q_0^2, c_0)}$ is the Jacobian which can be computed from the defining equation (2.1) and the kinematic parameterisations given in the appendix. Moreover, the Lorentz-invariant photon phase space integral reads

$$\begin{aligned}\int_{m_\gamma}^{E_\gamma^{\max}} d\Phi_\gamma &\equiv \frac{1}{(2\pi)^3}\int_{m_\gamma}^{E_\gamma^{\max}}\frac{d^3k}{2E_\gamma} \\ &= \frac{1}{2(2\pi)^3}\int_{m_\gamma}^{(E_\gamma^{(i)})^{\max}} dE_\gamma^{(i)}|\vec{k}^{\,(i)}|\int d\Omega_\gamma^{(i)}\Theta\big[f^{(i)}(E_\gamma^{(i)}, \theta_\gamma^{(i)}, \phi_\gamma^{(i)})\big]\,,\end{aligned} \tag{2.25}$$

with

$$(E_\gamma^{(1)})^{\max} = \frac{m_B^2 + m_\gamma^2 - (q+m_K)^2}{2m_B}\,, \quad (E_\gamma^{(4)})^{\max} = \frac{q_0^2 + m_\gamma^2 - (m_{\ell_1}+m_{\ell_2})^2}{2q_0}\,, \tag{2.26}$$

where the former and the latter correspond to the $\{q^2, \theta_\ell\}_{a=\ell}$ and $\{q_0^2, \theta_0\}_{a=0}$ variables respectively, and $q_a \equiv \sqrt{q_a^2}$ is understood in this context. The restriction on the angles is

$$\Theta\big[f^{(i)}(E_\gamma^{(i)}, \theta_\gamma^{(i)}, \phi_\gamma^{(i)})\big] = \begin{cases} 1 & i=1 \\ \Theta[D(E_\gamma^{(4)}, \theta_\gamma^{(4)}, \phi_\gamma^{(4)}, q_0^2, c_0)] & i=4 \end{cases}\,, \tag{2.27}$$

with the function D defined in (C.13). The reason why the restriction in the (4)-RF, appropriate for the $\{q_0^2, c_0\}$-variables, is non-trivial is that for certain given values of $\{q_0^2, c_0\}$, the true maximum photon energy is a function of the photon angles and is in general below $(E_\gamma^{(4)})^{\max}$. We find it most convenient to implement the kinematic restrictions via the step-function $\Theta(x)$.[5]

In the $\{q^2, \theta_\ell\}_{a=\ell}$ case, one can conveniently work with the Lorentz invariant variable $\bar{p}_B^2$, related to $E_\gamma^{(1)}$ as $2m_B E_\gamma^{(1)} = m_B^2 + m_\gamma^2 - \bar{p}_B^2$. Moreover, since the passage from $E_\gamma^{(1)}$ to $E_\gamma^{(2)}$ is independent of the photon angles the replacement $d\Omega_\gamma^{(1)} \to d\Omega_\gamma^{(2)}$ is allowed. The photon phase space then assumes the form

$$\int_{m_\gamma}^{E_\gamma^{\max}} d\Phi_\gamma \to \frac{1}{2^3(2\pi)^3}\int_{(q+m_K)^2}^{(m_B-m_\gamma)^2} d\bar{p}_B^2\frac{\lambda^{1/2}(m_B^2, \bar{p}_B^2, m_\gamma^2)}{m_B^2}\int d\Omega_\gamma^{(1,2)}\,. \tag{2.28}$$

The non-radiative $\bar{B} \to \bar{K}\ell_1\bar{\ell}_2$ rate is given by

$$d^2\Gamma_{\bar{B}\to\bar{K}\ell_1\bar{\ell}_2} = \frac{\rho_\ell|_{\bar{p}_B^2 \to m_B^2}}{m_B}\Big\{|\mathcal{A}^{(0)}|^2 + 2\mathrm{Re}[\mathcal{A}^{(0)}(\mathcal{A}^{(2)})^*] + \mathcal{O}(e^4)\Big\}\,dq^2 dc_\ell\,. \tag{2.29}$$

Since there is no photon-emission, in this case there is no difference between the $\{q^2, c_\ell\}$- and $\{q_0^2, c_0\}$-variables.

[5] In the limit of $m_{\ell_1,\ell_2} \to 0$, the step-function $\Theta(x)$ becomes redundant, since the function D is then positive for all kinematic configurations, as can be seen from (C.13).

JHEP12(2020)104

2.4.2 Introduction of a physical photon energy cut-off

As anticipated, to match experimental observations, we introduce a cut-off on the maximal value of $\bar{p}_B^2$ via the parameter $\delta_{\rm ex}$, defined in (2.4), satisfying

$$0 < \delta_{\rm ex} < \delta_{\rm ex}^{\rm inc} = 1 - \left(\frac{q + m_K}{m_B}\right)^2 . \tag{2.30}$$

The value $\delta_{\rm ex}^{\rm inc}$ corresponds to the minimal value of $\bar{p}_B^2$ in a fully photon-inclusive decay. This definition translates to the following photon-energy cut-off[6]

$$E_\gamma^{\max(1)} = \delta_{\rm ex} \frac{m_B}{2} , \tag{2.31}$$

A typical choice for $\delta_{\rm ex}$ in realistic experiments is $\delta_{\rm ex} = \mathcal{O}(0.1)$. With the inclusion of $\delta_{\rm ex}$, the integral (2.25) assumes the form

$$\int_{\delta_{\rm ex}} d\Phi_\gamma = \frac{1}{2^3(2\pi)^3} \int_{m_B^2(1-\delta_{\rm ex})}^{(m_B - m_\gamma)^2} d\bar{p}_B^2 \frac{\lambda^{1/2}(m_B^2, \bar{p}_B^2, m_\gamma^2)}{m_B^2} \int d\Omega_\gamma^{(2)} . \tag{2.32}$$

3 Cancellation of infrared divergences

In order to track the divergences it is convenient to split the differential rate as follows

$$\begin{aligned} d^2\Gamma_{\bar{B}\to\bar{K}\ell_1\bar{\ell}_2}(\delta_{\rm ex}) &= d^2\Gamma^{\rm LO} + \frac{\alpha}{\pi} \sum_{i,j} \hat{Q}_i \hat{Q}_j \left(\mathcal{H}_{ij} + \mathcal{F}_{ij}^{(a)}(\delta_{\rm ex})\right) dq_a^2 dc_a + \mathcal{O}(e^4) , \\ &= d^2\Gamma^{\rm LO} \left[1 + \Delta^{(a)}(q_a^2, c_a; \delta_{\rm ex})\right] dq_a^2 dc_a + \mathcal{O}(e^4) , \end{aligned} \tag{3.1}$$

where $d^2\Gamma^{\rm LO}$ corresponds to the zeroth order term in (2.29), the sums on the charges is understood as in (2.14), and $\mathcal{H}$ and $\mathcal{F}$ stand for the virtual and real contributions respectively. More precisely, $\mathcal{H}_{ij}$ and $\mathcal{F}_{ij}$ are related to the amplitudes as follows

$$\begin{aligned} \frac{\alpha}{\pi} \sum_{i,j} \hat{Q}_i \hat{Q}_j \mathcal{H}_{ij} &= \frac{1}{m_B} \rho_\ell|_{\bar{p}_B^2 \to m_B^2} 2{\rm Re}[\mathcal{A}^{(2)*}\mathcal{A}^{(0)}] , \\ \frac{\alpha}{\pi} \sum_{i,j} \hat{Q}_i \hat{Q}_j \mathcal{F}_{ij}^{(a)} &= \frac{1}{m_B} \int d\Phi_\gamma \, \rho_a \, |\mathcal{A}^{(1)}|^2 , \end{aligned} \tag{3.2}$$

where $d\Phi_\gamma$ and ρ_a are defined in (2.24) and (2.25) respectively.

In standard fashion, the integrals are split into divergent parts which can be done analytically and a necessarily regular part which is dealt with numerically. We parameterise this decomposition as follows

$$\begin{aligned} \mathcal{H}_{ij} &= \frac{d^2\Gamma^{\rm LO}}{dq^2 dc_\ell} \left(\tilde{\mathcal{H}}_{ij}^{(s)} + \tilde{\mathcal{H}}_{ij}^{(hc)}\right) + \Delta\mathcal{H}_{ij} , \\ \mathcal{F}_{ij}^{(a)}(\delta_{\rm ex}) &= \frac{d^2\Gamma^{\rm LO}}{dq^2 dc_\ell} \tilde{\mathcal{F}}_{ij}^{(s)}(\omega_s) + \tilde{\mathcal{F}}_{ij}^{(hc)(a)}(\underline{\delta}) + \Delta\mathcal{F}_{ij}^{(a)}(\underline{\delta}) , \end{aligned} \tag{3.3}$$

[6] When evaluating the photon phase space variable in the (4)-RF, appropriate for the $\{dq_0^2, dc_0\}$-variables, the cut-off can be converted by using $E_\gamma^{(1)} = \gamma_{q_0} E_\gamma^{(4)}(1 - \beta_{q_0} \cos\theta_\gamma^{(4)})$ cf. (C.11) for the Lorentz boost factors.

JHEP12(2020)104

with $\tilde{\mathcal{H}}_{ij}^{(s)}$ ($\tilde{\mathcal{H}}_{ij}^{(hc)}$) and $\tilde{\mathcal{F}}_{ij}^{(s)}$ ($\tilde{\mathcal{F}}_{ij}^{(hc)(a)}$), to be defined further below, containing all soft (hard-collinear) singularities, whereas $\Delta\mathcal{H}$ and $\Delta\mathcal{F}$ are regular (even in the limit $m_{\ell_{1,2}} \to 0$). In order to split the real emission part, besides the previously introduced physical cut-off $\delta_{\rm ex}$, we adopt the phase space slicing method [13], which requires the introduction of two auxiliary (unphysical) cut-offs $\omega_{s,c}$,

$$\underline{\delta} \equiv \{\delta_{\rm ex}, \omega_s, \omega_c\}\,, \quad \omega_s \ll 1\,, \quad \frac{\omega_c}{\omega_s} \ll 1\,. \tag{3.4}$$

We remind the reader that $\delta_{\rm ex}$ has been introduced for meaningful comparison with experimental data and mention for clarity that $\tilde{\mathcal{F}}_{ij}^{(hc)(a)}$ is singular in the $m_{\ell_{1,2}} \to 0$ limit but finite for $m_{\ell_{1,2}} \neq 0$.

As already implicit in the decomposition (3.3), soft divergences cancel at the differential level independently from the choice of variables. This is not the case for hard-collinear singularities, given that the hard-collinear integral ($\tilde{\mathcal{F}}_{ij}^{(hc)(a)}$) is not proportional to the non-radiative kinematics. Without the physical cut-off $\delta_{\rm ex}$, the cancellation of both types of divergences proceeds as in standard in textbooks discussions (see e.g. [14–16]). However, the choice of a photon energy cut-off, associated with a preferred frame, makes it significantly more involved compared to the semileptonic case [17]. A detailed discussion of the soft singularities and collinear logs follows below, along with the definitions of the $\tilde{\mathcal{F}}$ and $\tilde{\mathcal{H}}$. Particular emphasis is given to single out which observables are IR-safe and not.

3.1 Cancellation of soft divergences at differential level

The soft singularities in the virtual corrections are encoded in the triangle functions C_0 in (2.21) and the self energy contributions in (2.18). Combining them, we define

$$\begin{aligned}\tilde{\mathcal{H}}_{ij}^{(s)} &\stackrel{\rm def}{=} (1-\delta_{ij})(\hat{p}_i\cdot\hat{p}_j)\mathrm{Re}[C_0(m_i^2, m_j^2, (\hat{p}_i+\hat{p}_j)^2, m_i^2, m_\gamma^2, m_j^2)] + \delta_{ij}\times\delta Z_i^{(1)} \\ &= -r_{\rm soft}\left\{(1-\delta_{ij})\frac{\hat{p}_i\cdot\hat{p}_j}{m_i m_j}\frac{x_{ij}}{(1-x_{ij}^2)}\ln|x_{ij}| + \delta_{ij}\frac{1}{2}\right\} + \mathcal{O}(f_{\mathcal{R}})\,,\end{aligned} \tag{3.5}$$

where $f_{\mathcal{R}}$ stands for IR finite terms, including regularisation-dependent ones. The x_{ij}-variables are given by

$$x_{ij} \equiv \frac{\sqrt{y_{ij}}-1}{\sqrt{y_{ij}}+1}\,, \quad y_{ij} \equiv \frac{(\hat{p}_i+\hat{p}_j)^2-(m_i+m_j)^2+i0}{(\hat{p}_i+\hat{p}_j)^2-(m_i-m_j)^2+i0}\,. \tag{3.6}$$

Considering the soft part of the real emission amplitude, namely the Low part of the amplitude in (2.15), we define

$$\begin{aligned}\tilde{\mathcal{F}}_{ij}^{(s)}(\omega_s) &\stackrel{\rm def}{=} (2\pi)^2\int_{\omega_s}\frac{-p_i\cdot p_j}{(k\cdot p_i)(k\cdot p_j)}d\Phi_\gamma = (2\pi)^2\int_{\omega_s}\frac{-\hat{p}_i\cdot\hat{p}_j}{(k\cdot\hat{p}_i)(k\cdot\hat{p}_j)}d\Phi_\gamma \\ &= -K_{\mathcal{R}}(\omega_s)I_{ij}^{(0)} + \mathcal{O}(f_{\mathcal{R}}) \\ &= [r_{\rm soft} - 2\ln(\omega_s)]\left\{(1-\delta_{ij})\frac{\hat{p}_i\cdot\hat{p}_j}{m_i m_j}\frac{x_{ij}}{(1-x_{ij}^2)}\ln|x_{ij}| + \delta_{ij}\frac{1}{2}\right\} + \mathcal{O}(f_{\mathcal{R}})\,,\end{aligned} \tag{3.7}$$

where the $\mathcal{O}(f_{\mathcal{R}})$ terms can be found in appendix D.2. As can be checked, the sum $\tilde{\mathcal{H}}_{ij}^{(s)} + \tilde{\mathcal{F}}_{ij}^{(s)}(\omega_s)$ is free from soft divergences and this ensures their cancellation at the

JHEP12(2020)104

differential level.[7] This includes $\ln^2 m_{\ell_{1,2}}$-terms which cancel when the real and virtual terms are summed up: these are genuine soft-collinear terms, which cancels as a result of the cancellation of the soft divergences.[8] We note that as a result of these cancellations scheme dependent terms due to IR regularisation disappear as well.

The crucial step in evaluating (3.7) is that, neglecting finite terms, the integral over the photon energy and the photon angles factorises: the angular integral $I_{ij}^{(0)}$ alone becomes separately Lorentz invariant (i.e. frame independent) and can be performed in the RF of the radiating pair, where it is particularly simple (see appendix D for more details). The energy and angular integral evaluate to

$$K_{\mathcal{R}}(\omega_s) = -\frac{1}{2} r_{\text{soft}} + \ln\left(\frac{m_B}{\mu}\right) + \ln(\omega_s) + \mathcal{O}(\omega_s)\,, \tag{3.8}$$

and

$$I_{ij}^{(0)} = \begin{cases} 1 & i = j\,, \\ 2\frac{\hat{p}_i\cdot\hat{p}_j}{m_i m_j}\frac{x_{ij}}{1-x_{ij}^2}\ln|x_{ij}| & i \neq j\,. \end{cases} \tag{3.9}$$

We wish to emphasise that there are single collinear logs, $\ln m_{\ell_{1,2}}$, in $\tilde{\mathcal{H}}_{ij}^{(s)} + \tilde{\mathcal{F}}_{ij}^{(s)}(\omega_s)$ which match up with corresponding terms in $\tilde{\mathcal{H}}_{ij}^{(hc)} + \tilde{\mathcal{F}}_{ij}^{(hc)}(\underline{\delta})$. The procedure is therefore well set-up for tracking analytically after what phase space integration IR sensitive terms cancel against each other.

However, since there remain $\ln\omega_s$-terms in the analytic expression one might wonder whether this leads to a numerically stable integral. We have found that the phase space integral is stable when using a Monte Carlo integration on the photon variables. Alternatively, one might use the dipole subtraction method [18] as applied to QED [19–21].

3.2 Hard-collinear virtual contribution $\tilde{\mathcal{H}}^{(hc)}$

The hard-collinear virtual contribution, after summing over charges, is given by

$$\begin{aligned}\tilde{\mathcal{H}}^{(hc)} &\overset{\text{def}}{=} \sum_{i,j}\hat{Q}_i\hat{Q}_j\tilde{\mathcal{H}}_{ij}^{(hc)} = 2\hat{Q}_{\ell_1}\left(\hat{Q}_{\bar{\ell}_2}+\hat{Q}_{\bar{B}}+\hat{Q}_{\bar{K}}\right)\ln\left(\frac{m_{\ell_1}}{\mu}\right) + \{1\leftrightarrow 2\} \\ &= -2\hat{Q}_{\ell_1}^2\ln\left(\frac{m_{\ell_1}}{\mu}\right) + \{1\leftrightarrow 2\},\end{aligned} \tag{3.10}$$

where $\left(\frac{\mu^2}{4\pi^2}\right)^{\epsilon_{\text{UV}}} B_0(m^2,0,m^2) = \frac{1}{\bar{\epsilon}_{\text{UV}}} - 2\ln(m/\mu) + 2 + \mathcal{O}(\epsilon)$ was used and charge conservation was used in going from the first to the second line.

[7] Note that $x_{ij} < 0$ as the momenta p_i are assumed to be timelike with positive energy. Moreover, the individual $\mathcal{F}_{ij}$ are gauge dependent (the result is presented for $\xi = 1$), whereas in the sum over all charges gauge dependence disappears.

[8] In order to track the $\ln(m_\ell)$ terms, note that $x_{ij} \to -m_i m_j/(\hat{p}_i+\hat{p}_j)^2$ for $(\hat{p}_i+\hat{p}_j)^2 \gg m_{i,j}^2$. Moreover it is worth pointing out that one can write, $I_{ij}^{(0)} = \frac{1}{2\beta_{ij}}\ln\left(\frac{1+\beta_{ij}}{1-\beta_{ij}}\right)$, in terms of physically transparent variables with $\beta_{ij} = \frac{\beta_i+\beta_j}{1+\beta_i\beta_j}$ is the relativistic addition of the velocities of the two particles $\beta_i \equiv |\vec{p}_i|/E_i$ in the ij-RF.

JHEP12(2020)104

3.3 The hard-collinear integral $\tilde{\mathcal{F}}^{(hc,a)}$

We evaluate the hard-collinear integral using the phase space slicing method [13] following the specific recipe in ref. [22]. The integral is given by

$$\begin{aligned}\frac{\alpha}{\pi}\tilde{\mathcal{F}}^{(hc,a)}(\underline{\delta}) &= \frac{\alpha}{\pi}\sum_{i,j}\hat{Q}_i\hat{Q}_j\tilde{\mathcal{F}}_{ij}^{(hc,a)}(\underline{\delta}) \\ &= \frac{1}{m_B}\int_{\omega_s}^{\delta_{\rm ex}}\rho_a^{\ell_1||\gamma}(\omega_c)\,|\mathcal{A}^{(1)}_{\ell_1||\gamma}|^2 d\Phi_\gamma + \{1\leftrightarrow 2\}\,,\end{aligned} \tag{3.11}$$

where $|\mathcal{A}^{(1)}_{\ell_1||\gamma}|^2$ is the part of $|\mathcal{A}^{(1)}|^2$ proportional to $1/(k\cdot\ell_1)$ when $m_{\ell_1}\to 0$ which includes contributions beyond the Low term. Note that the photon-energy integral runs from ω_s till $\delta_{\rm ex}$, consistent with (3.3) where the soft modes are absorbed into $\tilde{\mathcal{F}}_{ij}^{(s)}(\omega_s)$. The phase space factor $\rho_a^{\ell_1||\gamma}(\omega_c)$ is defined as

$$\rho_a^{\ell_1||\gamma}(\omega_c) = \rho_a\Theta(\omega_c m_B^2 - k\cdot\ell_1)\,, \tag{3.12}$$

where ρ_a is defined in (2.24), the meaning of the integration boundaries can be inferred from (2.32), and the step-function encodes the phase space slicing. The quantity $\omega_c \ll 1$ then implies that k and ℓ_1 are nearly collinear.

3.3.1 Phase space slicing of the hard-collinear integral

In the phase space slicing method, the photon and the light particle it is emitted from, are effectively treated as a single particle. This follows up on the intuitive picture that a particle and its collinear photon are hard to disentangle. Below, we give the explicit expressions for $\ell_1||\gamma$, and the $\ell_2||\gamma$ case is obtained in a completely analogous fashion. Formally, one decomposes the phase space as follows

$$d\Phi_{\bar{B}\to\bar{K}\ell_1\bar{\ell}_2\gamma} = d\Phi_{\bar{B}\to\bar{K}\ell_{1\gamma}\bar{\ell}_2}d\Phi_\gamma\frac{E_{\ell_{1\gamma}}}{E_{\ell_1}}\,. \tag{3.13}$$

The collinear region is parameterised by $\ell_1 = z\ell_{1\gamma}$, where $\ell_{1\gamma}\equiv\ell_1+k$, assuming that the transverse part can be neglected in order to extract the collinear logs. The two parts in (3.13) then assume the form

$$\begin{aligned} d\Phi_\gamma\frac{E_{\ell_{1\gamma}}}{E_{\ell_1}} &\to \frac{1}{16\pi^2}dz\,d\ell_{1\gamma}^2\,, \\ d\Phi_{\bar{B}\to\bar{K}\ell_{1\gamma}\bar{\ell}_2} &\to \frac{1}{2^5(2\pi)^3}\frac{\lambda^{1/2}(m_B^2,q_0^2,m_K^2)}{m_B^2}dq_0^2dc_0\,. \end{aligned} \tag{3.14}$$

In those variables, the amplitude squared assumes the form (in the $\xi=1$ gauge)

$$\begin{aligned}|\mathcal{A}^{(1)}_{\ell_1||\gamma}|^2 &= \frac{e^2}{(k\cdot\ell_1)}\hat{Q}_{\ell_1}\left[\hat{Q}_{\ell_1}(1-z) - \frac{2z}{1-z}\left(\hat{Q}_{\bar{\ell}_2}+\hat{Q}_{\bar{B}}+\hat{Q}_{\bar{K}}\right) - \hat{Q}_{\ell_1}\frac{m_{\ell_1}^2}{k\cdot\ell_1}\right]|\mathcal{A}^{(0)}_{\ell_1\|\gamma}|^2 + \mathcal{O}(m_{\ell_1}^2) \\ &= \frac{e^2}{(k\cdot\ell_1)}\hat{Q}_{\ell_1}^2\left(\tilde{P}_{f\to f\gamma}(z) - \frac{m_{\ell_1}^2}{k\cdot\ell_1}\right)|\mathcal{A}^{(0)}_{\ell_1\|\gamma}(q_0^2,c_0)|^2\Big|_{\bar{B}\to\bar{K}\ell_{1\gamma}\bar{\ell}_2} + \mathcal{O}(m_{\ell_1}^2)\,,\end{aligned} \tag{3.15}$$

JHEP12(2020)104

where $|\mathcal{A}^{(0)}_{\ell_1\|\gamma}|^2 = |\mathcal{A}^{(0)}_{\bar{B}\to\bar{K}\ell_{1\gamma}\bar{\ell}_2}|^2$ and $\tilde{P}_{f\to f\gamma}(z)$ is the collinear emission part of the splitting function for a fermion to a photon[9]

$$\tilde{P}_{f\to f\gamma}(z) \equiv \left(\frac{1+z^2}{1-z}\right) , \tag{3.16}$$

and the $m^2_{\ell_1}/(k\ell_1)$ term is immaterial for the hard-collinear logs per se but of importance for the numerics as it captures $\ln\omega_s$ terms. The LO order matrix element squared in (3.15), is given in appendix B.1. The first line in (3.15) is gauge dependent whereas the second is not since charge conservation has been applied. This is further manifested by the appearance of the splitting function which is a universal object.

3.3.2 $\tilde{\mathcal{F}}^{(hc,0)}$, structure of collinear singularities in $dq_0^2 dc_0$

Taking (3.11) and using the integration measure $d\Phi_\gamma$ in (3.14) one arrives at

$$\begin{aligned}\tilde{\mathcal{F}}^{(hc,0)}(\underline{\delta}) = \frac{1}{2^{10}\pi^3 m_B^3}\Bigg(&\hat{Q}^2_{\ell_1}\int_{\max(z(\delta_{\rm ex}),0)}^{\max(z(\omega_s),0)} \tilde{f}^{(hc)}(c_0, m_{\ell_1}, \omega_c)dz \\ &+ \hat{Q}^2_{\ell_2}\int_{\max(z'(\delta_{\rm ex}),0)}^{\max(z'(\omega_s),0)} \tilde{f}^{(hc)}(-c_0, m_{\ell_2}, \omega_c)dz\Bigg) ,\end{aligned} \tag{3.17}$$

where the boundaries on z are determined by the phase space slicing cut-off ω_s and the real photon energy cut off $\delta_{\rm ex}$ (2.4),

$$z(\delta) = z(\delta, q_0^2, c_0) = 1 - \frac{\delta}{1-\hat{s}_{K\ell_2}(q_0^2, c_0)} , \tag{3.18}$$

with $\hat{s}_{K\ell_2} \equiv (\hat{p}_K + \hat{\ell}_2)^2 = \frac{1}{2}\left(1 - \hat{q}_0^2 + \hat{m}_K^2 - c_0\,\lambda^{1/2}\left(1, \hat{q}_0^2, \hat{m}_K^2\right)\right)$ and $z' = z|_{c_0\to -c_0}$.[10] The integrand in (3.17) reads

$$\tilde{f}^{(hc)}(c_0, m_\ell, \omega_c) = \lambda^{1/2}(m_B^2, q_0^2, m_K^2)|\mathcal{A}^{(0)}_{m_\ell\to 0}(q_0^2, c_0)|^2\left(\tilde{P}_{q\to q\gamma}(z)\, j^{hc} - j^{hc}_{(m_{\ell_1})}\right) , \tag{3.19}$$

with the LO amplitude squared given in appendix B.1 (in terms of q^2, c_ℓ though) and the j^{hc}'s are functions of z, m_{ℓ_1} and the collinear scale ω_c,

$$\begin{aligned} j^{hc}(z, \omega_c, m_{\ell_1}) &= \int_{\frac{1-z}{2z}m^2_{\ell_1}}^{\omega_c m_B^2} \frac{d(k\cdot\ell_1)}{k\cdot\ell_1} = \ln\frac{2\omega_c z}{\hat{m}^2_{\ell_1}(1-z)} , \\ j^{hc}_{(m_{\ell_1})}(z, \omega_c, m_{\ell_1}) &= \int_{\frac{1-z}{2z}m^2_{\ell_1}}^{\omega_c m_B^2} \frac{m^2_{\ell_1}\, d(k\cdot\ell_1)}{(k\cdot\ell_1)^2} = \frac{2z}{1-z} - \frac{\hat{m}^2_{\ell_1}}{\omega_c} , \end{aligned} \tag{3.20}$$

and the integration boundaries on $d\ell^2_{1\gamma}$ correspond to (3.12). Here and below, hatted quantities are normalised w.r.t. the m_B mass, i.e. $\hat{m}_K = m_K/m_B$.

[9] No prescription is required when $z \to 1$, in our case, as this soft region has been treated in another section and is cut off by ω_s. Cf. appendix A.1.1 for a discussion involving the full splitting function.

[10] Note that in the (4)-frame, the collinear limit forces the pair of particles (either $\ell_{1\gamma}$ and ℓ_2, or $\ell_{2\gamma}$ and ℓ_1) to move in opposite directions. Since c_0 is defined w.r.t. ℓ_1, this explains the $c_0 \to -c_0$ procedure to obtain the corresponding formulae for $\ell_2||\gamma$.

JHEP12(2020)104

In the case of the $\{q_0^2, c_0\}$-variables, as adapted in this section, (3.17) can be simplified considerably

$$\tilde{\mathcal{F}}^{(hc,0)}(\underline{\delta}) = \frac{\lambda^{1/2}(m_B^2, q_0^2, m_K^2)}{2^{10}\pi^3 m_B^3} \left(|\mathcal{A}^{(0)}(q_0^2, c_0)|^2 \, \hat{Q}_{\ell_1}^2 \, J^{(hc,0)}(\underline{\delta}) + \{1, c_0 \leftrightarrow 2, -c_0\} \right) , \quad (3.21)$$

and the remaining hard-collinear integral $J^{(hc,0)}$ is easily evaluated[11]

$$\begin{aligned} J^{(hc,0)}(\underline{\delta}) &= \int_{z(\delta_{\rm ex})}^{z(\omega_s)} dz \left(\tilde{P}_{q\to q\gamma}(z) \, j^{hc} - j^{hc}_{(m_{\ell_1})} \right) \\ &= A(\delta_{\rm ex}, \omega_s) \ln \frac{m_{\ell_1}^2}{2\omega_c m_B^2} + B(\delta_{\rm ex}, \omega_s, m_{\ell_1}) , \end{aligned} \quad (3.22)$$

where

$$\begin{aligned} A(\delta_{\rm ex}, \omega_s) &= \frac{1}{2}(z(\omega_s) - z(\delta_{\rm ex}))(2 + z(\omega_s) + z(\delta_{\rm ex})) + 2\ln\frac{\bar{z}(\omega_s)}{\bar{z}(\delta_{\rm ex})} \\ &\overset{z(\omega_s)\to 1}{\to} \frac{1}{2}\bar{z}(\delta_{\rm ex})(3 + z(\delta_{\rm ex})) + 2\ln\frac{\bar{z}(\omega_s)}{\bar{z}(\delta_{\rm ex})} \overset{z(\delta_{\rm ex})\to 0}{\to} \frac{3}{2} + 2\ln\bar{z}(\omega_s) , \\ B(\delta_{\rm ex}, \omega_s, m_\ell) &= \frac{1}{2}\Big[\Big(z(\delta_{\rm ex})^2 + 2z(\delta_{\rm ex})\Big) \ln\frac{z(\delta_{\rm ex})}{\bar{z}(\delta_{\rm ex})} - \ln\bar{z}(\delta_{\rm ex}) - 4\,{\rm Li}_2\,\bar{z}(\delta_{\rm ex}) \\ &\quad - 2\ln^2\bar{z}(\delta_{\rm ex}) - \left(3 + 2\frac{\hat{m}_\ell^2}{\omega_c}\right) z(\delta_{\rm ex}) - \{\delta_{\rm ex} \leftrightarrow \omega_s\}\Big] \quad (3.23) \\ &\overset{z(\omega_s)\to 1}{\to} \frac{1}{2}\Big[\Big(z(\delta_{\rm ex})^2 + 2z(\delta_{\rm ex})\Big) \ln\frac{z(\delta_{\rm ex})}{\bar{z}(\delta_{\rm ex})} - \ln\bar{z}(\delta_{\rm ex}) - 4\,{\rm Li}_2\,\bar{z}(\delta_{\rm ex}) \\ &\quad + \left(3 + 2\frac{\hat{m}_\ell^2}{\omega_c}\right)\bar{z}(\delta_{\rm ex}) - 2\ln^2\bar{z}(\delta_{\rm ex}) \ + 2\ln^2\bar{z}(\omega_s) + 4\ln\bar{z}(\omega_s)\Big] , \quad (3.24) \end{aligned}$$

with $\bar{z} \equiv 1 - z$ and the $z(\omega_s) \to 1$ limit has been used since $\omega_s \ll 1$. Moreover, A is the coefficient of the collinear log, for which we have also indicated the result for the photon-inclusive limit (i.e. $z(\delta_{\rm ex}) \to 0$). The hard-collinear logs from $\tilde{\mathcal{F}}^{(hc,0)}$ integrated over the full rate, starting from the soft cut-off ω_s, becomes

$$d^2\Gamma^{(0)}\Big|^{(hc)}_{\ell_1||\gamma,\,\ln m_{\ell_1}} = d^2\Gamma^{\rm LO}_{\bar{B}\to\bar{K}\ell_1\gamma\bar{\ell}_2} \left(\frac{\alpha}{\pi}\right) \hat{Q}_{\ell_1}^2 \left[\frac{3}{2} + 2\ln\bar{z}(\omega_s)\right] \ln m_{\ell_1} + \text{reg. terms} , \quad (3.25)$$

where "reg. terms" stands for terms which are finite in the $m_{\ell_1} \to 0$ limit.

We are now ready to show the cancellations of the $\ln m_{\ell_1}$-terms by assembling all pieces. Defining

$$\frac{d^2\Gamma}{dq_0^2 dc_0}\bigg|_{\ln m_{\ell_1}} = \frac{d^2\Gamma^{\rm LO}}{dq_0^2 dc_0} \left(\frac{\alpha}{\pi}\right) \hat{Q}_{\ell_1}^2 \ln m_{\ell_1} \times C_{\ell_1}^{(0)} , \quad (3.26)$$

[11] Note that the z-integration strictly speaking involves max conditions, cf. (3.17), and this is how we have performed the integral. However for $\omega_s, \delta_{\rm ex} \ll 1$ the z's are always larger than zero, hence the simplification.

JHEP12(2020)104

we find

$$C_{\ell_1}^{(0)} = \left[\frac{3}{2} + 2\ln\bar{z}(\omega_s)\right]_{\tilde{\mathcal{F}}^{(hc)}} + \left[-1 - 2\ln\bar{z}(\omega_s)\right]_{\tilde{\mathcal{F}}^{(s)}} + \left[\frac{3}{2} - 2\right]_{\tilde{\mathcal{H}}} = 0\,, \tag{3.27}$$

complete cancellation. As explicitly indicated, the first term in square brackets comes from the hard-collinear integral, (3.25), the second term from the soft integral in eq. (D.19) of appendix D.2, and the last term from the virtual corrections (here the $\frac{3}{2}$ originates from the Z-factors and the -2 from the B_0-functions in (3.10)). Note that the passage from $\bar{B} \to \bar{K}\ell_{1\gamma}\bar{\ell}_2$ in (3.25) to $\bar{B} \to \bar{K}\ell_1\bar{\ell}_2$ in (3.27) is justified since the lepton and the photon are collinear and can thus be treated as a single particle. The cancellation for the lepton $\bar{\ell}_2$ is of course completely analogous. It is worthwhile to point out that the hard-collinear logs, as well as the soft divergences, do cancel charge by charge as explicitly shown in appendix B.4. Note, that in general the cancellation at the differential level is spoiled by non photon-inclusiveness ($\delta_{\rm ex} < \delta_{\rm ex}^{\rm inc}$) and/or going over to the $\{q^2, c_\ell\}$-variables.

3.3.3 $\tilde{\mathcal{F}}^{(hc,\ell)}$, structure of collinear singularities in $dq^2 dc_\ell$

We now proceed to analyse the analogous question for the $\{q^2, c_\ell\}$-variables. Setting $m_K \to 0$, for simplicity, we have (for lepton ℓ_2, $c_\ell \to -c_\ell$)

$$q_0^2 = \frac{q^2}{z}\,, \quad c_0|_{m_K\to 0} = \frac{c_\ell(1+z)+1-z}{c_\ell(1-z)+1+z}\,, \tag{3.28}$$

and using

$$dq_0^2 dc_0 = 4(c_\ell(1-z)+1+z)^{-2} dq^2 dc_\ell\,, \tag{3.29}$$

the analogue of (3.17) becomes

$$\tilde{\mathcal{F}}^{(hc,\ell)}(\underline{\delta}) = \frac{\hat{Q}_{\ell_1}^2}{2^8\pi^3 m_B^3}\int_{\max(z_{\rm inc}(c_\ell),z_{\delta_{\rm ex}}(c_\ell))}^{\max(z_{\rm inc}(c_\ell),z_{\omega_s}(c_\ell))} dz \left[\frac{|\mathcal{A}^{(0)}(q_0^2,c_0)|^2\lambda^{1/2}(q_0^2,m_B^2,0)}{(c_\ell(1-z)+1+z)^2}\right.$$
$$\left.\times\left(\tilde{P}_{q\to q\gamma}(z)\, j^{hc} - j^{hc}_{(m_{\ell_1})}\right)\right] + \{1, c_\ell \leftrightarrow 2, -c_\ell\}\,, \tag{3.30}$$

where $c_0 = c_0(c_\ell)$ with regard to the symmetrisation over c_ℓ, $z_{\delta_{\rm ex}}(c_\ell)$ implements the photon energy cut (2.4) and the arguments have to be substituted by (3.28). The boundaries for the z-integral are given by[12]

$$z_{\rm inc}(c_\ell)|_{m_K\to 0} = \hat{q}^2\,, \quad z_\delta(c_\ell)|_{m_K\to 0} = \frac{1+\hat{q}^2-\delta+c_\ell(1-\hat{q}^2-\delta)}{1+\hat{q}^2+\delta+c_\ell(1-\hat{q}^2-\delta)}\,, \tag{3.31}$$

and obtained by solving (3.18) for $\delta = \delta_{\rm ex}^{\rm inc}, \omega_s, \delta_{\rm ex}$ as appropriate, with (3.28) in place. The phase space slicing condition is implemented via $z_{\omega_s}(c_\ell) < 1$.

[12] Note that the photon-inclusive case, $\delta_{\rm ex}^{\rm inc}$, corresponds to the minimum value of z, for a given q^2. In the limit of $m_K \to 0$, one can deduce, from (3.28), that this corresponds to $q_0^2 = m_B^2$, which then leads to $z_{\rm inc}(c_\ell)|_{m_K\to 0}$ in (3.31).

JHEP12(2020)104

The new aspect is that the $|\mathcal{A}^{(0)}(q_0^2, c_0)|^2$ cannot be factored out since it depends on z implicitly through q_0^2 and c_0. However, in the limit of $m_K \to 0$ and $m_{\ell_{1,2}} \to 0$, the amplitude squared (2.11) is simple enough,

$$|\mathcal{A}^{(0)}(q_0^2, c_0)|^2 = g_{\rm eff}^2(|C_V|^2 + |C_A|^2)\, 2(1-c_0^2)(1-\hat{q}_0^2)^2\, f_+^2(q_0^2)\,, \tag{3.32}$$

and the integral can be done analytically. Note that above $\{q_0^2, c_0\}$ are to be substituted as in (3.28).

Adding all the contributions, real and virtual, that contribute to the hard-collinear logs, one finds

$$\frac{d^2\Gamma}{dq^2 dc_\ell}\Big|_{\ln m_{\ell_{1,2}}} = \frac{\alpha}{\pi}(\hat{Q}_{\ell_1}^2 K_{\rm hc}(q^2, c_\ell)\ln m_{\ell_1} + \hat{Q}_{\ell_2}^2 K_{\rm hc}(q^2, -c_\ell)\ln m_{\ell_2})\,, \tag{3.33}$$

where $K_{\rm hc}(q^2, c_\ell)$ is a non-vanishing function (cf. appendix A.1.1 for a non-trivial cross-check). Plots of this quantity are shown in figure 7 for $(\ell_1, \bar{\ell}_2 = \ell^-, \ell^+)$, with $\ell = e, \mu$.

At last, we would like to mention that for $q^2 \to (m_{\ell_1} + m_{\ell_2})^2$ and $c_\ell \to -1$ the assumption that $k \cdot \ell_1$ is small compared to other scalar products breaks down and this leads to artificial enhancements. For example, the Jacobian factor in (3.30) becomes too large when q^2 is small and $c_\ell \to -1$. However, for a binned rate this effect is negligible and moreover for the $\{q_0^2, c_0\}$-variables there are no such issues at all.

At times we have made the $m_K \to 0$ approximation for simplicity in presentation. The full expressions of c_0 in terms of $\{q^2, c_\ell\}$ (eq. (3.28)), the Jacobian from $\{q_0^2, c_0\}$ to $\{q^2, c_\ell\}$ (eq. (3.29)), $s_{K\ell_2}$ in terms of $\{q^2, c_\ell\}$, the integrand for $\tilde{\mathcal{F}}^{(hc,\ell)}(\underline{\delta})$ (eq. (3.30)) and the limits of the z-integral (eq. (3.31)) can all be found in a Mathematica notebook appended to the arXiv version.

3.3.4 Cancellation of hard-collinear logs for the total differential rate

It is well-known that all IR divergences and IR sensitive terms ought to cancel at the level of the total, photon-inclusive, rate [23]. It is the aim of this section to verify this for the case at hand. The hard-collinear part of the total rate given by

$$\begin{aligned}
\tilde{\Gamma}^{(hc,\ell)}(\omega_s)\Big|_{\ln m_{\ell_1}} &\equiv \frac{\alpha}{\pi}\int_0^1 d\hat{q}^2 \int_{-1}^1 dc_\ell\, \tilde{\mathcal{F}}^{(hc,\ell)}\,,\\
\tilde{\Gamma}^{(hc,0)}(\omega_s)\Big|_{\ln m_{\ell_1}} &\equiv \frac{\alpha}{\pi}\int_0^1 d\hat{q}_0^2 \int_{-1}^1 dc_0\, \tilde{\mathcal{F}}^{(hc,0)}\,,
\end{aligned} \tag{3.34}$$

where we have assumed the $m_K \to 0$ limit.

In accordance with the general expectation, we find

$$\tilde{\Gamma}^{(hc)}\Big|_{\ln m_{\ell_1}} \equiv \tilde{\Gamma}^{(hc,0)}\Big|_{\ln m_{\ell_1}} = \tilde{\Gamma}^{(hc,\ell)}\Big|_{\ln m_{\ell_1}}\,, \tag{3.35}$$

equality at the level of the hard-collinear logs originating from the real radiation

$$\tilde{\Gamma}^{(hc)}(\omega_s)\Big|_{\ln m_{\ell_1}} = \frac{m_B \hat{Q}_{\ell_1}^2}{2^9\,(9\pi^3)} f_+^2 g_{\rm eff}^2(|C_V|^2 + |C_A|^2)\,[8 + 6\ln\omega_s + \mathcal{O}(\omega_s)]\ln m_{\ell_1}\,. \tag{3.36}$$

JHEP12(2020)104

Since we have explicitly shown the cancellation for $\frac{d^2\Gamma}{dq_0^2 dc_0}$, this implies that the hard-collinear logs cancel for the integrated $\int \frac{d^2\Gamma}{dq^2 dc_\ell} dq^2 dc_\ell$. The $\mathcal{O}(\omega_s)$-terms can be safely neglected, since $\omega_s \ll 1$, and in any case the same approximation has been used when evaluating the soft integrals, cf. appendix D.2.

3.4 On hard-collinear logs and structure-dependent terms

We turn to the important question as to whether further hard-collinear logs could be missing due to omitted structure-dependent corrections. Using gauge invariance, we are able to show that this is not the case. In doing so, we will further establish why the hard-collinear logs can be written as a sum of terms proportional to $\hat{Q}^2_{\ell_1,\bar{\ell}_2}$. At the end of the section, we give a physical argument of the previously established result that hard-collinear logs cancel at differential rate $\frac{d^2}{dq_0^2 dc_0}\Gamma$, that is when expressed in $\{q_0^2, c_0\}$-variables.

The starting point is to realise that hard-collinear logs $\ln m_{\ell_{1,2}}$ are generated by interference of

$$\frac{1}{k\cdot\ell_{1,2}} \tag{3.37}$$

denominators (k approaching $\ell_{1,2}$) with other terms. Without loss of generality, we may focus our attention to lepton ℓ_1. The real amplitude can be decomposed,

$$\mathcal{A}^{(1)} = \hat{Q}_{\ell_1} a^{(1)}_{\ell_1} + \delta\mathcal{A}^{(1)}\,, \tag{3.38}$$

into a term $\hat{Q}_{\ell_1} a^{(1)}_{\ell_1}$ with all terms proportional to $\hat{Q}_{\ell_1}$, and the remainder $\delta\mathcal{A}^{(1)}$. Note, that at this point we have not yet made use of charge conservation. From (2.13),

$$a^{(1)}_{\ell_1} = -e g_{\text{eff}} \bar{u}(\ell_1) \left[\frac{2\epsilon^*\cdot\ell_1 + \not{\epsilon}^* \not{k}}{2k\cdot\ell_1} \Gamma\cdot H_0(q_0^2) \right] v(\ell_2)\,, \tag{3.39}$$

which contains all $1/(k\cdot\ell_1)$-terms. It is seen that the structure-dependence of this term is encoded in the form factor H_0 (defined in (2.8)) only. For our purposes it is convenient to write the amplitude square, using (3.38), in terms of three terms

$$\sum_{\text{pol}} |\mathcal{A}^{(1)}|^2 = \sum_{\text{pol}} |\delta\mathcal{A}^{(1)}|^2 - \hat{Q}^2_{\ell_1} \sum_{\text{pol}} |a^{(1)}_{\ell_1}|^2 + 2\hat{Q}_{\ell_1} \text{Re}[\sum_{\text{pol}} \mathcal{A}^{(1)} a^{(1)*}_{\ell_1}]\,, \tag{3.40}$$

where it will be important that $\mathcal{A}^{(1)}$ is gauge invariant. By construction, the first term is manifestly free from hard-collinear logs $\ln m_{\ell_1}$. To simplify the discussion, we may use gauge invariance and set $\xi = 1$ in this section under which the polarisation sum, $\sum_{\text{pol}} \epsilon^*_\mu \epsilon_\nu = (-g_{\mu\nu} + (1-\xi)k_\mu k_\nu/k^2) \to -g_{\mu\nu}$, collapses to the metric term only. In this case, the second term evaluates to

$$\int d\Phi_\gamma\, \hat{Q}^2_{\ell_1} \sum_{\text{pol}} |a^{(1)}_{\ell_1}|^2 = \int d\Phi_\gamma\, \hat{Q}^2_{\ell_1} \frac{\mathcal{O}(m^2_{\ell_1}) + \mathcal{O}(k\cdot\ell_1)}{(k\cdot\ell_1)^2} = \mathcal{O}(1)\, \hat{Q}^2_{\ell_1} \ln m_{\ell_1}\,, \tag{3.41}$$

where we used $k - \ell_1 = \mathcal{O}(m^2_{\ell_1})$, valid in the collinear region. Note that the form factor part $H_0(q_0^2)$ does not participate in the photon phase space integration, and factorises when

JHEP12(2020)104

working with dq_0^2. We now turn to the third term. The crucial step in use is that gauge invariance $k\cdot\mathcal{A}^{(1)}=0$ implies $\ell_1\cdot\mathcal{A}^{(1)}=\mathcal{O}(m_{\ell_1}^2)$ in the collinear region and thus the third term assumes the form

$$\hat{Q}_{\ell_1}\sum_{\text{pol}}\mathcal{A}^{(1)}a_{\ell_1}^{(1)*}=c_1\,\hat{Q}_{\ell_1}^2\,\frac{\mathcal{O}(m_{\ell_1}^2)+\mathcal{O}(k\cdot\ell_1)}{(k\cdot\ell_1)^2}+c_2\,\hat{Q}_{\ell_1}\hat{Q}_X\,\frac{\mathcal{O}(m_{\ell_1})}{(k\cdot\ell_1)}+\dots\,, \tag{3.42}$$

where $X\in\{\bar{B},\bar{K},\bar{\ell}_2\}$ and the ellipses stand for less singular contributions. The c_1-term has the same origin as the one in (3.41). The c_2-term comes from interfering the spin dependent term in (3.39) with the $\hat{Q}_{\ell_1}$-independent part of $\mathcal{A}^{(1)}$ and it is by the use of the equation of motion, that one arrives at the $\mathcal{O}(m_{\ell_1})$-suppression[13]

$$\int d\Phi_\gamma\,\frac{\mathcal{O}(m_{\ell_1})}{(k\cdot\ell_1)}=\mathcal{O}(m_{\ell_1})\ln m_{\ell_1}\,, \tag{3.43}$$

as compared to (3.41). Hence we have established that all hard-collinear terms $\ln m_{\ell_1}$ can be written as a sum of terms proportional to $\hat{Q}_{\ell_1}^2$. It should be added that in making this statement, charge conservation was used since gauge invariance was assumed. All statements hold irrespective of any photon phase space restrictions such as an energy cut-off δ_{ex} or a photon angle cut (cf. section 4.2). Thus, any gauge invariant addition to the amplitude, due to structure-dependent terms, will not give rise to any additional $\ln m_{\ell_1}$-terms.

So far, our analysis has been concerned with the real amplitude only. Assuming that hard-collinear logs cancel charge by charge combination at the differential level in the $\{q_0^2,c_0\}$-variables, irrespective of the microscopic approach, the same conclusion applies to each virtual diagram.[14] For virtual diagrams, there is no distinction between $\{q_0^2,c_0\}$- and $\{q^2,c_\ell\}$-variables and thus the conclusion holds irrespective of the differential variables. As the reader might suspect, the same conclusions holds for lepton ℓ_2 by symmetry. Let us summarise these findings:

- Additional structure-dependent corrections, which are of course gauge invariant, will not give rise to any additional hard-collinear logs $\ln m_{\ell_{1,2}}$.[15]

- At the double-differential level, hard-collinear logs $\ln m_{\ell_{1,2}}$, real and virtual, can be written as a sum of terms proportional to $\hat{Q}_{\ell_{1,2}}^2$ consistent with our explicit evaluation using the phase space slicing method in eq. (3.25).

[13] In fact, this result is true more generally since the spin dependent part is proportional to the Lorentz-generator which, by contraction, is a boost into the direction of the photon. Let us assume that $m_{\ell_1}=0$. Since in the collinear limit, the photon and the lepton are parallel, the massless lepton is boosted in direction of movement. Since the helicity of a massless particle cannot be changed, the generator has to vanish. If the lepton mass is reinstalled, then there are terms of the form $m_{\ell_1}\ln m_{\ell_1}$ which are however safe.

[14] A physical argument of the correctness of this assumption is given in the last of paragraph of this section. In particular, we have verified this explicitly up to the second derivative of the form factor in our approach and produced a formal derivation that holds to all orders.

[15] This applies to either, approaches resolving the mesons by partons or an evaluation of the $B(K)_\gamma L_{1,2}$-diagrams, cf. figure 3, including higher terms in the expansion (2.7).

JHEP12(2020)104

To this end, let us give a physical explanation as to why hard-collinear logs $\ln m_{\ell_{1,2}}$ are to cancel at the differential level in $\{q_0^2, \theta_0\}$. In those variables, the decay corresponds to the disintegration of a scalar particle of mass q_0^2 which is an infrared-safe observable. Now, the angle θ_0 has no meaning when the decay axis, cf. figure 1, is decoupled and the $\bar{B}$ and the $\bar{K}$ are interpreted as a single particle of mass q_0^2. This observation is backed up by our explicit formal verification in eq. (3.26). In essence q_0^2 is an IR-safe kinematic variable and the entirety of the particles in q_0^2 can be viewed as the moral cousin of a jet.

4 Results for $\bar{B} \to \bar{K} e^+ e^-$ and $\bar{B} \to \bar{K} \mu^+ \mu^-$

The total radiative corrections are presented in section 4.1, followed by a discussion of the distortion of the spectrum due to γ-radiation in section 4.2. The size of the hard collinear logs and some comparison with older work is deferred to appendices A.1 and A.2 respectively. Before proceeding thereto, we summarise the input to the numerics below.

For the particles participating in the decay, the following masses are assumed: $m_e = 0.511\,\text{MeV}$, $m_\mu = 0.10565\,\text{GeV}$, $m_B = 5.28\,\text{GeV}$ and $m_K = 0.495\,\text{GeV}$. Other parameters are the Wilson coefficients, $C_9 = 4.035$ and $C_{10} = -4.25$ at $\mu_{UV} = 4.7\,\text{GeV}$ (the b-quark pole mass) and the fine structure constant, $1/\alpha = 137.036$. For the $B \to K$ form factors (2.8), the light-cone sum rules computation [24], including radiative correction up to twist-3, was used with updated Kaon distribution amplitude parameters[16]

$$\{f_+, f_-\}^{B\to K}(0) = \{0.271, -0.206\}\,, \quad \frac{d}{dq^2}\{f_+, f_-\}^{B\to K}(0) = \{0.0151, -0.0109\}\,, \tag{4.1}$$

where the uncertainty is roughly 15% if one additionally takes into account the error on the Kaon distribution amplitude. For the auxiliary cut-offs of the phase space slicing method, $\omega_s(e) = 2.5\cdot 10^{-3}$, $\omega_s(\mu) = 4\cdot 10^{-3}$, $\omega_c(e) = 1\cdot 10^{-2}\omega_s(e)$ and $\omega_c(\mu) = 2\cdot 10^{-2}\omega_s(\mu)$ lead to stable results. The hierarchy $\omega_c/\omega_s \ll 1$ is important since terms of this order are neglected.[17] Here, we refrain from a complete uncertainty analysis. Let us nevertheless mention the sources. There are the form factor uncertainties which can be largely reduced by considering correlations amongst the four numbers (4.1) entering the computations. Besides a more complete structure-dependent approach, cf. section 5.1, there are missing finite counterterms in the charged meson case, which we set to zero and refer the reader to the discussion in section 2.3. Concerning the latter, one might get a naive dimensional analysis estimate by varying the constant c, associated with $1/\epsilon_{\text{UV}} + c$, by a factor of 2. Adding these effects in quadrature results in an $\mathcal{O}(1\%)$-variation.

[16] For the Kaon distribution amplitude, the values $a_1^K(1\,\text{GeV}) = 0.115(34)$ and $a_2^K(1\,\text{GeV}) = 0.090(20)$ taken from the $N_f = 2+1$ lattice computation [25] (uncertainties were added in quadrature) were used. These values are consistent with earlier QCD sum rule computations [26–29].

[17] We refer the reader to [22] for an uncertainty analysis involving the auxiliary cut-offs.

JHEP12(2020)104

4.1 Radiative corrections as a function of q_0^2, c_0 and q^2, c_ℓ

We consider it most instructive to discuss the relative QED corrections, implicitly defined in (3.1),

$$\Delta^{(a)}(q_a^2, c_a; \delta_{\text{ex}}) = \left(\frac{d^2\Gamma^{\text{LO}}}{dq_a^2 dc_a}\right)^{-1} \frac{d^2\Gamma(\delta_{\text{ex}})}{dq_a^2 dc_a}\Big|_\alpha \,. \tag{4.2}$$

Above $|_\alpha$ stands for the inclusion of the $\mathcal{O}(\alpha)$-corrections only. The LO rate is given eq. (B.1). We further consider the relative single differential in $\frac{d}{dq_a^2}$

$$\Delta^{(a)}(q_a^2; \delta_{\text{ex}}) = \left(\frac{d\Gamma^{\text{LO}}}{dq_a^2}\right)^{-1} \frac{d\Gamma(\delta_{\text{ex}})}{dq_a^2}\Big|_\alpha \,, \tag{4.3}$$

where the numerator and denominator are integrated separately over $\int_{-1}^{1} dc_a$ respectively. In addition, we define the single differential in $\frac{d}{dc_a}$

$$\Delta^{(a)}(c_a, [q_1^2, q_2^2]; \delta_{\text{ex}}) = \left(\int_{q_1^2}^{q_2^2} \frac{d^2\Gamma^{\text{LO}}}{dq_a^2 dc_a} dq_a^2\right)^{-1} \int_{q_1^2}^{q_2^2} \frac{d^2\Gamma(\delta_{\text{ex}})}{dq_a^2 dc_a} dq_a^2\Big|_\alpha \,, \tag{4.4}$$

where the non-angular variable is binned. We would like to stress that it is important to integrate the QED correction and the LO separately as this corresponds to the experimental situation.

Results for $\Delta^{(a)}(q_a^2; \delta_{\text{ex}})$ and $\Delta^{(a)}(c_a, [q_1^2, q_2^2]; \delta_{\text{ex}})$ are shown in figures 4 and 5 respectively. Let us first focus on figure 4 where in the photon-inclusive case ($\delta_{\text{ex}} = \delta_{\text{ex}}^{\text{inc}}$, dashed line), one observes two important features: Approximate lepton-universality and the cancellation of the hard-collinear logs. In the q_0^2-variable, this happens at the differential level whereas for the q^2-variable, integration over the entire range is needed (the tendency thereto is visible in the plot of the r.h.s.). To be clear, the cancellation in the later case only occurs upon integration over the full q^2-range. We further remind the reader that in all cases the soft divergences cancel locally as explicitly shown in section 3.1. It is noticeable that for the charged case, there are $\mathcal{O}(2\%)$-effects in the q_0^2-variable due to "collinear logs", $\ln \hat{m}_K \approx -2.36$. These logs, of course, cancel upon integration over all differential variables. The impact of the photon energy cuts are large, cf. appendix A.1, and care needs to be taken when considering quantities like R_K for example. An important physical effect, visible in the plots on the right in figures 4, is the distortion of the q^2 distribution w.r.t. the non-radiative case. This is particularly prominent in the photon-inclusive limit as discussed in the next section.

The angular differential $\Delta^{(a)}(c_a, [q_1^2, q_2^2]; \delta_{\text{ex}})$ in figure 5 shows similar patterns in the photon-inclusive case ($\delta_{\text{ex}} = \delta_{\text{ex}}^{\text{inc}}$, dashed lines), e.g. lepton universality and small effects in the c_0-variable due to the cancellation of hard-collinear logs. In the electron case, there is a significant enhancement towards the endpoints $\{-1, 1\}$ which is due to the peculiar behaviour of the LO rate $d\Gamma^{\text{LO}} \propto (1 - c_\ell^2) + \mathcal{O}(m_\ell^2)$ (B.2). This is the same effect as the helicity suppression in a $\pi^- \to \ell^- \bar{\nu}$ decay and further explains why the effect is less prominent in the muon case. A more detailed analysis of the angles will follow in

JHEP12(2020)104

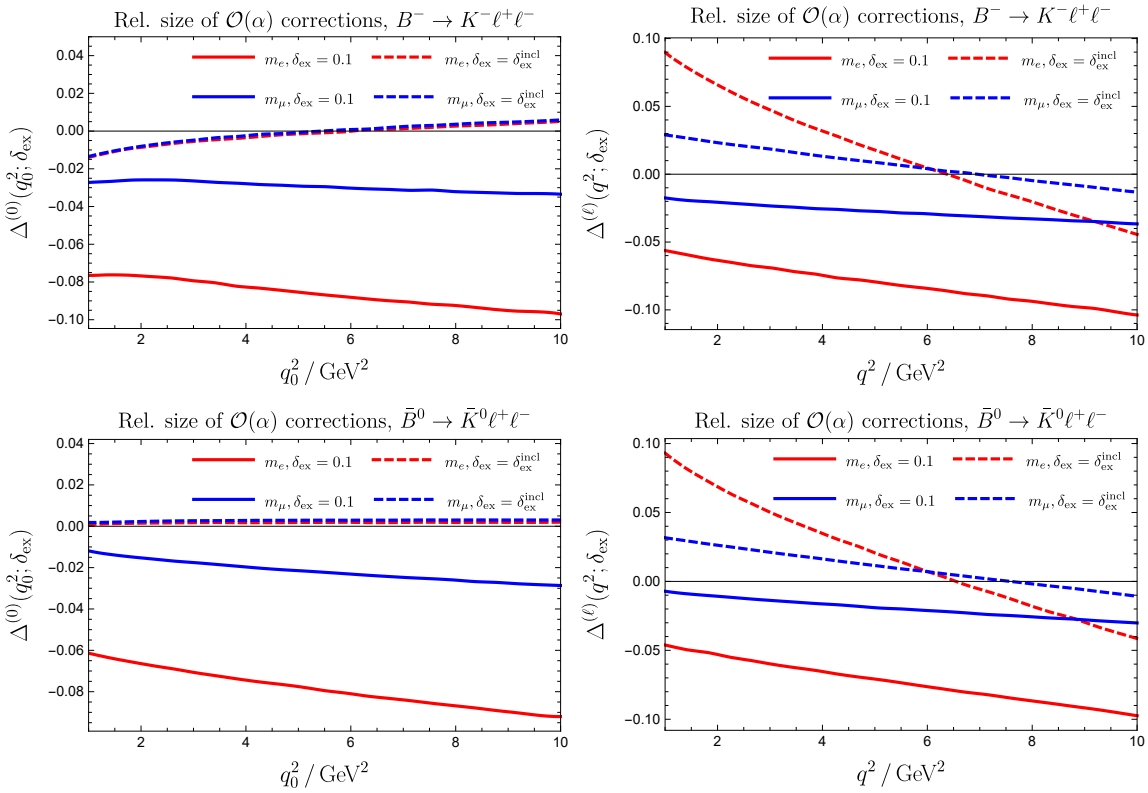

Figure 4. Total relative QED-corrections, cf. (4.3) for the definition, including finite terms. The upper and lower figures correspond to the charged and neutral modes in the q_0^2- and q^2-variables on the left and right respectively. In the photon-inclusive case ($\delta_{\rm ex} = \delta_{\rm ex}^{\rm inc}$, dashed lines), all IR sensitive terms cancel in the q_0^2 variable locally and in the q^2-variable when integrated which is nicely visible in both cases. In the charged case, however, we see finite effects of the $\mathcal{O}(2\%)$ due to $\ln \hat{m}_K$ "collinear logs" which do not cancel. An important aspect is the (approximate) lepton universality on the plots on the left. As is well-known, effects due to the photon energy cuts are sizeable since hard-collinear logs do not cancel in that case. This is in particular for electrons.

a forthcoming paper cf. comments in section 5.2. Cuts on the photon energy are again sizeable and the same remarks as before apply.

Plots of the hard-collinear logs $\ln m_\ell$ are deferred to appendix A.1. Moreover in appendix A.2 our results are compared to the earlier work [6] where virtual corrections were indirectly inferred and radiative corrections have been evaluated in terms of a radiator function depending on q^2 and q_0^2 only, and not on the photon-emission angle.

4.2 Distortion of the $\bar{B} \to \bar{K}\ell^+\ell^-$ spectrum due to γ-radiation

As discussed in section 3 the $\{q_0^2, \theta_0\}$-variables are safer than the $\{q^2, \theta_\ell\}$-variables because of the cancellation of the hard-collinear divergences. In this section, we wish to emphasise yet another reason why it is preferable to use the $\{q_0^2, \theta_0\}$-variables. This is sometimes called the migration of radiation or the distortion of the spectrum: at fixed q^2, effectively the radiative process is probed at a different $q_0^2 = (q+k)^2$ as a result of the photon carrying away momentum. If the spectrum has significant variations in q_0^2, this implies a

JHEP12(2020)104

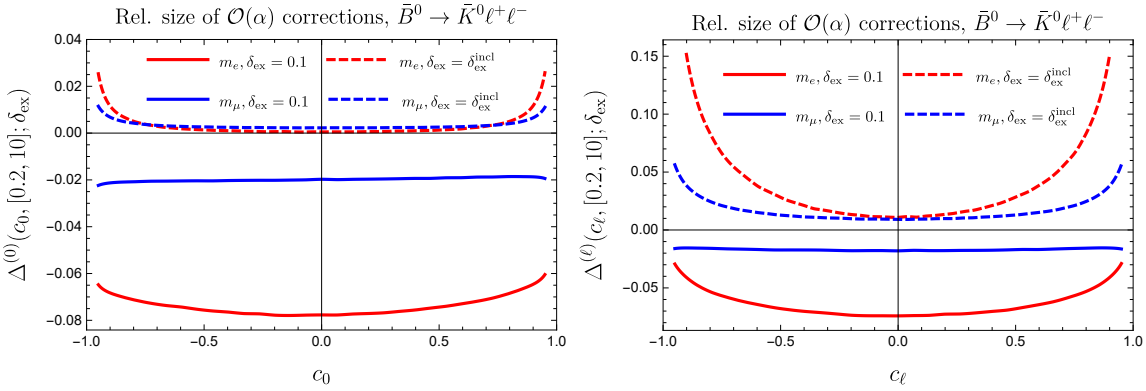

Figure 5. Total relative QED-corrections (4.4) in terms of $c_0 = \cos(\theta_0)$ $c_\ell = \cos(\theta_\ell)$ respectively for the electrically neutral hadron case. In the c_0-variable effects are small for $\delta_{\rm ex} = \delta_{\rm ex}^{\rm inc}$ cf. comments in text and previous figures. The enhanced effect towards the endpoints $\{-1, 1\}$ in the electron case is, partly, due to the special behaviour of the LO expression (B.2) which behaves like $\propto (1 - c_\ell^2) + \mathcal{O}(m_\ell^2)$ and explains why the effect is less pronounced for muons.

significant distortion in the kinematical distribution. This effect is indeed well-known from the determination of the J/Ψ-pole in $e^+e^- \to$ hadrons [30]. Generically, the more inclusive one gets in the photon energy and angle, the more pronounced it is, as in this case the radiative topologies (4-body) can be very different from the virtual ones (3-body).

Let us illustrate the effect by considering the hard-collinear radiation, $\tilde{\mathcal{F}}^{(hc,\ell)}(\underline{\delta})$ given in eq. (3.30). Assuming the $m_K = 0$ limit, for simplicity, the dz-intgegrand contains $|\mathcal{A}^{(0)}(q_0^2, c_0)|^2 \propto f_+(q_0^2)^2 = f_+(q^2/z)^2$ (cf. eq. (B.2) with $m_\ell = 0$) and $q_0^2 = q^2/z$ from eq. (3.28). Since $z < 1$ in general, it is clear that momentum transfers of a higher range are probed. For $c_\ell = -1$, maximising the effect, one gets

$$z_{\delta_{\rm ex}}(q^2)\Big|_{c_\ell=-1} = \frac{q^2}{q^2 + \delta_{\rm ex} m_B^2}\,, \quad (q_0^2)_{\rm max} = q^2 + \delta_{\rm ex} m_B^2\,, \tag{4.5}$$

upon using (3.31). Thus for $\delta_{\rm ex} = 0.15$ and $q^2 = 6\,\text{GeV}^2$ one finds $(q_0^2)_{\rm max} = 10.18\,\text{GeV}^2$ which is of course problematic when one wants to probe R_K in the $q^2 \in [1, 6]\,\text{GeV}^2$ range, given that the charmonia start to impact more severely well below $10\,\text{GeV}^2$. In the photon-inclusive case, the lower boundary becomes $z_{\rm inc}(c_\ell)|_{m_K\to 0} = \hat{q}^2$ by eq. (3.31) and $(q_0^2)_{\rm max} = m_B^2$. Hence, in that case the entire spectrum is probed for any fixed value of q^2 which confirms the earlier statement. As it can easily be understood, this would be rather problematic in $\bar{B} \to \bar{K}\ell^+\ell^-$ decays due to the large charmonia contributions (cf. comments below (2.12)), that would "contaminate" all the q^2 region below their masses. This is why in experimental analyses, stringent cuts on the photon energy (or the reconstructed B-meson mass) and its emission angle are implemented.

The effects described above are visible in both plots in figure 6. We stress that they are underestimated since a) we kept only one power in the derivative expansion and b) one would need to incorporate long-distance effects in addition. Note that for the virtual contributions, it is only when both hadrons are neutral that the derivative expansion can

JHEP12(2020)104

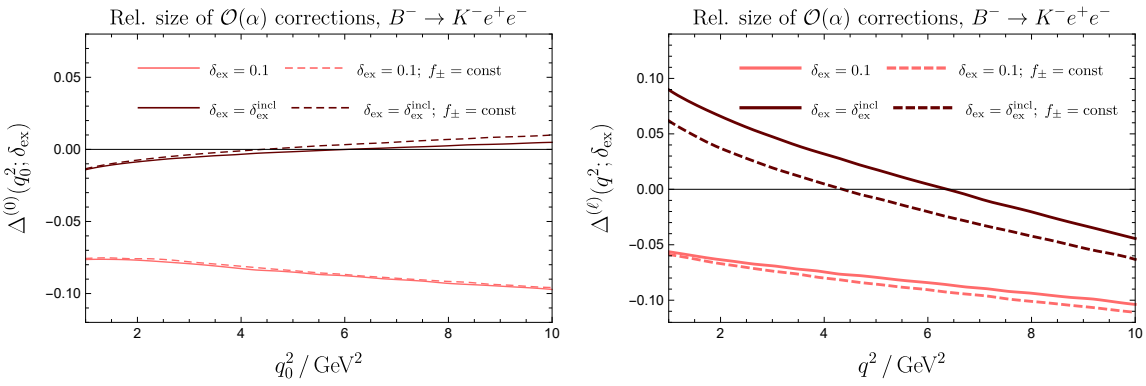

Figure 6. Plots of total relative QED corrections (4.2) for $B^- \to K^-\ell^+\ell^-$ comparing the constant form factor case versus taking one derivative correction into account with values given in (4.1) (cf. below (2.12) for further comments). Effects are more prominent in the photon-inclusive case ($\delta_{\rm ex} = \delta_{\rm ex}^{\rm inc}$) since there is more phase space for the q^2- and q_0^2-variables to differ. In the neutral case, we found that the effects are similar albeit slightly smaller.

be avoided. If this is not the case, it is important to take into account higher derivative corrections and perform the matching of the finite counterterms from QCD.

As alluded above, besides the cut on the reconstructed B-meson mass, in order to reduce the migration of radiation (or better the distortion of the q^2 spectrum) one can further restrict the photon's phase space in the photon's emission angle. From $q = q_0 - k$, taking into account (C.7), one gets $q^2 = q_0^2 - 2E_\gamma^{(1)}(E_{q_0}^{(1)} + |\vec{q}_0^{\,(1)}|\cos\theta_\gamma^{(1)})$. Then using the expression of the maximum photon energy in (2.31), one arrives at

$$(q_0^2)_{\rm max} = q^2 + \delta_{\rm ex} m_B (E_{q_0}^{(1)} + |\vec{q}_0^{\,(1)}|\cos\theta_\gamma^{(1)})\,. \tag{4.6}$$

Assuming again for simplicity the $m_K = 0$ limit where $E_{q_0}^{(1)} = (m_B^2 + q_0^2)/(2m_B)$ and $|\vec{q}_0^{\,(1)}| = (m_B^2 - q_0^2)/(2m_B)$, one finds

$$(q_0^2)_{\rm max} = \begin{cases} q^2 + \delta_{\rm ex} q_0^2 & \cos\theta_\gamma^{(1)} = -1 \quad \text{tight-angle cut} \\ q^2 + \delta_{\rm ex} m_B^2 & \cos\theta_\gamma^{(1)} = +1 \quad \text{max-angle} \end{cases}\,. \tag{4.7}$$

This means that for fixed q^2, and a cut of $\delta_{\rm ex} = 0.15$, the radiative process probes values of $(q_0^2)_{\rm max} = q^2/(1-\delta_{\rm ex}) \approx 1.18\,q^2$ (tight-angle cut) and $(q_0^2)_{\rm max} \approx q^2 + 4.18\,\text{GeV}^2$ (max-angle) respectively. Note that the maximum angle cut in the photon-emission gives the same result as the maximum lepton angle. This is because in the collinear limit ($\vec{\ell}_1 \propto \vec{k}$), the maximum lepton angle aligns $\vec{\ell}_1$ and $\vec{k}$ with the decay axis (x-axis, see figure 1), and this coincides with the maximum angle cut.

4.3 Remarks on the Lepton Flavour Universality ratio R_K

LFU ratios, such as R_K, are good observables to search for specific types of physics beyond the SM, namely new interactions that are not universal among the different lepton species. Owing to the cancellation of many hadronic uncertainties, these ratios can be predicted

JHEP12(2020)104

well up to LFU violating interactions. In the SM, LFU is broken by the fermion masses and, as such, sizeable effect could result from the logarithms of QED

$$R_K|_{q_0^2\in[q_1^2,q_2^2]\,\mathrm{GeV}^2} = \frac{\Gamma[\bar{B}\to\bar{K}\mu^+\mu^-]}{\Gamma[\bar{B}\to\bar{K}e^+e^-]}|_{q_0^2\in[q_1^2,q_2^2]\,\mathrm{GeV}^2} \approx 1+\Delta_{\mathrm{QED}}R_K\,, \tag{4.8}$$

as first quantified in [6]. Whereas for a meaningful comparison to experiment a purpose build Monte Carlo with complete differential treatment is desirable (cf. section 5.3), one may already raise the point that the precise treatment has a relevant impact.

For example, considering only the cuts on reconstructed B-meson mass in [1], the net QED correction that should be applied to R_K according to our analysis amounts to

$$\Delta_{\mathrm{QED}}R_K \approx \frac{\Delta\Gamma_{K\mu\mu}}{\Gamma_{K\mu\mu}}\bigg|^{m_B^{\mathrm{rec}}=5.175\,\mathrm{GeV}}_{q_0^2\in[1,6]\,\mathrm{GeV}^2} - \frac{\Delta\Gamma_{Kee}}{\Gamma_{Kee}}\bigg|^{m_B^{\mathrm{rec}}=4.88\,\mathrm{GeV}}_{q_0^2\in[1,6]\,\mathrm{GeV}^2} \approx +1.7\%\ , \tag{4.9}$$

whereas the correction has to be compared with the $\Delta_{\mathrm{QED}}R_K \approx +3\%$ quoted in [6] that, as explained in appendix A.2, takes into account an additional implicit tight cut on the photon-emission angle. Note that the different photon energy cuts for muons ($m_B^{\mathrm{rec}} = 5.175\,\mathrm{GeV} \leftrightarrow \delta_{\mathrm{ex}} = 0.0394$) and electrons ($m_B^{\mathrm{rec}} = 4.88\,\mathrm{GeV} \leftrightarrow \delta_{\mathrm{ex}} = 0.1458$) reduce the effect of QED corrections to R_K. In addition, $|\Delta_{\mathrm{QED}}R_K^{\mathrm{BIP}}| > |\Delta_{\mathrm{QED}}R_K^{\mathrm{INZ}}|$ has to be expected since the BIP computation [6] is more exclusive, in view of the tight photon-angle cut, than the explicit computation presented here. However, in both cases the overall impact of QED corrections in the LFU ratios (currently estimated by the experiment using PHOTOS) is not exceedingly large and below the current experimental error $R_K = 0.846^{+0.060+0.016}_{-0.054-0.014}$ [3].

5 Outlook

In this section, we briefly address various topics which go beyond the scope of this paper and are worthwhile to be pursued in future investigations.

5.1 Structure-dependent terms

In this work, we have treated the mesons as fundamental fields. The effective Lagrangian employed is able to perfectly describe their internal structure up to $\mathcal{O}(e^0)$. However, the electromagnetic probe sees the mesons as a structureless particle. Hence our effective Lagrangian corresponds to approximating a multipole expansion by the monopole term.

In the language of meson fields, one would need to build a systematic effective field theory with gauge invariant operators out of covariant derivatives and meson fields. This would include, amongst others, terms beyond minimal coupling of the form $(D^\mu B)^\dagger F_{\mu\nu}\, D^\nu K$. It is beyond doubt that in full QCD, the meson's partons give rise to such higher multipole emissions, which we referred to as structure-dependent terms.[18] The question is whether they are sizeable. For light-light systems, such as $K\to\pi$ decays, these terms are known to be small e.g. [31, 32] (unless the leading amplitude is accidentally suppressed). For

[18] The full theory, including QCD and QED, is needed to compute the corresponding Wilson coefficients. and counterterms when involving loops.

JHEP12(2020)104

heavy-light systems, this might change since the masses of the valence quarks introduce a sizeable asymmetry that will eventually be resolved.

A result established in this paper provides some protection. It was shown in section 3.4 that structure-dependent corrections do not lead to any additional hard-collinear logs. Since soft divergences cancel at the differential level, this means that the employed approximation captures all IR sensitive terms. However, it cannot be precluded that new and interesting hadronic effects, not directly related to infrared effects, could come into play. An example of which is provided by $B_s \to \mu^+\mu^-$, where it was found that the chirality suppression of the non radiative decay m_μ/m_b is lifted to $m_\mu/\Lambda_{\rm QCD}$ ("enhanced power corrections") when QED corrections are taken into account [33]. These authors develop QED corrections to B decays within the soft collinear effective theory (SCET) framework, recently extended to $B \to K\pi$ [34]. It allows for the resummation of different types of logarithms [35] but does not capture all $1/m_b$ effects. To what extent $1/m_b$-corrections are important in QED corrections to B-mesons decays is an interesting and open question. Another approach is lattice QCD, where the precision in Kaon physics per se demands the inclusion of QED corrections [36, 37] with first results in leptonic decays [38–40]. For B decays, in the region of fast recoiling particles, more work is needed because of too many exponentially growing modes that have to be captured by a fit or dealt with in some other way.

5.2 Moments of the differential distribution

A special feature of QED corrections is that they have genuine infrared effects when compared to the weak interaction with natural scale $m_W \gg m_B$. As pointed out in [41], this changes the angular distribution in that there is not a specific hierarchy of moments in the angles (cf. section 5 in this reference). Without QED corrections, it is the dimension of the effective Hamiltonian that limits the partial waves to its lowest numbers. Higher moments (in the partial wave expansion) are therefore absent or suppressed by further powers of m_b/m_W. Hence, measuring higher moments allows to measure QED effects. It is therefore interesting to scrutinise the size of these corrections from the theory side in order to identify the most sensitive moments and give further motivation to an experimental investigation. We will turn to this task in a forthcoming publication.

5.3 The $\bar{B} \to \bar{K}\ell^+\ell^-$ differential distribution through Monte Carlo

Our results can be used to estimate the radiative corrections to the $\bar{B} \to \bar{K}\ell^+\ell^-(\gamma)$ differential distribution semi-analytically.[19] As demonstrated, the choice of differential variables (which might be dictated by their accessibility in a given experiment) that we have in-

[19]The integration over the photon variables is done numerically and this is why we refer to them as semi-analytic.

JHEP12(2020)104

troduced (2.1) directly impacts in what way hard-collinear logs cancel. An alternative approach, more in line with current analysis techniques, is to build a Monte Carlo program for the numerical simulation of the radiative and the non-radiative processes, and evaluate the impact of the radiative corrections entirely numerically. This happens at an even more differential level by taking into account the photon kinematics on an event-by-event basis. Given the sizeable contributions from hard-collinear logs, it will be an important task to crosscheck the purpose-built Monte Carlo against standard tools used in experimental analysis. In this case, our virtual corrections are essential in that they provide the normalisation of the Monte Carlo code.[20] Within this approach, we are free to adopt the $\{q_0^2, c_0\}$ or the $\{q^2, c_\ell\}$-variables, since these are used to describe the simulated events and the experiment can produce a distribution in either of the variables by using local corrections factors. The final comparison with experiment is performed in a subsequent step after taking into account experimental efficiencies, resolutions, and cuts to reduce the background. Given our results in section 3, it is clear that the choice of $\{q_0^2, c_0\}$ is more convenient, since for each value of q_0^2 and c_0 the corresponding photon-inclusive rate is free from hard-collinear singularities. A detailed Monte Carlo code for $\bar{B} \to \bar{K}^{(*)}\ell^+\ell^-(\gamma)$, taking into account the finite $\mathcal{O}(\alpha)$ terms evaluated in this work, will be presented in a forthcoming publication.

It is worth stressing that most of the considerations presented in this work, and particularly the strategy outlined above to build a Monte Carlo code, apply if the final-state hadron is a narrow vector resonance (such as the $\bar{K}^*$), rather than a stable scalar meson. In the narrow-width approximation, we can neglect the interference of the radiation emitted by the final-state mesons, produced by the vector-meson decay, with the radiation from the B decay products (i.e. the radiation described in this work). In this limit (which is a rather good approximation in the $\bar{K}^*$ case, given that $\Gamma_{\bar{K}^*}/m_{\bar{K}^*} \approx 5\%$) the formalism is essentially identical, up to a richer form factor structure.

5.4 Remarks on charged-current semileptonic decays

In the main section, charges and masses were kept completely general, so that any semileptonic decay can be covered, including charged-current processes such as $\bar{B} \to D\ell\nu$. A significant difference to $\bar{B} \to \bar{K}\ell^+\ell^-$ is that the variable $\bar{p}_B^2$, defined as in (2.3), is not observable (because of the unidentified neutrino). Whereas this does not pose a problem for the Monte Carlo simulation discussed above, this is an issue for the semi-analytical determination of an $\mathcal{O}(\alpha)$ infrared-safe distribution of $\bar{B} \to D\ell\nu$.

One possibility to overcome this problem is to consider $\hat{p}_B^2 \equiv (p_B - p_\nu)^2$ as the effective photon energy variable. A photon energy cut-off, similar to (2.4), can be introduced as follows $\delta_{\rm SL}^{\rm ex} = (1 - p_{D\ell}^2/\hat{p}_B^2)$ which translates to $E_\gamma^* < \delta_{\rm SL}^{\rm ex}(p_{D\ell}/2)$ (E_γ^* is the photon energy in

[20] The Monte Carlo code requires the introduction of an (unphysical) soft cut-off Λ_s, below which the mode is treated as a three-body decay. The rate (3.1) is then split into, $d^2\Gamma(\delta_{\rm ex}) = [d^2\Gamma(\Lambda_s)]_{\rm MC_3} + \left[\frac{\alpha}{\pi}\sum_{i,j}\hat{Q}_i\hat{Q}_j(\mathcal{F}_{ij}^{(a)}(\delta_{\rm ex}) - \mathcal{F}_{ij}^{(a)}(\Lambda_s))\right]_{\rm MC_4} dq_a^2 dc_a$, a first term which is done semi-analytically with our computation and simulated with three-body kinematics, and a second term which is obtained through the simulation of the full four-body kinematics. Note that both terms are free from soft divergences and Λ_s is analogous to phase space slicing cut-off ω_s introduced in section 3.

JHEP12(2020)104

the D-lepton RF). The new aspect with regards to the FCNC case is that the lower cut-off on the energy variable, $(\hat{p}_B^2)_{\rm min} = p_{D\ell}^2/(1-\delta_{\rm SL}^{\rm ex})$, is dependent on a differential variable.[21]

Another strategy is to impose the minimal kinematic limits on $\bar{p}_{\rm vis}^2 \equiv (p_B - k - p_\nu)^2$ and accept all events with E_D and E_ν which lie within the non-radiative Dalitz-plot. This is the "traditional" approach adopted in refs. [17, 42, 43]. This can work in a clean environment, in K-factories, but would not be a feasible approach for the LHC collider environment. Incidentally, we note that the variables $(E_D,\, E_\nu)$ are an alternative choice to our $\{q^2, c_\ell\}$-variables. We finally stress that the approach followed in [44], where an effective cut on the photon energy is implemented irrespective of the photon-emission angle, might lead to a miss-estimate of the hard collinear logs (see the discussion in appendix A.2).

6 Conclusions

In this paper we have analysed the $\mathcal{O}(\alpha)$ corrections to a generic $M_H \to M_L \ell_1 \bar{\ell}_2$ decay, where $M_{H,L}$ are scalar mesons (of either parity). We have performed a complete calculation of these corrections within improved scalar QED, employing a mesonic effective Lagrangian (with a tower of effective operators) which provides an accurate description of the non-radiative hadronic form factors. We have shown by means of explicit computation that all soft divergences cancel at the double differential level (section 3.1), irrespective of the choice of the variables used to describe the "visible" kinematics. On the other hand, we have demonstrated that the hard-collinear logs can survive, even in the photon-inclusive limit, depending on the variables employed to describe the photon-inclusive distribution. More precisely, they cancel in the case of the $\{q_0^2, c_0\}$- but not the $\{q^2, c_\ell\}$-variables defined in eq. (2.1).

Our analysis goes well beyond, in terms of accuracy and generality, w.r.t. previous analytical treatments of radiative effects in $M_H \to M_L \ell_1 \bar{\ell}_2$ decays. Still, some open issues remain, as discussed in section 5.1. In particular the matching of the residual UV ambiguities with QCD (which would allow the inclusion of QED effects to the Wilson coefficients [45, 46]) and resolving the photon interaction with the quarks themselves. As we have shown, gauge invariance ensures that such ambiguities cannot induce $\ln m_\ell$-enhanced corrections (section 3.4). This implies, in particular, that these corrections have a negligible impact on the experimental determination of the LFU ratios.

Our analysis indicates that great care must be taken when comparing theoretical with experimental data, given that radiative corrections for the electron modes can easily exceed the 10%-level (as already indicated by previous analyses). As discussed in appendix A.2, the overall impact of QED corrections on integrated LFU ratios, such as R_K, is not too large, especially given the current cuts applied on the reconstructed invariant mass for electron and muon modes [3]. On the other hand, differential observables are subject

[21] Alternatively, one could trade $\bar{p}_B$ with $\bar{p}_{\rm vis} \equiv p_B - k - p_\nu$. The upper cut-off on $\bar{p}_B^2$ is then to be replaced by a lower cut-off on $\bar{p}_{\rm vis}^2$ and the adaption of our formalism requires to work with a finite neutrino mass. It is understood that this approach might be challenging on the numerical side.

JHEP12(2020)104

to potentially larger effects.[22] In particular, as we have shown in section 4.2, a sizeable lepton-non-universal distortion of the dilepton invariant mass spectrum occurs if the latter is expressed in term of the $\{q^2, c_\ell\}$-variables. To overcome this problem the best way to report data is in terms of the of the $\{q_0^2, c_0\}$ distribution (as currently done by most experiments), where the "dangerous" hard-collinear logs ($\ln m_\ell$) cancel at the differential level. In the case of the LHCb experiment, where q_0^2 is not directly measurable, this is done after comparing the results with a Monte Carlo code and correcting for the effect of the QED radiation. In this context, we note that our analysis provides the theoretical groundwork to build a Monte Carlo program with a complete differential treatment of radiative corrections and an accurate parameterisation of the hadronic form-factors (possibly including also long-distance contributions), which represents a key ingredient for a precise comparison between data and theoretical predictions in the future.

Acknowledgments

We would like to thank Andrea Pattori for collaboration at the very early stages of this work. Useful discussion with Melissa van Beekveld, Stefan Dittmaier, Giulio Falcioni, Antonin Portelli, Marek Schönherr, Jennifer Smillie and Gabor Somogyi are acknowledged. RZ and SN are grateful to the UZH and the Pauli Center for the hospitality in Zürich during various stays while working on this project. RZ is supported by an STFC Consolidated Grant, ST/P0000630/1. SN is supported by a Higgs Scholarship and an Edinburgh Global Research Scholarship. GI has received funding from the European Research Council (ERC) under the European Union's Horizon 2020 research and innovation programme under grant agreement 833280 (FLAY), and by the Swiss National Science Foundation (SNF) under contract 200021–175940.

A Additional plots and further numerical results

A.1 The size of hard-collinear logarithms as a function of $\delta_{\rm ex}$ and q^2

It is of interest to investigate the size of the collinear logs. We do this by normalising against the non-radiative differential rate, as done previously in section 4.1,

$$\Delta_{\rm hc}^{(a)}(q_a^2, c_a; \delta_{\rm ex}) = \Delta^{(a)}(q_a^2, c_a; \delta_{\rm ex})\Big|_{\ln \hat{m}_{\ell_{1,2}}} = \left(\frac{d^2\Gamma^{\rm LO}}{dq_a^2 dc_a}\right)^{-1} \frac{d^2\Gamma(\delta_{\rm ex})}{dq_a^2 dc_a}\Big|_{\ln \hat{m}_{\ell_{1,2}}}, \tag{A.1}$$

where the terms on the r.h.s. can be found in eqs. (B.1) and (3.33) respectively. Charged and neutral meson modes are not distinguished as they contain the same collinear divergences as the latter are strictly proportional to the lepton charges, i.e. independent of the hadron charges. Thus, there is only one basic mode of interest for the hard-collinear logs per lepton pair final state. The integrated quantities $\Delta_{\rm hc}^{(a)}(q^2; \delta_{\rm ex})$ and $\Delta_{\rm hc}^{(a)}(c_\ell, [q_1^2, q_2^2]; \delta_{\rm ex})$ are defined in complete analogy to eqs. (4.3) and (4.4) respectively.

[22] Even for total decay rates (non-LFU type) there can be relevant effects such as the $\ln m_K$-logs discussed in section 4.1.

JHEP12(2020)104

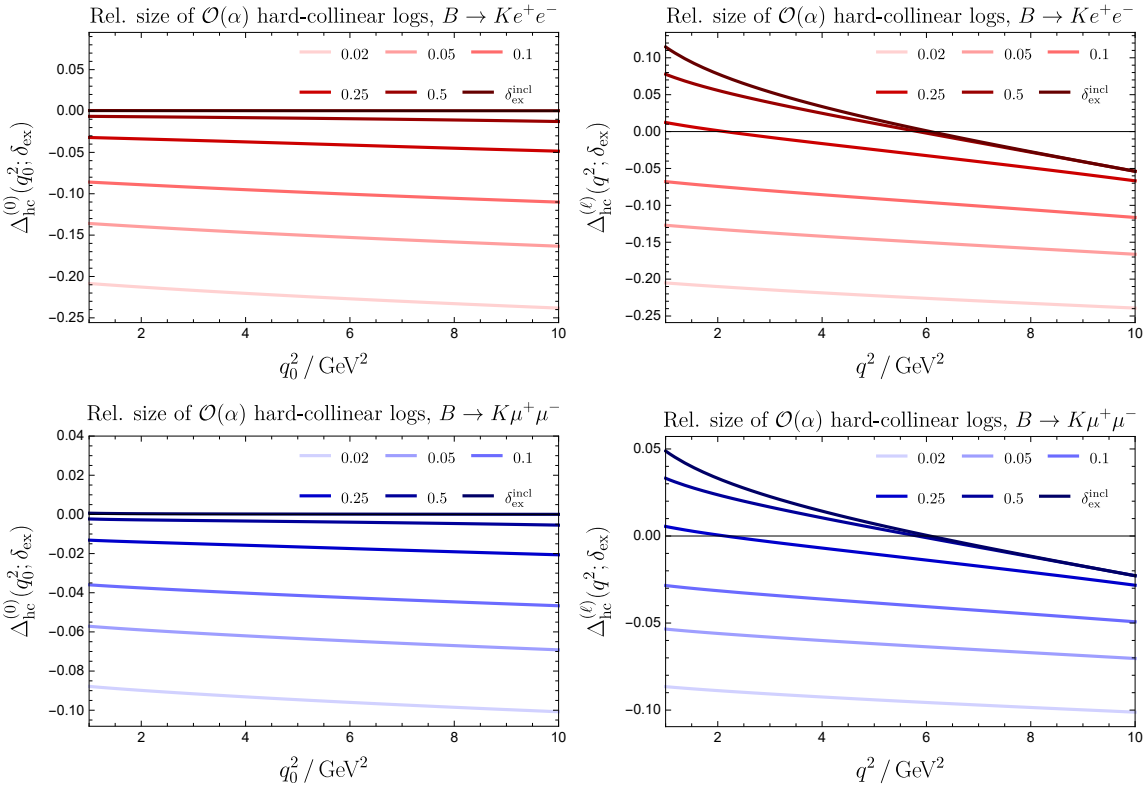

Figure 7. Hard-collinear logs $\Delta_{\rm hc}^{(a)}(q_a^2;\delta_{\rm ex})$ as a function of q_a^2 for the electron and muon (top) and (bottom) respectively. The quantity is shown for various photon energy cut-offs $\delta_{\rm ex}$ (2.4). It is noted that for $\delta_{\rm ex} = \delta_{\rm ex}^{\rm inc}$, the cancellation of the logs can be seen, though not completely, as we only show a restricted interval of q^2. Bottom and top figures are similar by a scaling factor cf. (A.2) and the explanation above it.

Plots of $\Delta_{\rm hc}^{(a)}(q_a^2;\delta_{\rm ex})$ are shown in figure 7 for different photon energy cuts $\delta_{\rm ex}$ (2.4) for electrons and muons with larger effects for the former because of the size of $\ln \hat{m}_e$ versus $\ln \hat{m}_\mu$ logs. In the photon-inclusive case, the cancellation of the hard-collinear logs is visible at the differential level in the q_0^2-variable. For the q^2-variable, the hard-collinear logs cancel when integrated over the entire q^2-interval, the tendency of which can be inferred from the plots on the reduced interval $q^2_{\rm max} < 10\,{\rm GeV}^2$. The reader is reminded that hatted quantities are normalised w.r.t. to the B-mass, $\hat{m}_{\ell_{1,2}} = m_{\ell_{1,2}}/m_B$. Hence one expects

$$R_{\rm hc} = \frac{\Delta_{\rm hc}^{(a)}(q_a^2;\delta_{\rm ex})|_{\bar{B}\to\bar{K}e^+e^-}}{\Delta_{\rm hc}^{(a)}(q_a^2;\delta_{\rm ex})|_{\bar{B}\to\bar{K}\mu^+\mu^-}} \approx \frac{\ln(\hat{m}_e)}{\ln(\hat{m}_\mu)} \approx 2.363\,, \tag{A.2}$$

with corrections of the order of $\mathcal{O}(m_e^2 \ln(\hat{m}_e) - m_\mu^2 \ln(\hat{m}_\mu))$. Inspection of the plots shows that this is indeed the case. We would like to stress that extracting the hard-collinear logs on their own is slightly ambiguous as one needs to normalise them (hatted notation). The unambiguous way to show them is through the full plots in the main text. Nevertheless, they illustrate nicely the effect of the photon energy cut.

JHEP12(2020)104

A.1.1 Comparison of $\bar{B} \to \bar{K}\ell^+\ell^-$ to the inclusive case $b \to s\ell^+\ell^-$

It is interesting to compare our results to the inclusive rate in [46] with regard to the hard-collinear logs. Let us define

$$\Delta^{(\ell)}_{\rm hc}(\hat{q}^2) = \frac{2\alpha\,\hat{Q}^2_{\ell_1}}{\pi}\left(\frac{1}{\Gamma^{\rm LO}}\frac{d\Gamma^{\rm LO}(\hat{q}^2)}{d\hat{q}^2}\right)^{-1}\tilde{\Delta}^{(\ell)}_{\rm hc}(\hat{q}^2)\,, \tag{A.3}$$

where $\hat{Q}^2_{\ell_1} = \hat{Q}^2_{\bar{\ell}_2}$ and $m_{\ell_1} = m_{\ell_2} \equiv m_\ell$ have been assumed. Then, it is known that the collinear logs of the electron can be extracted from (e.g. chapter 17 [47])[23]

$$\tilde{\Delta}^{(\ell)}_{\rm hc}(\hat{q}^2) = \frac{1}{\Gamma^{\rm LO}}\left(\int_{\hat{q}^2}^1 \frac{dz}{z} P_{f\to f\gamma}(z)\frac{d\Gamma^{\rm LO}(\hat{q}^2/z)}{d\hat{q}^2/z}\right)\ln\frac{\Lambda_b}{m_\ell}\,, \tag{A.4}$$

where $\Lambda_b = \mathcal{O}(m_b)$ is some reference scale, $P_{f\to f\gamma}(z)$ is the full leading order splitting function

$$P_{f\to f\gamma}(z) = \frac{1+z^2}{(1-z)_+} + \frac{3}{2}\delta(1-z)\,, \tag{A.5}$$

and $1/(1-z)_+$ is the plus distribution $\int_0^1 dz f(z)/(1-z)_+ = \int_0^1 dz(f(z)-f(1))/(1-z)$. Note that by construction, the hard-collinear logs cancel in the total rate. This can be seen by reversing the order of integration and adopting the change of variable $\hat{q}^2/z = \hat{q}_0^2$ to arrive at $\int_0^1 d\hat{q}^2\tilde{\Delta}^{(\ell)}_{\rm hc}(\hat{q}^2) \propto \int_0^1 dz P_{f\to f\gamma}(z) = 0$. Now, the zeroth moment of the splitting function vanishes since it corresponds to the anomalous dimension of the (conserved) electromagnetic current. Conversely, (A.4) can be deduced from eq. (3.15) by integrating over dc_0, substituting $q_0^2 = q^2/z$ and then integrating over z. From (3.16), the full splitting function is then easily deduced by adding a delta function ansatz $A\delta(1-z)$ and regularising the $1/(1-z)$ such that the soft divergences cancel (which leads to the plus distribution).

The leading order differential rates are given by

$$\frac{1}{\Gamma^{\rm LO}}\frac{d\Gamma^{\rm LO}(\hat{q}^2)}{d\hat{q}^2} = \begin{cases} 2(1-\hat{q}^2)^2(2\hat{q}^2+1) & b\to s\ell^+\ell^- \\ 4(1-\hat{q}^2)^3 & \bar{B}\to\bar{K}\ell^+\ell^- \end{cases}\,, \tag{A.6}$$

where the $m_s \to 0$ limit is implied in [46] and for simplicity we have assumed the $m_K \to 0$ limit and a constant form factor. Note that the factor $\hat{\lambda}_B^{1/2} = \lambda^{1/2}(1,\hat{m}_K^2,\hat{q}^2)|_{m_K\to 0} = 1-\hat{q}^2$ is the square root of the Källén-function and as such related to the three velocity of the strange particle in the B-meson's RF. Its power in the rate is determined by the interaction and the spin of the particle (e.g. if it were $\bar{B}\to\bar{K}^*\ell^+\ell^-$ then $d\Gamma^{\rm LO}\propto(1-\hat{q}^2)$ [48]). The

[23] From section 5 in [46], one can extract a similar formula for the collinear logs

$$\tilde{\Delta}^{(\ell)}_{\rm hc}(\hat{q}^2) = \frac{1}{\Gamma^{\rm LO}}\left(\int_{\hat{q}^2}^1 \frac{dz}{z}\tilde{P}_{f\to f\gamma}(z)\frac{d\Gamma^{\rm LO}(\hat{q}^2/z)}{d\hat{q}^2/z} - \int_0^1 dz\tilde{P}_{f\to f\gamma}(z)\frac{d\Gamma^{\rm LO}(\hat{q}^2)}{d\hat{q}^2}\right)\ln\frac{\Lambda_b}{m_\ell}\,,$$

where $\tilde{P}_{f\to f\gamma}(z)$ (3.16) is the collinear emission part of the splitting function. Soft divergences at $z\to 1$ cancel between the two integrals. Translating into our notation from [46] demands $x = 1-z$, $\hat{s} = \hat{q}^2$ and $\tilde{P}_{f\to f\gamma}(z)$ is the part collinear in $f_\gamma^{(m)}$ up to factors of proportionality properly accounted for. Our formula (A.4) can be recovered upon using that $\int dz P_{f\to f\gamma}(z) = 0$.

JHEP12(2020)104

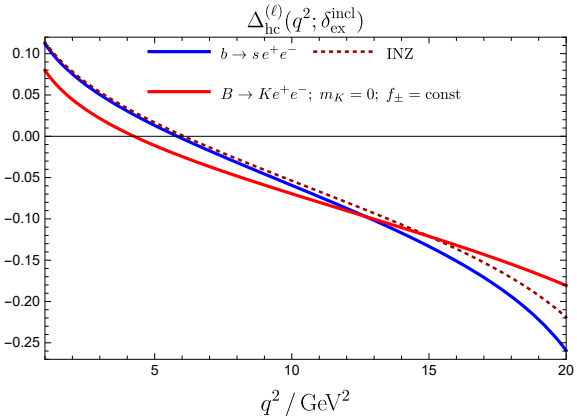

Figure 8. Comparison of hard-collinear logs in $b \to se^+e^-$ (solid blue line) versus $\bar{B} \to \bar{K}e^+e^-(\gamma)$ with no photon energy cut, constant form factors and $m_K \to 0$ (solid red line) corresponding to eqs. (A.7). This illustrates the spin-dependance of the hard-collinear which can be traced back to the LO differential rates in the case at hand cf. (A.6). For further comparison, we have added the full result in the dotted red line for this paper with no photon energy cut either. The agreement at low q^2 of the latter with the $b \to se^+e^-$ is somewhat accidental.

factor $2\hat{q}^2 + 1$ originates from the s-quark's spin summation. One finds

$$\tilde{\Delta}_{\rm hc}^{b\to s\ell^+\ell^-}(s) = 2\left(\left(6s^2-4s^3-1\right)\ln s + 2\,(1-s)^2\,(2s+1)\ln(1-s) + \frac{12s^2-8s^3-3s-1}{3}\right),$$

$$[5pt]\,\tilde{\Delta}_{\rm hc}^{\bar{B}\to\bar{K}\ell^+\ell^-}(s) = 4\left(\left(2s^3-6s^2+3s-1\right)\ln s + 2\,(1-s)^3\ln(1-s) + \frac{4s^3-6s^2+6s-6}{3}\right). \quad \text{(A.7)}$$

The basic form is similar in both cases and we observe the $\ln q^2$-term leading to enhanced collinear emission at low q^2 which can be interpreted as a migration of the photon radiation cf. section 4.2. We wish to stress again that $\tilde{\Delta}_{\rm hc}^{\bar{B}\to\bar{K}\ell^+\ell^-}$ receives corrections due to finite m_K and non-constant form factor and that $\delta_{\rm ex} = \delta_{\rm ex}^{\rm inc}$ was assumed. Both of these features are included in the comparison plot figure 8. We have checked that integrating (3.33) over $\int_{-1}^{1} dc_\ell$ reproduces the $\tilde{\Delta}_{\rm hc}^{\bar{B}\to\bar{K}\ell^+\ell^-}$-expression in (A.7). This comparison provides another non-trivial cross-check of our analysis.

A.2 Comparison with earlier work on $\bar{B} \to \bar{K}\ell^+\ell^-$

We compare our results to those presented in [6]. The analysis of [6], which first investigated the impact of LFU breaking in $\bar{B} \to \bar{K}\ell^+\ell^-$ induced by QED corrections, is a simplified analysis based on the following three principles/assumptions:

i. indirect determination of virtual corrections by imposing the absence of log-enhanced terms in the photon-inclusive $d\Gamma/dq_0^2$ spectrum (for any value of q_0^2);

ii. constructing a radiator function depending on q^2 and q_0^2 only, which describs the probability of a dilepton pair (of invariant mass q^2) to originate from momentum transfer q_0^2, after photon-emission;

JHEP12(2020)104

iii. neglecting lepton-flavour universal radiative corrections, such as those induced by the emissions from meson legs only.

As proved in general terms in this paper, assumption i. is correct and provides an efficient way to determine the radiator function. Our analysis shows that the non-log enhanced terms are small in the neutral-meson case (as shown in figure 4). They do exceed the 1% level in the charged-meson case, but this is a lepton-flavour universal effect.

On the other hand, while assumption ii. is a legitimate choice, it is incompatible with the goal of estimating radiative corrections implementing only a cut on the reconstructed B-meson mass:[24] the radiator in [6] is obtained by integrating over all photon angles; however, as already discussed in 4.2, in the B-RF the relation connecting q_0^2 and q^2 does not only depend on $m_B^{\rm rec}$ but also on the photon's emission angle. To overcome this problem, in [6] the maximal q_0^2 value affecting the spectrum at a given q^2 value has been determined imposing the tight cut defined in (4.7). This choice corresponds to the *minimal* value of $(q_0^2)_{\rm max}$ obtainable with an experimental cut on photons not emitted forward with respect to $\vec{q}$ (in the B-RF). Incidentally, we note that a cut of this type is implemented in the experimental analysis to avoid a large migration effect (e.g. charmonium resonances at low q^2, cf. section 4.2). This is the most important difference among the two approaches. As illustrated in figure 9, the net effect is quite sizeable, especially for the electrons at low values of q^2.

In practice, the implicit cut applied in [6] on the photon-emission angle removes some hard-collinear logs. We may track the difference on the collinear logs analytically. We demonstrate this for the q_0^2-spectrum since the expression (3.21) is much simpler than the corresponding one for q^2 in (3.30). Let us consider

$$\frac{d\Gamma}{dq_0^2} = \frac{\alpha}{\pi}\left[\frac{d\Gamma}{dq_0^2}\right]^{\rm LO}\left(A_0 \ln\delta_{\rm ex} + C_0\right)\ln m_\ell + \text{non-collinear}\,. \tag{A.8}$$

The coefficients A_0 and C_0 are obtained by integrating eq. (9) — using the boundary conditions implied by eq. (10) of [6] — w.r.t. to x (which is our z and moreover $1-\delta^2 = \delta_{\rm ex}$), and the expression in (3.21) with $z(\omega_s) \to 1$ but finite $\delta_{\rm ex}$. Not surprisingly, we find

$$A_0 = A_0^{\rm INZ} = A_0^{\rm BIP} = -4\,. \tag{A.9}$$

This is the universal coefficient of the soft-collinear singularity (double log), which is independent of the boundary conditions. Incidentally, we note that this coefficient is also the same for the $\frac{d\Gamma}{dq^2}$-distribution. Low's theorem guarantees that the single $\ln\delta_{\rm ex}$-term is identical. For the C_0 term, however, there are differences

$$\begin{aligned} C_0^{\rm INZ} &= -\frac{25}{3} + 2\ln\hat{q}_0^2 + 2\frac{(1-\hat{m}_K^2+\hat{q}_0^2)^2}{\hat{\lambda}} - R\ln\left[\frac{1-\hat{m}_K^2+\hat{q}_0^2-\hat{\lambda}^{1/2}}{1-\hat{m}_K^2+\hat{q}_0^2+\hat{\lambda}^{1/2}}\right] + \mathcal{O}(\delta_{\rm ex}) \\ C_0^{\rm BIP} &= \left(-3 - 4\ln\left[1+\frac{\hat{m}_K^2}{1-\hat{q}_0^2}\right]\right) + \mathcal{O}(\delta_{\rm ex})\,, \end{aligned} \tag{A.10}$$

[24] We note that a radiator function depending on q^2 and q_0^2 only is sufficient to estimate the distortion of the q^2 spectrum in the absence of a photon-energy cut, as for instance done in Higgs-collider physics [49].

JHEP12(2020)104

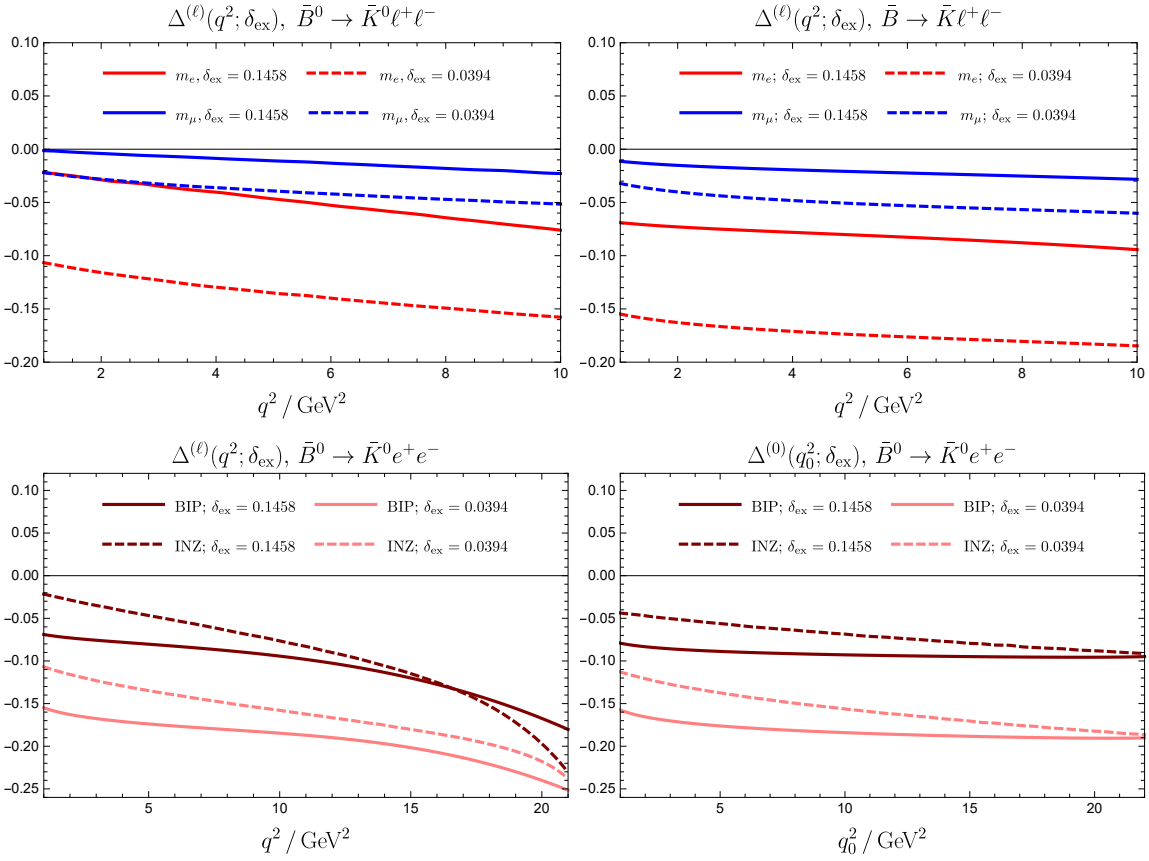

Figure 9. Relative effects of relative corrections as a function of q^2, in the neutral case, with the cuts on $m_B^{\rm rec}$ used in [6] computed in this work (top left) vs. those presented in [6] (top right). The bottom left and bottom right plots compare our results with those in [6] for the q^2 and q_0^2-spectrum respectively. The translation between the notation of this reference and ours is $\delta_{\rm ex} = 1-(m_B^{\rm rec}/m_B)^2$ with $(\bar{p}_B = m_B^{\rm rec})$ and $\{0.1458, 0.1, 0.0394\} \leftrightarrow m_B^{\rm rec} = \{4.88, 5.009, 5.175\}$ GeV.

where $\hat{\lambda} \equiv \lambda(1, \hat{m}_K^2, \hat{q}_0^2)$ and

$$R = 2(1+\hat{q}_0^2-\hat{m}_K^2)\left(\frac{1}{\hat{\lambda}^{1/2}} - \frac{2\hat{q}_0^2}{\hat{\lambda}^{3/2}}\right). \tag{A.11}$$

Note that in [6], only the leading term in m_K^2 was kept in $(q_0^2)_{\rm max}$ and thus, for meaningful comparison, one has to assume the $m_K \to 0$ limit

$$\begin{aligned} C_0^{\rm INZ} &= -\frac{19}{3} + 8\frac{\hat{q}_0^2}{(1-\hat{q}_0^2)^2} + 4\frac{(3-\hat{q}_0^2)}{(1-\hat{q}_0^2)^3}\hat{q}_0^4 \ln\hat{q}_0^2 + \mathcal{O}(\delta_{\rm ex}) \overset{\hat{q}_0^2\to 1}{\longrightarrow} -3 + \mathcal{O}(\delta_{\rm ex}) + \mathcal{O}(\hat{q}_0^2-1) \\ C_0^{\rm BIP} &= -3 + \mathcal{O}(\delta_{\rm ex})\,. \end{aligned} \tag{A.12}$$

Agreement is found at the kinematic endpoint $\hat{q}_0^2 \to 1$ (including $\mathcal{O}(\delta_{\rm ex})$-terms). This is to be expected since the cut on $(q_0^2)_{\rm max}$ is independent of the photon-emission angle, whereas differences are maximal at low q_0^2 values, consistent with the numerical findings in figure 9 (bottom-right).

JHEP12(2020)104

To better understand the agreement at large $\hat{q}_0^2$ illustrated in (A.12), consider (3.18), with $\delta = \delta_{\rm ex}$, which corresponds to the case where the photon becomes collinear with ℓ_1. With a non-zero Kaon mass, $(\hat{q}_0^2)_{\rm max} = (1-\hat{m}_K)^2$, and thus the lower limit for the z-integration becomes

$$z_{\rm INZ}(\delta_{\rm ex}, (\hat{q}_0^2)_{\rm max}, c_0) = 1 - \frac{\delta_{\rm ex}}{1-\hat{m}_K}\,, \tag{A.13}$$

where the c_0-dependence drops (and thus the same z limit applies for ℓ_2). Now, consider $q_0^2 = q^2 + m_B \delta_{\rm ex}(E_{q_0}^{(1)} + |\vec{q}_0^{\,(1)}| \cos\theta_\gamma^{(1)})$, which is the defining principle behind eq. (10) of [6], where $E_{q_0}^{(1)}$ and $|\vec{q}_0^{\,(1)}|$ are given in (C.8). Substituting $q^2 = z q_0^2$, one gets

$$z_{\rm BIP} = 1 - \frac{m_B\,\delta_{\rm ex}}{q_0^2}(E_{q_0}^{(1)} + |\vec{q}_0^{\,(1)}| \cos\theta_\gamma^{(1)}) \overset{\hat{q}_0^2 \to (\hat{q}_0^2)_{\rm max}}{\longrightarrow} 1 - \frac{\delta_{\rm ex}}{1-\hat{m}_K}, \tag{A.14}$$

which matches (A.13). This explains the agreement at large $\hat{q}_0^2$ in (A.12) and in figure 9. Note that the $\theta_\gamma^{(1)}$ dependence drops in the limit of $\hat{q}_0^2 \to (\hat{q}_0^2)_{\rm max}$, analogous to the c_0 dependence in (A.13). The c_0-independence (or equivalently $\theta_\gamma^{(1)}$) at $(\hat{q}_0^2)_{\rm max}$ happens since the Kaon's three-momentum vanishes and the (1)- and (4)-RF become equivalent and thus, there cannot be any non-trivial angular dependance.

On the other hand, the same argument does *not* apply to the differential rate in q^2. As $q^2 \to q^2_{\rm max}$, the range of allowed photon energies becomes more and more restricted. The cut $\bar{p}_B^2 > m_B^2(1-\delta_{\rm ex})$ on its own is independent of q^2, and it is for this reason that one needs the maximum condition imposed on the lower limit of the z-integration in (3.30). For larger q^2, the kinematic restriction on z, denoted by $z_{\rm inc}$, becomes more important than the restriction on z due to the photon energy cut $\delta_{\rm ex}$. This is why the two INZ-curves in the bottom left plot in figure 9 approach each other for large q^2.

In summary, from the comparison of our work with [6] we may deduce the following two lessons or insights.

a) The indirect determination of virtual logs in the photon-inclusive $d\Gamma/dq_0^2$-spectrum, which is the key assumption behind both the approach of ref. [6] and PHOTOS [5], is correct.

b) A meaningful comparison between theory and experiment (in a collider environment) cannot be done by only considering the two non-radiative variables $(\{q_a^2, c_a\})$ and the cut on the reconstructed B-meson mass, but it requires a detailed information on the (inevitable) photon-emission angle cut as their impact is sizeable.

Whereas point a) is reassuring in view of the current treatment of R_K, point b) indicates the necessity to build a Monte Carlo program with a complete differential treatment of radiative corrections and an accurate parameterisation of the hadronic form factors (with the effective inclusion of long-distance effects, which we recall are *not* included in PHOTOS), in order to check the impact of the QED corrections on the kinematical distributions at the %-level, with the explicit cuts applied in experiments. This task, for which this paper lays the groundwork, is devoted to a future publication.

JHEP12(2020)104

B Explicit results of the computation

B.1 Leading order differential rate

The leading order amplitude rate is easily computed from (2.29) and the amplitude $\mathcal{A}^{(0)}_{\bar{B}\to\bar{K}\ell_1\bar{\ell}_2}$ (2.11) and is rather simple

$$\frac{d^2}{dq^2 dc_\ell}\Gamma^{\rm LO}(q^2,c_\ell) = \frac{\rho_\ell|_{\bar{p}_B^2\to m_B^2}}{m_B}|\mathcal{A}^{(0)}|^2 = \; 2|g_{\rm eff}|^2\frac{\rho_\ell|_{\bar{p}_B^2\to m_B^2}}{m_B}\times$$

$$\Big[|C_V|^2\Big(\lambda_B f_+(q^2)^2(1-(\Delta\bar{m}_\ell)^2-\frac{\lambda_\ell}{q^4}c_\ell^2)\; + (\Delta m_{BK}^2)^2(\Delta\bar{m}_\ell)^2 f_0(q^2)^2(1-\bar{m}_{\ell_1\ell_2}^2)$$

$$- 2\Delta\bar{m}_{BK}^2\,\bar{m}_{\ell_1\ell_2}\,\Delta\bar{m}_\ell\, f_0(q^2)f_+(q^2)\lambda_B{}^{1/2}\lambda_\ell^{1/2}c_\ell\Big) + |C_A|^2\Big(\bar{m}_{\ell_1\ell_2}\leftrightarrow\Delta\bar{m}_\ell\Big)\Big]\,, \tag{B.1}$$

where $\lambda_\ell = \lambda(q^2,m_{\ell_1}^2,m_{\ell_2}^2)$, $\Delta\bar{m}_\ell = \bar{m}_{\ell_1}-\bar{m}_{\ell_2}$, $\bar{m}_{\ell_1\ell_2} = \bar{m}_{\ell_1}+\bar{m}_{\ell_2}$, $\Delta m_{BK}^2 = m_B^2-m_K^2$, with ρ_ℓ as in (2.24), and all barred quantities are dimensionless by division with q. In the limit of equal lepton masses ($m_{\ell_1}=m_{\ell_2}\equiv m_\ell$), the above equation reduces to

$$\frac{d^2}{dq^2 dc_\ell}\Gamma^{\rm LO}(q^2,c_\ell) = 2|g_{\rm eff}|^2\frac{\rho_\ell|_{\bar{p}_B^2\to m_B^2}}{m_B}\Big(|C_V|^2(\lambda_B f_+(q^2)^2(1-\beta_\ell^2c_\ell^2))+ \tag{B.2}$$

$$|C_A|^2(\lambda_B f_+(q^2)^2(1-c_\ell^2)\beta_\ell^2+4f_0(q^2)^2\bar{m}_\ell^2(\Delta m_{BK}^2)^2)\Big)\,,$$

with $\beta_\ell=\sqrt{1-4m_\ell^2/q^2}$ and $\lambda_B=\lambda(m_B^2,q^2,m_K^2)$.

B.2 Virtual amplitude $\mathcal{A}^{(2)}_{\bar{B}\to\bar{K}\ell_1\bar{\ell}_2}$

As the computation of the QED corrections including the tower of operators (2.7) is anew, to the best of our knowledge, we present the explicit amplitudes prior to integration. The $B, K_{L_{1,2}}$ and $P_{L_{12}}$ and $P_{B,K}$ graphs are non-trivially amended. This is true in particular for the P-graphs.

The BL_{12}-graphs read

$$\mathcal{A}^{(2)}_{BL_{1,2}} = ig_{\rm eff}\hat{Q}_{\bar{B}}e^2\int_k(2p_B+k)^\nu\Delta_{\nu\rho}(k)\Delta_B(l)\tilde{H}_0^{\mu(B)}(q_0^2)\bar{u}(\hat{Q}_{\ell_1}\gamma^\rho S_1(r)\Gamma_\mu-\hat{Q}_{\bar{\ell}_2}\Gamma_\mu S_2(r)\gamma^\rho)v\,,$$

with shorthands $\bar{u}\equiv\bar{u}(\ell_1)$, $v\equiv v(\ell_2)$, $(2\pi)^4\int_k=\int d^4k$, momentum assignments $(r,l)=(\pm[\ell_1(\ell_2)+k],p_B+k)$, with notation borrowed from the real emission case (cf. below (2.13)),

$$f_\pm(q_0^2)=\sum_{n\geq0}\frac{f_\pm^{(n)}(0)}{n!}(q_0^2)^n\,,\quad P_n\equiv P_n(q^2,q_0^2)=\sum_{m=0}^n(q^2)^{(n-m)}(q_0^2)^m\,, \tag{B.3}$$

with $q_0=q+k$ and k being the loop integration momentum k. Moreover $\tilde{H}_0^{(B)}(q_0^2)=H_0(q_0^2)|_{p_B\to p_B+k}$, and the q_0^2 in the argument indicates that the form factor is to be expanded as above and propagators are given by

$$\Delta_M(k)=\frac{1}{k^2-m_M^2}\,,\quad S_i(k)=\frac{\not{k}+m_{\ell_i}}{k^2-m_{\ell_i}^2}\,,\quad \Delta_{\mu\nu}(k)=-\frac{g_{\mu\nu}}{k^2}+(1-\xi)\frac{k_\mu k_\nu}{k^4}\,. \tag{B.4}$$

JHEP12(2020)104

The $KL_{1,2}$-graphs are analogous

$$\mathcal{A}^{(2)}_{KL_{1,2}} = -ig_{\text{eff}}\hat{Q}_{\bar{K}}e^2\int_k (2p_K - k)^\nu \Delta_{\nu\rho}(k)\Delta_K(l)\tilde{H}_0^{\mu(K)}(q_0^2)\bar{u}(\hat{Q}_{\ell_1}\gamma^\rho S_1(r)\Gamma^\mu - \hat{Q}_{\bar{\ell}_2}\Gamma^\mu S_2(r)\gamma^\rho)v\,,$$

where $(r,l) = (\pm[\ell_1(\ell_2)+k], p_K - k)$ and $\tilde{H}_0^{(K)}(q_0^2) = H_0(q_0^2)|_{p_K\to p_K-k}$. The $PL_{1,2}$ and $P_{B,K}$ graphs read

$$\mathcal{A}^{(2)}_{PL_{1,2}} = -ig_{\text{eff}}e^2\int_k F^{L_{1,2}}_{\mu\rho}\bar{u}(\hat{Q}_{\ell_1}\gamma^\rho S_1(r)\Gamma_\mu - \hat{Q}_{\bar{\ell}_2}\Gamma_\mu S_2(r)\gamma^\rho)v\,, \tag{B.5}$$

$$\mathcal{A}^{(2)}_{P_{B,K}} = ig_{\text{eff}}e^2 L_0^\mu\int_k \hat{Q}_{\bar{B}}F^B_{\mu\rho}\,\Delta_B(p_B+k)(2p_B+k)^\rho - \hat{Q}_{\bar{K}}\,F^K_{\mu\rho}\,\Delta_K(p_K-k)(2p_K-k)^\rho\,,$$

with $r = \pm(\ell_1(\ell_2)+k)$, L_0 defined in (2.12) and the loop momentum k enters the expressions

$$F^{L_{1,2}}_{\mu\rho} = F_{\mu\rho}(p_B, p_K, q_0^2)\,,\quad F^B_{\mu\rho} = F_{\mu\rho}(p_B+k, p_K, q^2)\,,\quad F^K_{\mu\rho} = F_{\mu\rho}(p_B, p_K-k, q^2)\,,$$

where the common functional form $F_{\mu\rho}$ is given by

$$\begin{aligned}F_{\mu\rho}(p_B,p_K,q^2) &= (\hat{Q}_{\bar{B}}\mp\hat{Q}_{\bar{K}})\Delta_{\mu\rho}(k)f_\pm(q^2)\\ &\quad + (\hat{Q}_{\bar{B}}+\hat{Q}_{\bar{K}})(p_B\pm p_K)_\mu(q+q_0)^\nu\Delta_{\nu\rho}(k)\sum_{n\geq 1}\frac{f_\pm^{(n)}(0)}{n!}P_{n-1}\,.\end{aligned} \tag{B.6}$$

The BK-vertex correction is given by

$$\mathcal{A}^{(2)}_{BK} = ig_{\text{eff}}\hat{Q}_{\bar{B}}\hat{Q}_{\bar{K}}e^2\int_k (2p_B-k)^\beta\Delta_{\beta\kappa}(k)(2p_K-k)^\kappa L_0\cdot\tilde{H}_0^{(BK)}\,\Delta_B(l)\Delta_K(r)\,,$$

where $l = (p_B - k)$ and $r = (p_K - k)$ and $\tilde{H}_0^{(BK)} = H_0(q^2)|_{(p_B,p_K)\to(p_B-k,p_K-k)}$. The lepton vertex correction, which can be found in many textbooks, reads

$$\mathcal{A}^{(2)}_{L_1L_2} = ig_{\text{eff}}\hat{Q}_{\ell_1}\hat{Q}_{\bar{\ell}_2}e^2H_0^\mu(q^2)\int_k \Delta_{\alpha\beta}(k)\,\bar{u}\gamma^\alpha S_1(l)\Gamma_\mu S_2(r)\gamma^\beta v\,, \tag{B.7}$$

with $l = k + \ell_1-$ and $r = k - \ell_2$.

B.3 Gauge invariance of the real amplitude $\mathcal{A}^{(1)}_{\bar{B}\to\bar{K}\ell_1\bar{\ell}_2\gamma}$

The real amplitude is given in eq. (2.13). Explicit verification of gauge invariance of this amplitude is instructive. In essence, we will flesh out the steps described at the end of section 2.2. Gauge invariance follows from the charge conservation (2.14) and inspecting the four terms in (2.13), it is far from obvious how this will work out since the individual terms depend on the hadronic form factor in a non-uniform way e.g. $\hat{Q}_{\bar{\ell}_2,\ell_1}H_0(q_0^2)$, $\hat{Q}_{B,K}\bar{H}^{(B,K)}(q^2),\ldots$. A special rôle is played by the contact terms arising from diagram P in figure 2. From the viewpoint of the effective Lagrangian, these terms arise from replacing ordinary derivatives with covariant ones and from the viewpoint of the Ward identity, they are induced by the derivatives acting on the U(1) gauge transformation.

JHEP12(2020)104

At first, we consider lines two and three of the amplitude

$$\begin{aligned}\mathcal{A}_{23}^{(1)} &\propto \hat{Q}_{\bar{B}}\, L_0{\cdot}\bar{H}_0^{(B)}(q^2)\frac{\epsilon^*{\cdot}p_B}{k{\cdot}p_B} \;+\hat{Q}_{\bar{K}}\, L_0{\cdot}\bar{H}_0^{(K)}(q^2)\frac{\epsilon^*{\cdot}p_K}{k{\cdot}p_K}\\ &\quad+(\hat{Q}_{\bar{B}}-\hat{Q}_{\bar{K}})\, L_0{\cdot}\epsilon^*\, f_+(q^2)+(\hat{Q}_{\bar{B}}+\hat{Q}_{\bar{K}})\, L_0{\cdot}\epsilon^*\, f_-(q^2)\\ &\overset{\epsilon\to k}{\to}(\hat{Q}_{\bar{B}}+\hat{Q}_{\bar{K}})L_0{\cdot}H_0(q^2)\,,\end{aligned}\tag{B.8}$$

and notice that a gauge transformation combines these two parts into an expression which will combine with the first line

$$\begin{aligned}\mathcal{A}_1^{(1)} &\propto \bar{u}(\ell_2)\left[\hat{Q}_{\ell_1}\,\frac{2\epsilon^*{\cdot}\ell_1+\not{\epsilon}^*\not{k}}{2k{\cdot}\ell_1}\Gamma{\cdot}H_0(q_0^2)+\hat{Q}_{\bar{\ell}_2}\,\Gamma{\cdot}H_0(q_0^2)\frac{2\epsilon^*{\cdot}\ell_2+\not{k}\not{\epsilon}^*}{2k{\cdot}\ell_2}\right]v(\ell_1)\\ &\overset{\epsilon\to k}{\to}(\hat{Q}_{\bar{\ell}_2}+\hat{Q}_{\ell_1})L_0{\cdot}H_0(q_0^2)\,,\end{aligned}\tag{B.9}$$

except that the argument of the form factors is q_0^2 in one case and q^2 in the other case. This is remedied, of course, by the fourth line

$$\begin{aligned}\mathcal{A}_4^{(1)} &\propto (\hat{Q}_{\bar{B}}+\hat{Q}_{\bar{K}})L_0{\cdot}(p_B\pm p_K)(2\epsilon^*{\cdot}q)\sum_{n\geq 1}\frac{f_\pm^{(n)}(0)}{n!}P_{n-1}\\ &\overset{\epsilon\to k}{\to}(\hat{Q}_{\bar{B}}+\hat{Q}_{\bar{K}})L_0{\cdot}(p_B\pm p_K)\sum_{n\geq 1}\frac{f_\pm^{(n)}(0)}{n!}\Delta_q^{2n}\\ &=(\hat{Q}_{\bar{B}}+\hat{Q}_{\bar{K}})L_0{\cdot}(H_0(q_0^2)-H_0(q^2))\,,\end{aligned}\tag{B.10}$$

which follows from $\Delta_q^2=2q{\cdot}k$ and $\Delta_q^2P_{n-1}=\Delta_q^{2n}$ and $\Delta_q^{2n}\equiv(q_0^2)^n-(q^2)^n$ as before. Adding them all together, one obtains

$$\mathcal{A}^{(1)}|_{\epsilon\to k}\propto L_0{\cdot}H_0(q_0^2)\sum_i\hat{Q}_i=0\,,\tag{B.11}$$

the explicit gauge invariance of the real amplitude.

B.4 Cancellation of hard-collinear logs charge by charge

Whereas for the cancellation of soft divergences charge conservation was not assumed, this is not true for the hard-collinear logs $\ln m_\ell$ cf. section 3.3.2. The aim of this appendix is to show that this assumption is unnecessary, i.e. that hard-collinear logs cancel charge by charge combination. Charge conservation is though necessary for gauge invariance or conversely imposing gauge invariance implies charge conservation. Using charge conservation can still be convenient such as for the photon-inclusive hard-collinear log formula (A.4).

First, we focus on the soft contribution $\mathcal{F}^{(s)}(\omega_s)|_{\ln m_{\ell_1}}\equiv\sum_{i,j}\hat{Q}_i\hat{Q}_j\mathcal{F}_{ij}^{(s)}(\omega_s)|_{\ln m_{\ell_1}}$ to the hard-collinear log. In the limit of $m_{\ell_1}\to 0$, using eqs. (D.8), (D.9), (D.10), (D.17) and (D.19), one gets

$$\mathcal{F}^{(s)}(\omega_s)|_{\ln m_{\ell_1}}=\ln m_{\ell_1}\left[-\hat{Q}_{\ell_1}^2+2\hat{Q}_{\ell_1}\left(\hat{Q}_{\bar{\ell}_2}+\hat{Q}_{\bar{B}}+\hat{Q}_{\bar{K}}\right)\ln\bar{z}(\omega_s)\right],\tag{B.12}$$

JHEP12(2020)104

where we have used $\bar{z}(\omega_s) = \frac{\omega_s m_B}{2E_{\ell_1}}$, as explained below eq. (D.19). Next, the virtual contribution, $\tilde{\mathcal{H}}|_{\ln m_{\ell_1}} \equiv \sum_{i,j} \hat{Q}_i \hat{Q}_j \left(\tilde{\mathcal{H}}_{ij}^{(s)} + \tilde{\mathcal{H}}_{ij}^{(hc)}\right)\Big|_{\ln m_{\ell_1}}$, using eqs. (2.18), (3.5) and (3.10), is given by

$$\tilde{\mathcal{H}}|_{\ln m_{\ell_1}} = \ln m_{\ell_1} \left[\frac{3}{2}\hat{Q}_{\ell_1}^2 + 2\hat{Q}_{\ell_1}\left(\hat{Q}_{\bar{\ell}_2} + \hat{Q}_{\bar{B}} + \hat{Q}_{\bar{K}}\right)\right]. \tag{B.13}$$

Moreover, $\mathcal{F}^{(hc)}(\underline{\delta})|_{\ln m_{\ell_1}} \equiv \sum_{i,j} \hat{Q}_i \hat{Q}_j \mathcal{F}_{ij}^{(hc)}(\underline{\delta})|_{\ln m_{\ell_1}}$ is given by

$$\mathcal{F}^{(hc)}(\underline{\delta})|_{\ln m_{\ell_1}} = \ln m_{\ell_1} \left[-\frac{1}{2}\hat{Q}_{\ell_1}^2 - 2\hat{Q}_{\ell_1}\left(\hat{Q}_{\bar{\ell}_2} + \hat{Q}_{\bar{B}} + \hat{Q}_{\bar{K}}\right)(1 + \ln \bar{z}(\omega_s))\right]. \tag{B.14}$$

In obtaining (B.14), we followed the procedure in section 3.3.2 without using charge conservation in eq. (3.15).

Finally, adding the three contributions, one finds (with ordering as above)

$$\begin{aligned}\left[\mathcal{F}^{(s)}(\omega_s) + \tilde{\mathcal{H}} + \mathcal{F}^{(hc)}(\underline{\delta})\right]\Big|_{\ln m_{\ell_1}} &= [2\ln \bar{z}(\omega_s) + 2 - 2(1 + \ln \bar{z}(\omega_s))] \cdot \hat{Q}_{\ell_1}(\hat{Q}_{\bar{\ell}_2} + \hat{Q}_{\bar{B}} + \hat{Q}_{\bar{K}}) \\ &\quad + \left[-1 + \frac{3}{2} - \frac{1}{2}\right] \cdot \hat{Q}_{\ell_1}^2 = 0\,,\end{aligned} \tag{B.15}$$

that the hard-collinear cancel charge by charge (without the need for charge conservation).

C Kinematics and other conventions

In this section, we collect a few conventions used throughout the paper to improve readability. We make use of the abbreviation $c_a = \cos\theta_a$ and $s_a = \sin\theta_a$ where the label a stands either for ℓ or 0 and its meaning on the main kinematic variables is depicted in (2.1). The matrix elements $\langle 0|B^\dagger(x)|\bar{B}(p_B)\rangle = e^{-ip_B\cdot x}$, $\langle K(p_K)|K^\dagger(x)|0\rangle = e^{ip_K\cdot x}$ provide the link to the mesonic states $\bar{B}$ and $\bar{K}$ of valence quarks b and s. Whenever there is no ambiguity, we use $p = \sqrt{p^2}$ and hatted quantities are understood to be divided by m_B in order to render them dimensionless e.g. $\hat{q}^2 \equiv q^2/m_B^2$. We use dimensional regularisation with $d = 4 - 2\epsilon$.

C.1 Kinematics in terms of the $\{q^2, \theta_\ell\}$-variables

The main frame is the $\bar{p}_B$-RF, which will serve to define the photon energy cut-off. In this frame, the momenta are parametrised as follows[25]

$$\begin{aligned}k^{(2)} &= (E_\gamma^{(2)}, -\cos\theta_\gamma|\vec{k}_\gamma^{(2)}|, -\sin\theta_\gamma\cos\phi_\gamma|\vec{k}_\gamma^{(2)}|, -\sin\theta_\gamma\sin\phi_\gamma|\vec{k}_\gamma^{(2)}|)\,,\\ \bar{p}_B^{(2)} &= (\bar{p}_B, 0, 0, 0)\,, \quad q^{(2)} = (\bar{p}_B - p_K)^{(2)} = (\bar{p}_B - E_K^{(2)}, |\vec{p}_K|, 0, 0) = (E_q^{(2)}, |\vec{p}_K|, 0, 0)\,,\\ p_K^{(2)} &= (E_K^{(2)}, -|\vec{p}_K|, 0, 0)\,,\end{aligned} \tag{C.1}$$

[25] All four-momenta are understood with lower Lorentz indices e.g. $(k^{(2)})_\mu$. It is understood that $\theta_\gamma \equiv \theta_\gamma^{(2)}, \phi_\gamma \equiv \phi_\gamma^{(2)}$ for brevity. If the angles do not refer to the (2)-frame, then they will be indicated.

JHEP12(2020)104

where

$$E_K^{(2)} = \sqrt{|\vec{p}_K^{(2)}|^2 + m_K^2} = \frac{1}{2\bar{p}_B}(\bar{p}_B^2 - q^2 + m_K^2)\,, \qquad |\vec{p}_K^{(2)}| = \frac{\lambda^{1/2}(\bar{p}_B^2, q^2, m_K^2)}{2\bar{p}_B}\,,$$
$$E_\gamma^{(2)} = \sqrt{|\vec{k}_\gamma^{(2)}|^2 + m_\gamma^2} = \frac{1}{2\bar{p}_B}\left(m_B^2 - \bar{p}_B^2 - m_\gamma^2\right)\,, \quad |\vec{k}_\gamma^{(2)}| = \frac{\lambda^{1/2}(\bar{p}_B^2, m_B^2, m_\gamma^2)}{2\bar{p}_B}\,,$$
$$E_q^{(2)} = \sqrt{|\vec{p}_K^{(2)}|^2 + q^2} = \frac{1}{2\bar{p}_B}(\bar{p}_B^2 + q^2 - m_K^2)\,, \tag{C.2}$$

consistent with $\bar{p}_B - E_K^{(2)} = E_q^{(2)}$. The Källén function,

$$\lambda(s, m_1^2, m_2^2) = (s - (m_1 - m_2)^2)(s - (m_1 + m_2)^2)\,, \tag{C.3}$$

is related to the spatial momentum in $1 \to 2$ decay [7]. The momenta $\ell_{1,2}$ depend on the angle of the lepton ℓ_1 w.r.t. to the decay axis in the q-RF

$$\ell_1^{(2)} = (\gamma(E_{\ell_1}^{(3)} + \beta\cos\theta_\ell|\vec{\ell}_1^{(3)}|), \gamma(\beta E_{\ell_1}^{(3)} + \cos\theta_\ell|\vec{\ell}_1^{(3)}|), -|\vec{\ell}_1^{(3)}|\sin\theta_\ell, 0)\,,$$
$$\ell_2^{(2)} = (\gamma(E_{\ell_2}^{(3)} - \beta\cos\theta_\ell|\vec{\ell}_1^{(3)}|), \gamma(\beta E_{\ell_2}^{(3)} - \cos\theta_\ell|\vec{\ell}_1^{(3)}|), +|\vec{\ell}_1^{(3)}|\sin\theta_\ell, 0)\,, \tag{C.4}$$

where the energy and momenta are defined in the q-RF and are given by

$$E_{\ell_{1,2}}^{(3)} = \sqrt{|\vec{\ell}_1^{(3)}|^2 + m_{\ell_{1,2}}^2} = \frac{1}{2q}(q^2 + m_{\ell_{1,2}}^2 - m_{\ell_{2,1}}^2)\,, \quad |\vec{\ell}_1^{(3)}| = \frac{\lambda^{1/2}(q^2, m_{\ell_1}^2, m_{\ell_2}^2)}{2q}\,, \tag{C.5}$$

and $q \equiv \sqrt{q^2}$, whenever it is clear that q is not a vector, such as in $E_q^{(3)} = E_{\ell_1}^{(3)} + E_{\ell_2}^{(3)} = q$. The boost velocity β and γ-factor are given by

$$\beta = \frac{|\vec{p}_K^{(2)}|}{E_q^{(2)}}\,, \quad \gamma = \frac{E_q^{(2)}}{q}\,, \tag{C.6}$$

where $|\vec{q}| = |\vec{p_K}|$ was used.

C.2 Kinematics in terms of the $\{q_0^2, \theta_0\}$-variables

We start by defining kinematic variables in the p_B-RF, denoted by (1). Defining the x-axis along the direction of $\vec{q}_0$, one has

$$p_B^{(1)} = (m_B, 0, 0, 0)\,, \quad q_0^{(1)} = (E_{q_0}^{(1)}, |\vec{q}_0^{(1)}|, 0, 0)\,, \quad p_K^{(1)} = (E_K^{(1)}, -|\vec{q}_0^{(1)}|, 0, 0)\,. \tag{C.7}$$

The momenta ℓ_1, ℓ_2, and k, will be defined in frame (4), and

$$E_K^{(1)} = m_B - E_{q_0}^{(1)} = \frac{1}{2m_B}(m_B^2 - q_0^2 + m_K^2)\,,$$
$$E_{q_0}^{(1)} = \sqrt{|\vec{q}_0^{(1)}|^2 + q_0^2} = \frac{1}{2m_B}(m_B^2 + q_0^2 - m_K^2)\,, \quad |\vec{q}_0^{(1)}| = \frac{\lambda^{1/2}(m_B^2, q_0^2, m_K^2)}{2m_B}\,. \tag{C.8}$$

JHEP12(2020)104

Frame (1) is useful for imposing the cut-off on the photon energy, cf. eq. (2.31). For the phase space integration, we pick the independent variables $|\vec{k}_\gamma^{(4)}|$, $\theta_\gamma^{(4)}$, $\phi_\gamma^{(4)}$, all defined in the q_0-RF, which we denote as the (4)-frame. There, the four-momenta are given by

$$\begin{aligned}
k^{(4)} &= (E_\gamma^{(4)}, -\cos\theta_\gamma^{(4)}|\vec{k}_\gamma^{(4)}|, -\sin\theta_\gamma^{(4)}\cos\phi_\gamma^{(4)}|\vec{k}_\gamma^{(4)}|, -\sin\theta_\gamma^{(4)}\sin\phi_\gamma^{(4)}|\vec{k}_\gamma^{(4)}|)\,, \\
p_B^{(4)} &= \gamma_{q_0} m_B\,(1, -\beta_{q_0}, 0, 0)\;, \quad q_0^{(4)} = (q_0, 0, 0, 0)\,, \\
p_K^{(4)} &= \gamma_{q_0}\left(\left(E_K^{(1)} + \beta_{q_0}|\vec{q}_0^{\,(1)}|\right), -\left(|\vec{q}_0^{\,(1)}| + \beta_{q_0}E_K^{(1)}\right), 0, 0\right)\,,
\end{aligned} \tag{C.9}$$

where $E_\gamma^{(4)} = \sqrt{|\vec{k}_\gamma^{(4)}|^2 + m_\gamma^2}$ and the boost factors from the p_B-RF to the q_0-RF are given by

$$\beta_{q_0} = \frac{|\vec{q}_0^{\,(1)}|}{E_{q_0}^{(1)}}\,, \quad \gamma_{q_0} = \frac{E_{q_0}^{(1)}}{q_0}\,. \tag{C.10}$$

We choose the axes such that $\vec{\ell}_1^{\,(4)}$ lies in the $xy-$plane. Then

$$\ell_1^{(4)} = \left(E_{\ell_1}^{(4)}, |\vec{\ell}_1^{\,(4)}|c_0, -|\vec{\ell}_1^{\,(4)}|s_0, 0\right), \tag{C.11}$$

where θ_0 (recall $c_0 \equiv \cos\theta_0$) is the angle between $\vec{\ell}_1^{\,(4)}$ and the x-axis in the q_0-RF (cf. figure 1), and $E_{\ell_1}^{(4)} = (|\vec{\ell}_1^{\,(4)}|^2 + m_{\ell_1}^2)^{1/2}$. $\ell_2^{(4)}$ is found by momentum conservation via $\ell_2^{(4)} = (q_0 - \ell_1 - k)^{(4)}$. Solving for $|\vec{\ell}_1^{\,(4)}|$ is quite complicated, and the explicit result is given by

$$|\vec{\ell}_1^{\,(4)}| = \frac{AB + \sqrt{D}}{C^2 - B^2}\,, \tag{C.12}$$

where

$$\begin{aligned}
A &\equiv q_0^2 - 2q_0E_\gamma^{(4)} + m_{\ell_1}^2 - m_{\ell_2}^2 + m_\gamma^2\,, \\
B &\equiv 2E_\gamma^{(4)}\beta_\gamma\left(\cos\theta_\gamma^{(4)}\;c_0 - \sin\theta_\gamma^{(4)}\;\cos\phi_\gamma^{(4)}\;s_0\right)\,, \\
C &\equiv 2q_0 - 2E_\gamma^{(4)}\,, \\
D &\equiv A^2B^2 + (C^2 - B^2)(A^2 - C^2m_{\ell_1}^2)\,,
\end{aligned} \tag{C.13}$$

where $\beta_\gamma = ((E_\gamma^{(4)})^2 - m_\gamma^2)^{\frac{1}{2}}/E_\gamma^{(4)}$. Using the above, one can also calculate $\omega^2 \equiv 2(|\vec{\ell}_1^{\,(4)}|E_q^{(4)} + \partial_{|\vec{\ell}_1^{\,(4)}|}[\vec{k}\cdot\vec{\ell}_1]^{(4)}E_{\ell_1}^{(4)})$, needed in (2.24). It reads

$$\omega^2 = 2\left(|\vec{\ell}_1^{\,(4)}|(q_0 - E_\gamma^{(4)}) + E_{\ell_1}^{(4)}E_\gamma^{(4)}\beta_\gamma(\sin\theta_\gamma^{(4)}\;\cos\phi_\gamma^{(4)}\;s_0 - \cos\theta_\gamma^{(4)}\;c_0)\right). \tag{C.14}$$

D Soft integral $\mathcal{F}_{ij}^{(s)}$

D.1 IR sensitive part with photon mass and dimensional regularisation

The $\mathcal{F}_{ij}^{(s)}$ integral is IR-divergent and has to be regulated. We discuss dimensional regularisation and photon mass regularisation in this appendix. The regularised integral, denoted

JHEP12(2020)104

by an $\mathcal{R}$-subscript, is

$$\left[\mathcal{F}_{ij}^{(s)}(\omega_s)\right]_{\mathcal{R}} = \int [d\Phi_\gamma]_{\mathcal{R}} \left[\frac{-(E_\gamma^{(n)})^2\, p_i\cdot p_j}{(k\cdot p_i)(k\cdot p_j)}\right] = \frac{1}{2\pi}\int_0^{(E_\gamma^{(n)})^{\max}} \frac{dE_\gamma^{(n)}}{E_\gamma^{(n)}} \rho_{\mathcal{R}}^{E}\, I_{ij}^{(\mathcal{R},n)}(E_\gamma^{(n)})\,, \quad \text{(D.1)}$$

where

$$I_{ij}^{\mathcal{R}}(E_\gamma^{(n)}) \equiv \int d\Omega_\gamma^{(n)}\; \rho_{\mathcal{R}}^{\Omega^{(n)}} \left[\frac{-(E_\gamma^{(n)})^2\, p_i\cdot p_j}{(k\cdot p_i)(k\cdot p_j)}\right], \quad \text{(D.2)}$$

and $(E_\gamma^{(1,2)})^{\max} = \frac{\omega_s m_B}{2}$ corresponds to the expression in (2.31) with $\delta_{\text{ex}} \to \omega_s \ll 1$ for which the two frames become equivalent and

$$\rho_{\mathcal{R}}^{E} = \begin{cases} \frac{\Gamma(1-\epsilon)}{\Gamma(1-2\epsilon)}\left(\frac{E_\gamma^{(n)}}{\sqrt{\pi}\mu}\right)^{-2\epsilon} & \text{dim-reg} \\ \theta(E_\gamma^{(n)} - m_\gamma) & m_\gamma \end{cases}, \qquad \rho_{\mathcal{R}}^{\Omega^{(n)}} = \begin{cases} (\sin\theta_\gamma\, \sin\phi_\gamma)^{-2\epsilon} & \text{dim-reg} \\ \frac{|\vec{k}_\gamma^{(n)}|}{E_\gamma^{(n)}} & m_\gamma \end{cases}, \quad \text{(D.3)}$$

and in addition one needs to set $m_\gamma \to 0$ in dim-reg. We will argue that the angular integral is Lorentz-invariant when the regulator is removed. We may restore Lorentz invariance of (D.1) by removing the photon energy cut-off. In a second step, we remove the regulator, $\rho_{\mathcal{R}}^{E}, \rho_{\mathcal{R}}^{\Omega^{(n)}} \to 1$. Then, the integral, which is frame- and scheme-independent, factorises into an energy integral K and an angular integral $I_{ij}^{(0)}$, where the superscript (0) indicates that the regulator has been removed. Since the energy integral is Lorentz invariant on its own, this implies the Lorentz-invariance of the finite $I_{ij}^{(0)}$-integral.

Focussing on the IR sensitive part, we keep $\rho_{\mathcal{R}}^{E}$ to regulate the divergent energy integral and remove the angular regularisation $\rho_{\mathcal{R}}^{\Omega^{(n)}} \to 1$ which is a useful limit as the integral still factorises into a doable energy integral and the Lorentz invariant $I_{ij}^{(0)}$-part,

$$\left[\mathcal{F}_{ij}^{(s)}\right]_{\mathcal{R}} = -K_{\mathcal{R}}(\omega_s)\; I_{ij}^{(0)} + \mathcal{O}(f,\mathcal{R})\,, \quad \text{(D.4)}$$

where

$$I_{ij}^{(0)} = I_{ij}^{(0,n)} \equiv \int d\Omega_\gamma^{(n)} \left[\frac{-(E_\gamma^{(n)})^2\, p_i\cdot p_j}{(k\cdot p_i)(k\cdot p_j)}\right] = (3.9)\,, \quad \text{(D.5)}$$

and we have used the Lorentz invariance of $I_{ij}^{(0,n)}$. We note that while $\rho_{\mathcal{R}}^{\Omega^{(n)}} \to 1$ captures all IR sensitive terms, it misses constant terms, indicated by $\mathcal{O}(f,\mathcal{R})$. These terms are determined in DR in the next section.

In DR, the $K_{\mathcal{R}}(\omega_s)$ integral evaluates to

$$K_\epsilon(\omega_s) = \int_0^{(E_\gamma^{(n)})^{\max}} \frac{dE_\gamma^{(n)}}{E_\gamma^{(n)}} \frac{\Gamma(1-\epsilon)}{\Gamma(1-2\epsilon)}\left(\frac{E_\gamma^{(n)}}{\sqrt{\pi}\mu}\right)^{-2\epsilon} = -\frac{1}{2} r_{\text{soft}} + \ln\left(\frac{\omega_s m_B}{\mu}\right) + \mathcal{O}(\epsilon), \quad \text{(D.6)}$$

whereas in photon mass regularisation the result is

$$K_{m_\gamma}(\omega_s) = \int_{m_\gamma}^{(E_\gamma^{(n)})^{\max}} \frac{dE_\gamma^{(n)}}{E_\gamma^{(n)}} = -\frac{1}{2} r_{\text{soft}} + \ln\left(\frac{\omega_s m_B}{2\mu}\right) + \mathcal{O}(m_\gamma)\,, \quad \text{(D.7)}$$

and we note the additional factor of 2 in the logarithm as compared to the DR result.

JHEP12(2020)104

D.2 Soft integrals in dimensional regularisation

In this section, we calculate the soft integrals fully analytically up $\mathcal{O}(\epsilon^0)$ to using dimensional regularisation. We perform the integrals by introducing a soft cut-off ω_s, and the result is obtained up to $\mathcal{O}(\omega_s)$ corrections, which can be safely neglected since $\omega_s \ll 1$.

The integrals have the general form

$$\mathcal{F}_{ij}^{(s)}(\omega_s) = \frac{(\pi\mu^2)^\epsilon}{2\pi}\frac{\Gamma(1-\epsilon)}{\Gamma(1-2\epsilon)}\int_0^{(E_\gamma^{(n)})^{\max}}\frac{dE_\gamma^{(n)}}{\left(E_\gamma^{(n)}\right)^{1+2\epsilon}}\int_0^\pi\frac{d\theta_\gamma}{\sin^{2\epsilon-1}\theta_\gamma}\int_0^\pi\frac{d\phi_\gamma}{\sin^{2\epsilon}\phi_\gamma}\left[\frac{-(E_\gamma^{(n)})^2\, p_i{\cdot}p_j}{(k{\cdot}p_i)(k{\cdot}p_j)}\right].$$

We have a total of 10 soft integrals to evaluate, corresponding to the different cases of i and j. Most of them can be evaluated using the results in the appendix of [50] and [22] (see also [51]). For $i = j$, we can write them as

$$\mathcal{F}_{ii}^{(s)}(\omega_s) = \left[\frac{1}{2}r_{\text{soft}} - \ln\left(\frac{\omega_s m_B}{\mu}\right)\right] + \frac{1}{2\beta_i}\ln\left(\frac{1+\beta_i}{1-\beta_i}\right), \tag{D.8}$$

where r_{soft} refers to the DR version in (2.20), and all β_i are measured in the p_B-RF, with $k = 0$, since we are in the soft limit.[26] We note that in the soft limit, the (1)- and (2)-frames are the same, and thus, we will use the two interchangeably in this section. Further, we can isolate the collinear logs in the case of small lepton masses by considering

$$\frac{1}{2\beta_i}\ln\left(\frac{1+\beta_i}{1-\beta_i}\right) = \frac{1}{2\beta_i}\ln\left(\frac{(1+\beta_i)^2}{1-\beta_i^2}\right) \overset{m_i\to 0}{\longrightarrow} \frac{1}{2}\ln\frac{4E_i^2}{m_i^2} = -\ln m_i + \text{non-div}\,. \tag{D.9}$$

We now list the integrals corresponding to $i \neq j$. The simplest one is

$$\mathcal{F}_{iB}^{(s)}(\omega_s) = \left[\frac{1}{2}r_{\text{soft}} - \ln\left(\frac{\omega_s m_B}{\mu}\right)\right] I_{iB}^{(0)} + \frac{1}{2\beta_i}\left[\text{Li}_2\left(\frac{2\beta_i}{1+\beta_i}\right) + \frac{1}{4}\ln^2\left(\frac{1+\beta_i}{1-\beta_i}\right)\right], \tag{D.10}$$

where $I_{iB}^{(0)}$ can be obtained by using $j = B$ in eq. (3.9). The 3 other non-diagonal integrals require more work since they are not attributed to the frame in which the integral is evaluated. One can recast the remaining integrals as

$$\mathcal{F}_{ij}^{(s)}(\omega_s) = \left[\frac{1}{2}r_{\text{soft}} - \ln\left(\frac{\omega_s m_B}{\mu}\right)\right]\Omega_{ij}\,, \tag{D.11}$$

where $\Omega_{ij} = \Omega(\beta_i, \beta_j, \tau_{ij})$,

$$\Omega(\beta_i,\beta_j,\tau_{ij}) = P_{ij}\int_0^\pi\frac{d\theta_\gamma}{\sin^{2\epsilon-1}\theta_\gamma}\int_0^\pi\frac{d\phi_\gamma}{\sin^{2\epsilon}\phi_\gamma} \times\left[\frac{1}{(1-\beta_i\cos\theta_\gamma)(1-\beta_j\cos\theta_\gamma\cos\chi_{ij}-\beta_j\sin\theta_\gamma\cos\phi_\gamma\sin\chi_{ij})}\right], \tag{D.12}$$

where $\cos\chi_{ij} = 2\tau_{ij} - 1$, $\sin\chi_{ij} = \sqrt{1-\cos^2\chi_{ij}}$ and $P_{ij} = (1-\beta_i\beta_j(2\tau_{ij}-1))/2\pi$.

[26] The reason for measuring all β_i in the p_B-RF is that it is the same frame in which we impose the cut-off on the photon energy, cf. eq. (2.31).

JHEP12(2020)104

Before matching β_i, β_j and τ_{ij} to the cases we have, consider $\Omega(\beta_i, \beta_j, \tau_{ij})$. For $\beta_i \neq 1$ and $\beta_j \neq 1$, the result to $\mathcal{O}(\epsilon)$ is not known in the literature. This is needed for isolating the collinear logs, since they arise from the $\mathcal{O}(\epsilon)$ part of the angular integrals multiplied by the $1/\epsilon$ from the r_{soft}.

However, through [52], we were able to get an expression for $\Omega(\beta_i, \beta_j, \tau_{ij})$. The result is

$$\Omega_{ij} = \frac{\pi\, P_{ij}}{2\, C_{ij}} \Bigg\{ \ln\left(\frac{v_{ij}+C_{ij}}{v_{ij}-C_{ij}}\right) + \epsilon \Bigg[-\ln\left(\frac{1-C_{ii}}{1+C_{ii}}\right) \ln\left(\frac{R_{ij}+S_{ij}}{R_{ij}-S_{ij}}\right) + \left(\sum_{a,b=1}^{4} \left[-1+2\left(\delta_{a2}+\delta_{a3}\right)\right] \left[1-2\left(\delta_{b3}+\delta_{b4}\right)\right] G(r_{ij}^{(a)}, r_{ij}^{(b)}, 1) \right) \Bigg] \Bigg\} . \tag{D.13}$$

The functions $G(a, b, 1)$ are generalised polylogarithms of weight 2, and for our parameters a and b the following representation holds

$$\begin{aligned} G(a,b,1) &= \mathrm{Li}_2\left(\frac{b-1}{b-a}\right) - \mathrm{Li}_2\left(\frac{b}{b-a}\right) + \ln\left(1-\frac{1}{b}\right) \ln\left(\frac{1-a}{b-a}\right) , \\ G(a,a,1) &= \frac{1}{2} \ln^2\left(1-\frac{1}{a}\right) , \end{aligned} \tag{D.14}$$

and

$$\begin{aligned} r_{ij}^{(1)} &= \frac{f_{ij}-\sqrt{g_{ij}}}{h_{ij}} , & r_{ij}^{(2)} &= \frac{f_{ij}+\sqrt{g_{ij}}}{h_{ij}} , \\ r_{ij}^{(3)} &= r_{ij}^{(1)}|_{\beta_{i,j}\to-\beta_{i,j}} , & r_{ij}^{(4)} &= r_{ij}^{(2)}|_{\beta_{i,j}\to-\beta_{i,j}} , \\ f_{ij} &= \beta_i \left(\beta_j \left(1-2\tau_{ij}\right)+1\right) , & h_{ij} &= \beta_i \left(\beta_j + 2 - 4\tau_{ij}\right) + \beta_j , \\ g_{ij} &= \beta_i^2 \left(4\beta_j^2 \tau_{ij} \left(\tau_{ij}-1\right)+1\right) + \beta_i\beta_j(2-4\tau_{ij}) \ +\beta_j^2 , \\ R_{ij} &= C_{ii} v_{ij} C_{jj} - 8 v_{ii} v_{jj} + v_{ij} , & S_{ij} &= \left(C_{ii}+C_{jj}\right) C_{ij} , \\ C_{ij} &= \sqrt{v_{ij}^2 - 4 v_{ii} v_{jj}} , & C_{ii} &= \sqrt{1-4v_{ii}} , & C_{jj} &= \sqrt{1-4v_{jj}} , \\ v_{ij} &= \frac{1}{2}\left(1-\beta_i\beta_j\left(2\tau_{ij}-1\right)\right) , & v_{ii} &= \frac{1}{4}\left(1-\beta_i^2\right) , & v_{jj} &= \frac{1}{4}\left(1-\beta_j^2\right) , \end{aligned}$$

with no summation over indices implied. For the matching, we consider the momenta p_K, ℓ_1 and ℓ_2 in the (2)-frame. Thus, for $\mathcal{F}^{(s)}_{K\ell_{1,2}}(\omega_s)$, one has

$$\beta_K = \frac{|\vec{p}_K^{\,(2)}|}{E_K^{(2)}} , \quad \beta_{\ell_{1,2}} = \frac{|\vec{\ell}_{1,2}^{\,(2)}|}{E_{1,2}^{(2)}} , \quad \tau_{K\ell_{1,2}} = \frac{1}{2}\left(1-\frac{\ell_{1,2,x}^{(2)}}{|\vec{\ell}_{1,2}^{\,(2)}|}\right) , \tag{D.15}$$

where $\ell_{1,2,x}^{(2)}$ corresponds to the x-component of $\ell_{1,2}^{(2)}$. Recall that the β_i's can be evaluated either in the (1)-RF or (2)-RF as these are equivalent in the $k \to 0$ limit assumed here.

Finally, for $\mathcal{F}^{(s)}_{\ell_1\ell_2}(\omega_s)$, before the matching can be performed, one needs to perform a 3D rotation to eliminate the y-component of one of the momenta, for which we choose ℓ_1.

JHEP12(2020)104

Thus, one has ($\beta_{\ell_{1,2}}$ is given above)

$$\tau_{\ell_1\ell_2} = \frac{1}{2}\left(1 + \frac{\ell^{(2)}_{2,x}\cos\alpha - \ell^{(2)}_{2,y}\sin\alpha}{|\vec{\ell}^{(2)}_2|}\right), \tag{D.16}$$

where, as before, the subscript on ℓ_2 denotes the corresponding component of ℓ_2. The angle of rotation α is defined via $\cos\alpha = \frac{\ell^{(2)}_{1,x}}{|\vec{\ell}^{(2)}_1|}$ and $\sin\alpha = \sqrt{1-\cos^2\alpha}$. Taking the limit of small lepton masses, one can isolate the collinear logs and obtain

$$\begin{aligned}
\mathcal{F}^{(s)}_{\ell_1\ell_2}(\omega_s) &= \left[\frac{1}{2}\Delta_\epsilon - \ln(\omega_s m_B)\right] I^{(0)}_{\ell_1\ell_2} + \left(\frac{1}{2}\ln^2 m_{\ell_1} - \ln m_{\ell_1}\ln\left(2E^{(1)}_{\ell_1}\right) + \{1\leftrightarrow 2\}\right) + \text{finite}\,,\\
\mathcal{F}^{(s)}_{K\ell_1}(\omega_s) &= \left[\frac{1}{2}\Delta_\epsilon - \ln(\omega_s m_B)\right] I^{(0)}_{K\ell_{1,2}} + \frac{1}{2}\ln^2 m_{\ell_1} - \ln m_{\ell_1}\ln\left(2E^{(1)}_{\ell_1}\right) + \text{finite}\,.
\end{aligned} \tag{D.17}$$

We now collect all single logs in $\mathcal{F}^{(s)}(\omega_s) \equiv \sum_{i,j}\hat{Q}_i\hat{Q}_j\mathcal{F}^{(s)}_{ij}(\omega_s)$. To this end, consider the divergent parts of the different limits of $I^{(0)}_{ij}$.

$$I^{(0)}_{ij} \to \begin{cases} -\ln m_i & m_i \ll m_K, m_B \\ -\ln m_i - \ln m_j & m_i \approx m_j \ll m_K, m_B \end{cases}. \tag{D.18}$$

Assembling all bits and pieces, and using charge conservation, we obtain

$$\begin{aligned}
\mathcal{F}^{(s)}(\omega_s)|_{\ln m_{\ell_{1,2}}} &= \hat{Q}^2_{\ell_1}\ln m_{\ell_1}(2\ln 2E^{(1)}_{\ell_2} - (1 + 2\ln(\omega_s m_B)) + \{1\leftrightarrow 2\}\\
&= \hat{Q}^2_{\ell_1}\ln m_{\ell_1}\left[-1 - 2\ln(\bar{z}(\omega_s))\right] + \{1\leftrightarrow 2\}\,,
\end{aligned} \tag{D.19}$$

where we have used $2\hat{E}^{(1)}_{\ell_1} \equiv 1 - \hat{s}_{K\ell_2}$ to arrive at the final result, and $\bar{z}(\omega_s) \equiv 1 - z(\omega_s)$ with $z(\omega_s)$ given in eq. (3.18).

E Passarino-Veltman functions

The aim of this appendix is to give a minimal self-contained discussion of the Passarino-Veltman functions appearing in our results. The integrals are defined in [53],

$$I_n \equiv \frac{(2\pi\mu)^{4-d}}{i\pi^2}\int \mathrm{d}^d l \frac{1}{(l^2 - m_0^2 + i0)((l+\ell_1)^2 - m_1^2 + i0)((l+\ell_1+\ell_2)^2 - m_2^2 + i0)\ldots}, \tag{E.1}$$

where $n = 1, 2, 3, 4$ form a complete 1-loop basis and are usually referred to as A_0, B_0, C_0, D_0 respectively. For our case, $n = 1, 2, 3$ are sufficient. The A_0 and B_0 functions are given to $\mathcal{O}(\varepsilon^0)$, with $d = 4 - 2\varepsilon$,

$$\begin{aligned}
A_0\left(m^2\right) &= m^2\left(\frac{1}{\hat{\epsilon}_{\text{UV}}} + 1 - \ln\left(\frac{m^2}{\mu^2}\right)\right) + \mathcal{O}(\varepsilon)\,,\\
B_0(s, m_0^2, m_1^2) &= \left(\frac{1}{\hat{\epsilon}_{\text{UV}}} + 2 - \ln\frac{m_0 m_1}{\mu^2} + \frac{m_0^2 - m_1^2}{s}\ln\frac{m_1}{m_0} - \frac{m_0 m_1}{s}\left(\frac{1}{r} - r\right)\ln r\right) + \mathcal{O}(\varepsilon)\,,
\end{aligned} \tag{E.2}$$

where $r = -\frac{1}{2}(-b + \sqrt{b^2 - 4})$ with $b = -\frac{s - m_0^2 - m_1^2 + i0}{m_0 m_1}$, and $\frac{1}{\hat{\epsilon}_{\text{UV}}}$ is given in eq. (2.19).

JHEP12(2020)104

The C_0 function used is $C_0(s,t,u,m_0^2,m_1^2,m_2^2)$, where the cuts of the momenta $\{s,t,u\}$ start at $\{(m_0+m_1)^2,(m_0+m_2)^2,(m_1+m_2)^2\}$ respectively. This is the same convention used in FeynCalc [54, 55] and [53].

The C_0 function can be found in the review paper [56] (eq. B.5), valid for small photon mass (up to $\mathcal{O}(m_\gamma^2)$ corrections) in mass regularisation and to $\mathcal{O}(\epsilon^0)$ in DR,

$$C_0 = \frac{x_{ij}}{m_i m_j (1-x_{ij}^2)} \left\{ \left(\ln\left(\frac{m_i m_j}{\mu^2}\right) - r_{\text{soft}} \right) \ln(x_{ij}) - \frac{1}{2}\ln^2(x_{ij}) + 2\ln(x_{ij})\ln(1-x_{ij}^2) \right.$$
$$\left. + \frac{1}{2}\ln^2\left(\frac{m_i}{m_j}\right) - \frac{\pi^2}{6} + \text{Li}_2(x_{ij}^2) + \text{Li}_2\left(1 - x_{ij}\frac{m_i}{m_j}\right) + \text{Li}_2\left(1 - x_{ij}\frac{m_j}{m_i}\right) \right\}, \tag{E.3}$$

where $C_0 \equiv C_0(m_i^2, m_j^2, (\hat{p}_i+\hat{p}_j)^2, m_i^2, m_\gamma^2, m_j^2)$, r_{soft} is defined in (2.20), and

$$x_{ij} \equiv \frac{\sqrt{y_{ij}}-1}{\sqrt{y_{ij}}+1}, \quad y_{ij} \equiv \frac{(\hat{p}_i+\hat{p}_j)^2-(m_i+m_j)^2+i0}{(\hat{p}_i+\hat{p}_j)^2-(m_i-m_j)^2+i0}. \tag{E.4}$$

References

[1] LHCb collaboration, *Test of lepton universality using $B^+ \to K^+\ell^+\ell^-$ decays*, *Phys. Rev. Lett.* **113** (2014) 151601 [arXiv:1406.6482] [INSPIRE].

[2] LHCb collaboration, *Test of lepton universality with $B^0 \to K^{*0}\ell^+\ell^-$ decays*, *JHEP* **08** (2017) 055 [arXiv:1705.05802] [INSPIRE].

[3] LHCb collaboration, *Search for lepton-universality violation in $B^+ \to K^+\ell^+\ell^-$ decays*, *Phys. Rev. Lett.* **122** (2019) 191801 [arXiv:1903.09252] [INSPIRE].

[4] S. Bifani, S. Descotes-Genon, A. Romero Vidal and M.-H. Schune, *Review of Lepton Universality tests in B decays*, *J. Phys. G* **46** (2019) 023001 [arXiv:1809.06229] [INSPIRE].

[5] N. Davidson, T. Przedzinski and Z. Was, *PHOTOS interface in C++: Technical and Physics Documentation*, *Comput. Phys. Commun.* **199** (2016) 86 [arXiv:1011.0937] [INSPIRE].

[6] M. Bordone, G. Isidori and A. Pattori, *On the Standard Model predictions for R_K and R_{K^*}*, *Eur. Phys. J. C* **76** (2016) 440 [arXiv:1605.07633] [INSPIRE].

[7] Particle Data Group collaboration, *Review of Particle Physics*, *PTEP* **2020** (2020) 083C01 [INSPIRE].

[8] M. Beneke, T. Feldmann and D. Seidel, *Systematic approach to exclusive $B \to Vl^+l^-$, $V\gamma$ decays*, *Nucl. Phys. B* **612** (2001) 25 [hep-ph/0106067] [INSPIRE].

[9] M. Dimou, J. Lyon and R. Zwicky, *Exclusive Chromomagnetism in heavy-to-light FCNCs*, *Phys. Rev. D* **87** (2013) 074008 [arXiv:1212.2242] [INSPIRE].

[10] J. Lyon and R. Zwicky, *Isospin asymmetries in $B \to (K^*,\rho)\gamma/l^+l^-$ and $B \to Kl^+l^-$ in and beyond the standard model*, *Phys. Rev. D* **88** (2013) 094004 [arXiv:1305.4797] [INSPIRE].

JHEP12(2020)104

[11] A. Khodjamirian, T. Mannel and Y.M. Wang, $B \to K\ell^+\ell^-$ *decay at large hadronic recoil*, *JHEP* **02** (2013) 010 [arXiv:1211.0234] [INSPIRE].

[12] B. Kubis and R. Schmidt, *Radiative corrections in* $K \to \pi\ell^+\ell^-$ *decays*, *Eur. Phys. J. C* **70** (2010) 219 [arXiv:1007.1887] [INSPIRE].

[13] R. Ellis, D.A. Ross and A.E. Terrano, *The Perturbative Calculation of Jet Structure in* e^+e^- *Annihilation*, *Nucl. Phys. B* **178** (1981) 421 [INSPIRE].

[14] S. Weinberg, *The quantum theory of fields. Vol. 1: Foundations*, Cambridge University Press, (2005).

[15] T. Muta, *Foundations of quantum chromodynamics*, Second edition, vol. 57., World Scientific, (1998).

[16] G.F. Sterman, *An introduction to quantum field theory*, Cambridge University Press, (1993).

[17] E.S. Ginsberg, *Radiative corrections to the k-l-3 +- dalitz plot*, *Phys. Rev.* **162** (1967) 1570 [*Erratum ibid.* **187** (1969) 2280] [INSPIRE].

[18] S. Catani and M.H. Seymour, *A general algorithm for calculating jet cross-sections in NLO QCD*, *Nucl. Phys. B* **485** (1997) 291 [*Erratum ibid.* **510** (1998) 503] [hep-ph/9605323] [INSPIRE].

[19] S. Dittmaier, *A general approach to photon radiation off fermions*, *Nucl. Phys. B* **565** (2000) 69 [hep-ph/9904440] [INSPIRE].

[20] S. Dittmaier, A. Kabelschacht and T. Kasprzik, *Polarized QED splittings of massive fermions and dipole subtraction for non-collinear-safe observables*, *Nucl. Phys. B* **800** (2008) 146 [arXiv:0802.1405] [INSPIRE].

[21] M. Schönherr, *An automated subtraction of nlo ew infrared divergences*, *Eur. Phys. J. C* **78** (2018) 119.

[22] B.W. Harris and J.F. Owens, *The two cutoff phase space slicing method*, *Phys. Rev. D* **65** (2002) 094032 [hep-ph/0102128] [INSPIRE].

[23] F. Bloch and A. Nordsieck, *Note on the Radiation Field of the electron*, *Phys. Rev.* **52** (1937) 54 [INSPIRE].

[24] P. Ball and R. Zwicky, *New results on* $B \to \pi, K, \eta$ *decay formfactors from light-cone sum rules*, *Phys. Rev. D* **71** (2005) 014015 [hep-ph/0406232] [INSPIRE].

[25] RQCD collaboration, *Light-cone distribution amplitudes of pseudoscalar mesons from lattice QCD*, *JHEP* **08** (2019) 065 [*Addendum ibid.* **11** (2020) 037] [arXiv:1903.08038] [INSPIRE].

[26] V.M. Braun and A. Lenz, *On the* SU(3) *symmetry-breaking corrections to meson distribution amplitudes*, *Phys. Rev. D* **70** (2004) 074020 [hep-ph/0407282] [INSPIRE].

[27] P. Ball and R. Zwicky, SU(3) *breaking of leading-twist K and K* distribution amplitudes: A reprise*, *Phys. Lett. B* **633** (2006) 289 [hep-ph/0510338] [INSPIRE].

[28] P. Ball and R. Zwicky, *Operator relations for* SU(3) *breaking contributions to K and K* distribution amplitudes*, *JHEP* **02** (2006) 034 [hep-ph/0601086] [INSPIRE].

[29] K.G. Chetyrkin, A. Khodjamirian and A.A. Pivovarov, *Towards NNLO Accuracy in the QCD Sum Rule for the Kaon Distribution Amplitude*, *Phys. Lett. B* **661** (2008) 250 [arXiv:0712.2999] [INSPIRE].

JHEP12(2020)104

[30] M. Greco, G. Pancheri-Srivastava and Y. Srivastava, *Radiative Corrections for Colliding Beam Resonances*, *Nucl. Phys. B* **101** (1975) 234 [INSPIRE].

[31] G. D'Ambrosio and G. Isidori, $K \to \pi\pi\gamma$ *decays: A search for novel couplings in kaon decays*, *Z. Phys. C* **65** (1995) 649 [hep-ph/9408219] [INSPIRE].

[32] G. D'Ambrosio, G. Ecker, G. Isidori and H. Neufeld, $K \to \pi\pi\pi\gamma$ *in chiral perturbation theory*, *Z. Phys. C* **76** (1997) 301 [hep-ph/9612412] [INSPIRE].

[33] M. Beneke, C. Bobeth and R. Szafron, *Enhanced electromagnetic correction to the rare B-meson decay* $B_{s,d} \to \mu^+\mu^-$, *Phys. Rev. Lett.* **120** (2018) 011801 [arXiv:1708.09152] [INSPIRE].

[34] M. Beneke, P. Böer, J.-N. Toelstede and K.K. Vos, *QED factorization of non-leptonic B decays*, *JHEP* **11** (2020) 081 [arXiv:2008.10615] [INSPIRE].

[35] M. Beneke, C. Bobeth and R. Szafron, *Power-enhanced leading-logarithmic QED corrections to* $B_q \to \mu^+\mu^-$, *JHEP* **10** (2019) 232 [arXiv:1908.07011] [INSPIRE].

[36] N. Carrasco et al., *QED Corrections to Hadronic Processes in Lattice QCD*, *Phys. Rev. D* **91** (2015) 074506 [arXiv:1502.00257] [INSPIRE].

[37] C.T. Sachrajda et al., *Radiative corrections to semileptonic decay rates*, *PoS* **LATTICE2019** (2019) 162 [arXiv:1910.07342] [INSPIRE].

[38] D. Giusti et al., *First lattice calculation of the QED corrections to leptonic decay rates*, *Phys. Rev. Lett.* **120** (2018) 072001 [arXiv:1711.06537] [INSPIRE].

[39] M. Di Carlo et al., *Light-meson leptonic decay rates in lattice QCD+QED*, *Phys. Rev. D* **100** (2019) 034514 [arXiv:1904.08731] [INSPIRE].

[40] A. Portelli, *Electromagnetic corrections to leptonic decays*, talk given at *37th International Symposium on Lattice Field Theory*, Wuhan, China, June 2019.

[41] J. Gratrex, M. Hopfer and R. Zwicky, *Generalised helicity formalism, higher moments and the* $B \to K_{J_K}(\to K\pi)\bar{\ell}_1\ell_2$ *angular distributions*, *Phys. Rev. D* **93** (2016) 054008 [arXiv:1506.03970] [INSPIRE].

[42] V. Cirigliano, M. Knecht, H. Neufeld, H. Rupertsberger and P. Talavera, *Radiative corrections to K(l3) decays*, *Eur. Phys. J. C* **23** (2002) 121 [hep-ph/0110153] [INSPIRE].

[43] V. Cirigliano, M. Giannotti and H. Neufeld, *Electromagnetic effects in K(l3) decays*, *JHEP* **11** (2008) 006 [arXiv:0807.4507] [INSPIRE].

[44] S. de Boer, T. Kitahara and I. Nisandzic, *Soft-Photon Corrections to* $\bar{B} \to D\tau^-\bar{\nu}_\tau$ *Relative to* $\bar{B} \to D\mu^-\bar{\nu}_\mu$, *Phys. Rev. Lett.* **120** (2018) 261804 [arXiv:1803.05881] [INSPIRE].

[45] C. Bobeth, P. Gambino, M. Gorbahn and U. Haisch, *Complete NNLO QCD analysis of* $\bar{B} \to X(s)\ell^+\ell^-$ *and higher order electroweak effects*, *JHEP* **04** (2004) 071 [hep-ph/0312090] [INSPIRE].

[46] T. Huber, E. Lunghi, M. Misiak and D. Wyler, *Electromagnetic logarithms in* $\bar{B} \to X_s l^+ l^-$, *Nucl. Phys. B* **740** (2006) 105 [hep-ph/0512066] [INSPIRE].

[47] M.E. Peskin and D.V. Schroeder, *An Introduction to quantum field theory*, Addison-Wesley, Reading, U.S.A., (1995).

[48] G. Hiller and R. Zwicky, *(A)symmetries of weak decays at and near the kinematic endpoint*, *JHEP* **03** (2014) 042 [arXiv:1312.1923] [INSPIRE].

JHEP12(2020)104

[49] M. Bordone, A. Greljo, G. Isidori, D. Marzocca and A. Pattori, *Higgs Pseudo Observables and Radiative Corrections*, *Eur. Phys. J. C* **75** (2015) 385 [arXiv:1507.02555] [INSPIRE].

[50] W. Beenakker, H. Kuijf, W.L. van Neerven and J. Smith, *QCD Corrections to Heavy Quark Production in $p\bar{p}$ Collisions*, *Phys. Rev. D* **40** (1989) 54 [INSPIRE].

[51] G. Somogyi, *Angular integrals in d dimensions*, *J. Math. Phys.* **52** (2011) 083501 [arXiv:1101.3557] [INSPIRE].

[52] G. Somogyi, private communication.

[53] A. Denner, *Techniques for calculation of electroweak radiative corrections at the one loop level and results for W physics at LEP-200*, *Fortsch. Phys.* **41** (1993) 307 [arXiv:0709.1075] [INSPIRE].

[54] R. Mertig, M. Böhm and A. Denner, *FEYN CALC: Computer algebraic calculation of Feynman amplitudes*, *Comput. Phys. Commun.* **64** (1991) 345 [INSPIRE].

[55] V. Shtabovenko, R. Mertig and F. Orellana, *New Developments in FeynCalc 9.0*, *Comput. Phys. Commun.* **207** (2016) 432 [arXiv:1601.01167] [INSPIRE].

[56] S. Dittmaier, *Separation of soft and collinear singularities from one loop N point integrals*, *Nucl. Phys. B* **675** (2003) 447 [hep-ph/0308246] [INSPIRE].

JHEP12(2020)104